

ABSTRACT

THOMPSON, JAMES R. Analysis of Market Returns Using Multifractal Time Series and Agent-Based Simulation. (Under the direction of James R. Wilson.)

Many types of financial time series, most notably market returns, have been found to exhibit long-range memory as well as dramatic day-to-day swings that cannot be adequately represented by light-tailed distributions such as the normal distribution. In particular, this means that for such time series, the sum of covariances at all time lags is not defined because the covariance function does not converge to zero fast enough as the time lag increases. Moreover in such time series, often the tails of the marginal density converge to zero so slowly that higher-order marginal moments such as skewness and kurtosis fail to exist. Therefore conventional methods for analyzing simulation-generated time series cannot generally be applied to high-fidelity simulations of financial markets.

Building on earlier work in fractal geometry and fractal time series, in 1997 Mandelbrot et al. proposed the multifractal model of asset returns (MMAR) as an alternative to the ARCH models for analyzing time series exhibiting volatility clustering, long-range dependence, and heavy-tailed returns. Mandelbrot et al. defined the multifractal spectrum as the renormalized probability density function of the Hölder exponents observed in the time series; and they used the multifractal spectrum to measure the ability of MMAR to match the statistical properties of real data. In 2002 Kantelhardt et al. formulated multifractal detrended fluctuation analysis (MF-DFA), an algorithm for extracting the multifractal spectrum from a time series.

Many economists have recently adopted agent-based simulation for modeling financial markets. Fads based on new products, shocks related to world events, scandals involving company leaders, or outright criminal activity can drastically change the processes and relationships governing a market. Already there is evidence that agent-based models yield more accurate approximations to the true or observed behavior in financial markets compared with approximations achieved with conventional discrete-event models. Agent-based models exhibit emergent behaviors that have been linked to non-Gaussian interaction metrics and singularities in the time series they generate.

To analyze market-return time series exhibiting volatility clustering, long-range dependence, or heavy-tailed marginals, we exploit multifractal analysis and agent-based simulation. We develop a robust, automated software tool for extracting the multifractal spectrum of a time series based on MF-DFA. Guidelines are given for setting MF-DFA's parameters in practice. The software is tested on simulated data with closed-form monofractal and multifractal spectra as well as on observed data, and the results are analyzed. We also present a prototype agent-based financial market model and analyze its output using MF-DFA. The ultimate objective is to expand this model to study the effects of microlevel agent behaviors on the macrolevel time series output as analyzed by MF-DFA. Finally we explore the potential for validating agent-based models using MF-DFA.

Analysis of Market Returns Using Multifractal
Time Series and Agent-Based Simulation

by
James R. Thompson

A dissertation submitted to the Graduate Faculty of
North Carolina State University
in partial fulfillment of the
requirements for the Degree of
Doctor of Philosophy

Industrial Engineering

Raleigh, North Carolina

2013

APPROVED BY:

Russell King

Peter Bloomfield

Julie Ivy

James R. Wilson
Chair of Advisory Committee

DEDICATION

For Roy Goss

BIOGRAPHY

James R. Thompson, a native of Athens, Georgia, has lived in a number of cities around the world, settling in Washington, D.C. in 2003. He completed his graduate work in Industrial and Systems Engineering at North Carolina State University, and his undergraduate work in the same field at Georgia Institute of Technology. James' circuitous career has included (in no particular order) manufacturing engineer, logistics manager, construction project manager, strategic sourcing manager, consultant, teacher, painter, Christmas tree farmer, cattle-hand, lifeguard and Marine. He is an avid rugby player and can be found most Saturday afternoons running at scrum-half or wing, and most Sunday mornings wondering if he should take up a lower-impact sport.

ACKNOWLEDGEMENTS

First, I would like to thank my advisor, Dr. Jim Wilson. His willingness to pursue topics outside the normal realm of Industrial Engineering, and his belief that my rather obscure ideas “had legs” is the primary reason this dissertation came to pass. I would also like to thank Dr. Russell King. Dr. King originally recruited me to North Carolina State, and he was a constant source of advice and support as I made the adjustment from working professional back to academia. I owe special thanks to Dr. Peter Bloomfield for serving on my committee and keeping me grounded on the time series analysis side of things. I also would like to thank Dr. Yahya Fathi and Dr. Juile Ivy for their contributions and support.

Ella Fitzgerald once said “I stole everything that I heard, but mostly I stole from the horns.” And it is to my horn section that I owe special thanks. To my mother, Glenda Goss, for her constant support; to my father, Jimmy Thompson, for his guidance through the years that included *The Intelligent Investor* as a birthday gift in 2003; to my sister, Beth Thompson, for inspiring me to pursue my dreams; to the Raleigh Vipers Rugby Club for giving me the outlet I needed to get through this endeavor; and to my many friends on the Washington Irish Rugby Club for their endless support.

Finally, and most importantly, I owe a deep debt of gratitude to Emily Coccia. Her unwavering support over the last four years is the primary reason any of this was possible. Her confidence in me far outstripped my own, and for that I am more grateful than words can express. Time and again she has proven that she can remain supportive longer than I can remain irrational.

TABLE OF CONTENTS

LIST OF TABLES	vii
LIST OF FIGURES	viii
Chapter 1 Introduction	1
Chapter 2 Multifractal Analysis	6
2.1 Introduction	6
2.1.1 Fractals	6
2.2 Fractal Times Series	8
2.2.1 The Hurst Exponent and Fractional Brownian Motion	8
2.2.2 The Hölder Exponent and The Multifractal Formalism	12
2.3 Multifractal Analysis Background and Literature Review	16
2.4 Multifractal Detrended Fluctuation Analysis	25
2.4.1 The Algorithm	25
2.4.2 Important Notes on Parameter Selection	27
2.5 Software Implementation and Testing	32
2.5.1 Java Application	32
2.5.2 Testing on Known Multifractals	33
2.5.3 Brownian Motion	34
2.5.4 Multifractal Binomial Measure	43
2.6 Summary	50
Chapter 3 Applications of MF-DFA to Empirical Data	51
3.1 Introduction	51
3.2 The General Electric Data	52
3.3 Methods and Results	55
3.3.1 Traditional Time Series Analysis	55
3.3.2 Multifractal Time Series Analysis	69
3.4 Discussion	72
Chapter 4 Agent-based Modeling and the Zero-Intelligence Financial Market	73
4.1 Introduction	73
4.2 Agent-Based Modeling Background and Literature Review	74
4.2.1 Applications in Economics	74
4.2.2 Behavioral Logic	76
4.2.3 Review of Available Software	77
4.2.4 Zero-Intelligence Financial Markets	79
4.3 The Model	80
4.3.1 Continuous Double Auction Structure	80
4.3.2 Experiments	83
4.4 Results	86
4.4.1 The thin-tailed simulation	86

4.4.2	The heavy-tailed simulation	89
4.4.3	Multifractal Results	94
4.5	Discussion	99
Chapter 5	The Positive-Intelligence Financial Market	101
5.1	Introduction	101
5.2	Literature Review	103
5.3	The Model	105
5.3.1	The Order Book	105
5.3.2	The Agents	106
5.3.3	The Modified Gompertz Differential Equation	110
5.3.4	Model Mechanics	111
5.4	Exploratory Analysis	114
5.5	Multifractal Results	121
5.6	Discussion	126
Chapter 6	Conclusions and Future Research	130
6.1	Summary	130
6.2	Conclusions	131
6.3	Future Research	132
REFERENCES	135
APPENDIX	140
Appendix A	141
A.1	The Multifractal Binomial Measure	141
A.2	Simulating the Multifractal Binomial Measure	142

LIST OF TABLES

Table 2.1	Scale vs Coverings	7
Table 3.1	GE TAQ Data: 2000 to 2003	55
Table 3.2	GE Data AR Parameters	59
Table 5.1	Positive-Intelligence Parameters	112
Table 5.2	80% Grahamists with Adaptation	122
Table 5.3	80% Grahamists without Adaptation	124
Table 5.4	Grahamists Results Comparison	124
Table 5.5	Grahamists Paired <i>t</i> -test	125

LIST OF FIGURES

Figure 2.1	Standard Brownian Motion	10
Figure 2.2	Fractional Brownian Motion	11
Figure 2.3	Standard Brownian Motion: 2^{16} points	35
Figure 2.4	Brownian Motion Multifractal Spectrum	36
Figure 2.5	Fluctuation Functions of Brownian Motion	37
Figure 2.6	Fractional Brownian Motion H-comparison	38
Figure 2.7	Multifractal Spectra of Fractional Brownian Motion	39
Figure 2.8	Standard Brownian Motion Shuffle Test	40
Figure 2.9	Fractional Brownian Motion Shuffle Test	41
Figure 2.10	Fractional Brownian Motion Shuffle Test	42
Figure 2.11	Binomial Measure	43
Figure 2.12	Binomial Measure c.d.f.	44
Figure 2.13	Multifractal Spectrum of Binomial Measure	45
Figure 2.14	Binomial Measure Shuffle Test	46
Figure 2.15	Random Binomial Measure	47
Figure 2.16	Random vs Stochastic Multifractal	48
Figure 2.17	Multifractal Comparison: Brownian Motion vs Binomial Measure	49
Figure 3.1	GE Adjusted Daily Closing Price	53
Figure 3.2	GE TAQ Price	54
Figure 3.3	GE First Difference	56
Figure 3.4	GE First Difference	57
Figure 3.5	GE ACF and PACF	58
Figure 3.6	GE AR(4) Residuals	60
Figure 3.7	GE AR(4) QQ-plot	61
Figure 3.8	GE AR(4) Histogram	62
Figure 3.9	GE AR(4) ACF and PACF	63
Figure 3.10	GE GARCH(1,1) Residuals	64
Figure 3.11	GE GARCH(1,1) Histogram	65
Figure 3.12	GE GARCH(1,1) ACF and PACF	66
Figure 3.13	GE AR+GARCH QQ	67
Figure 3.14	GE AR+GARCH Histogram	68
Figure 3.15	GE Multifractal Spectrum	69
Figure 3.16	GE Shuffle Test	70
Figure 3.17	GE Standard Models	71
Figure 4.1	Double Auction Order Book	81
Figure 4.2	Zero-Intelligence Model	82
Figure 4.3	Zero-Intelligence Heavy-Tailed Time Series	84
Figure 4.4	Zero-Intelligence Thin-Tailed Time Series	85
Figure 4.5	Thin-Tailed Difference Time Series	86
Figure 4.6	Thin-Tailed ACF and PACF	87

Figure 4.7	Thin-Tailed Residuals	88
Figure 4.8	Thin-Tailed Residuals QQ	89
Figure 4.9	Heavy-Tailed Difference Time Series	90
Figure 4.10	Heavy-Tailed ACF and PACF	91
Figure 4.11	Heavy-Tailed Residuals	92
Figure 4.12	Heavy-Tailed Residuals QQ	93
Figure 4.13	Thin-Tailed Multifractal Spectrum	95
Figure 4.14	Heavy-Tailed Multifractal Spectrum	97
Figure 4.15	Simulated Multifractal Spectra Comparison	98
Figure 4.16	Multifractal Spectrum Compared with GE	100
Figure 5.1	Positive-Intelligence Model	113
Figure 5.2	Price Time Series by Grahamists	115
Figure 5.3	Price vs Steps by Grahamists	116
Figure 5.4	Price Difference by Grahamists	117
Figure 5.5	Price Difference 80% Grahamists	117
Figure 5.6	80% Grahamists ACF	118
Figure 5.7	80% Grahamists PACF	118
Figure 5.8	80% Grahamists GARCH QQ	119
Figure 5.9	Multifractal Spectra by Grahamists	120
Figure 5.10	80% Grahamists Multifractal Spectra	121
Figure 5.11	Agent-Adaptation Comparison	123
Figure 5.12	Multifractal Spectra Adaptation Off	123
Figure 5.13	Positive-Intelligence Shuffle Test	125
Figure 5.14	GE Multifractal Spectra by Year	127
Figure 5.15	Multifractal Comparisons	129
Figure 6.1	GE Multifractal Spectra	134

Chapter 1

Introduction

The analysis of empirical time series data remains something of an art form, in that there is no fixed prescription; indeed multiple techniques are often considered appropriate, although they may yield different results. The challenge to the researcher is to construct a theoretical model informed by observations and then validate that model with repeated experimentation. An important example is the modeling of financial times series as lognormal processes. This practice represents an evolution of Louis Bachelier's *The Theory of Speculation*, published in 1900. Bachelier's dissertation is thought to be the first application of Brownian motion as a model of asset returns, in this case, on the French stock market [18]. Given that negative prices are prevented by market structure, a natural extension to Bachelier's theory was to model the asset as having lognormal increments. This model retains the tractable mathematics associated with the Gaussian distribution, while making the model more realistic. Unfortunately, it still does not adequately explain many of the characteristics observed in financial data. Most notable are the instances of nonconstant variance, long memory, volatility clustering, and heavy tails observed in returns.

By 1963 a number of publications began to question the Gaussian approach, and Benoit Mandelbrot published his analysis of US cotton prices [54] in an effort to thoroughly dispute the notion that price changes are independent and identically distributed (i.i.d.) Gaussian random variables. Building on the work of Vilfredo Pareto and Paul Lévy, Mandelbrot generalized Bachelier's theory and defined what he called a *stable Paretian* distribution. Applying this distribution to cotton prices between 1900 and 1950, he was able to show the underlying parameters of the distribution differed only by the scale parameter — that is, when analyzed at different time scales the distribution of the price changes were simply horizontal translates of each other in doubly logarithmic plots, but otherwise all scales exhibited the same properties. This power law relationship between different time scales of the same data set became the foundation of Mandelbrot's work in fractal geometry.

Volatility clustering was ultimately addressed by Robert Engle. His paper introducing autoregressive conditional heteroscedastic (ARCH) models substantially updated the tool set employed in econometrics [21]. The basic idea was not only to condition the mean on the previous observations of the process

back to an appropriate lag, but also to condition the variance of the process on previous observations back to an appropriate lag. This approach has been effective in improving forecasts of financial data, as it retains some short-term memory of a drastic change in the asset. Naturally this approach leads to a cluster of volatility and seemingly updates the original Gaussian-based model with another layer of Gaussian variables. Engle himself noted that the ARCH model might be “an approximation to a more complex regression,” which clearly improves upon the constant-variance models, but still is not the true underlying model of asset prices.

Mandelbrot and others remained unconvinced that another Gaussian patch was the solution to the divide between theory and observation in time series analysis. Building on his work in fractal geometry, Mandelbrot et al. proposed the multifractal model of asset returns (MMAR) [59]. Interestingly enough, they retained the assumption of Brownian motion, but distorted the time scale. That is, they assumed that traders in the marketplace operate differently as the market environment evolves over time. In their basic example, “trading time” was sampled from a cumulative distribution function constructed from a multiplicative cascade, and this variable was then used as the time parameter in Brownian motion. The result was a time series exhibiting heavy tails in returns, long memory that decays as a power law, and volatility clustering.

MMAR is multifractal because fluctuations of the time series it generates scale not as one power law, but as a spectrum of power laws. In geometric terms, this means the time series exhibits a spectrum of Hölder exponents that are related to the fractal dimension of an object, and the points in time that support a given Hölder exponent constitute a fractal set. Mandelbrot was aware that most multifractals have a dominant dimension, and thus a histogram of the relative frequencies of these exponents would collapse into a single spike in the limit. He therefore defined the *multifractal spectrum* (sometimes called the *singularity spectrum*) as the renormalized probability density function of the Hölder exponents, $f(\alpha)$ [58]. This multifractal spectrum defines the stochastic fractal construction of multifractal data. As Calvet and Fisher noted [13], the multifractal spectrum identifies “events that happen many times in the construction but at a vanishing frequency.”

On a different side of economic research, other early assumptions were being questioned. The theory of market participants behaving rationally, that is in the manner of greatest expected profit to themselves, was being challenged by empirical observation as well. In 1979, Kahneman and Tversky published their seminal paper on prospect theory [40]. They directly challenged the precepts of expected utility theory and supported their claims with psychological experiments where subjects had to make decisions in situations involving risk. Their work upended expected utility theory and arguably led to a new approach to economics known as *behavioral economics*. As a result, economists began trying to model different behaviors of market participants on a microlevel to analyze the effects on the market economy at large.

Keeping pace with these changes, the field of computer simulation has experienced its own evolution. The traditional approach for modeling systems with a large number of stochastic variables has been discrete-event simulation (DES). In DES models, the state variables are updated only at points in time

when an event impacts their status. As the availability of computing power and data storage capacity have increased, however, the concept of agent-based modeling has become more appealing [62].

The difference between these two approaches comes down to their focus, but in general DES is the natural precursor to agent-based modeling. DES models focus on the processes of a system — that is, the sequence of events “seen” by homogeneous agents (called “entities” in DES) as those agents move through the system and are impacted by the events. Agent-based models in contrast focus on the agents, allowing them a degree of influence over which events they experience. As such, the agents’ reactions to system events are heterogeneous, and the impact of microlevel behaviors on macrolevel system output can be analyzed. This difference appears subtle at first, especially given the power of current DES software to specify vectors of attributes for the entities. However, according to North and Macal in order to qualify as an agent-based simulation rather than DES, the agents must [62]:

- be able to adapt within their current situation;
- be capable of modifying their future behavior based on their past experiences;
- be autonomous; and
- be heterogeneous.

Given the level of “intelligence” possessed by the agents, agent-based models are well suited for modeling systems consisting of people or organizations that make individual decisions based on their view of the available information. As such, many social networks and systems are being increasingly modeled with agent-based techniques. Economics, in particular, has adopted agent-based modeling to test theories of behavioral economics, the formation of prices under uncertainty, and the impact of market structure on market participants and their actions [74].

The agents in agent-based modeling differ from entities in discrete event modeling by possessing their own internal logic that enables them to learn and update their decision thresholds based on their experiences in the simulation. Thus, even a set of agents starting out with the same logic will ultimately experience different events within the random simulation and therefore evolve into heterogeneous virtual beings. One can think of this learning process as the elimination of some behaviors and the adoption of others. Those behaviors that are eliminated obviously contribute to the construction of the simulated environment, and thus its output, but do so at a vanishing frequency.

Already there is evidence that agent-based models get closer to modeling the true or observed behavior in markets. Agent-based models exhibit emergent behaviors, defined by North and Macal as “system reactions where the complete results are more than the sum of the individual components’ results.” These behaviors have been linked to non-Gaussian interaction metrics [16] and singularities in the time series they generate. Farmer et al. have modeled financial markets that exhibit volatility clustering and heavy-tailed returns [26] simply due to the rules for trading in a double auction order book.

Though agent-based simulation has provided a number of insights into how complex systems arise, the problem of validating these models against empirical observation remains. They are often used to isolate a single behavior (or a small set of behaviors) in the hopes that this will provide some intuitive sense of what goes on in real systems. Similarly the concept of a multifractal spectrum encapsulating the stochastic properties of a multifractal construction has mostly been applied to simulated time series with a closed-form multifractal spectrum. The theoretical results are then compared to the simulated results, but applications to actual observed data are limited.

In this dissertation we present a robust tool for extracting the multifractal spectrum from a time series that implements the multifractal detrended fluctuation analysis (MF-DFA) algorithm. Some aspects of MF-DFA are enhanced with guidelines for parameter choice, and software for performing MF-DFA in a timely manner is described. We test the software on simulated data with closed-form multifractal (and monofractal) spectra to ensure the statistical accuracy of our program. We discuss the interpretation of the multifractal spectrum in the context of time series data and illustrate its practical utility in financial analysis. We then employ MF-DFA on fine scale New York Stock Exchange data and present an in-depth analysis of the results. Next we present an agent-based financial market model and analyze its output with MF-DFA. We expand our prototype zero-intelligence, single-asset financial market to include intelligent traders and a risk-free asset to study the effects of microlevel agent behaviors on the macrolevel time series output as analyzed by MF-DFA. Finally, we illustrate the potential for validating agent-based models using MF-DFA and thus being able to “tune” the agent-based simulation to the multifractal spectrum of empirical data. This process involves first analyzing the degree of multifractality due to long-range correlation rather than a heavy-tailed distribution in the price movements, and then ensuring the agents possess a behavioral structure that imitates or otherwise generates this degree of sequential time dependence.

The rest of this dissertation is organized as follows. In Chapter 2 we introduce the concept of fractals and multifractals in the context of time series analysis. We discuss the mathematical background of the multifractal spectrum and review some of the methods for its extraction. We present multifractal detrended fluctuation analysis and its advantages and shortcomings. We also describe the software we developed to implement this analysis, and give results of its performance on simulated data. In Chapter 3 we perform an in-depth time series analysis on fine-scale data from the New York Stock Exchange. We start with standard time series techniques, such as ARMA and GARCH, and compare those results with multifractal analysis. In Chapter 4 we discuss agent-based simulation. In particular, we focus on the application of agent-based models in economics and their ability to model behaviors on a microlevel while producing a macrolevel output. We also discuss the software available to implement agent-based models and the reasoning behind our selection of MASON as the software platform used to build our agent-based models of financial markets [65]. We close the chapter with a presentation of our zero-intelligence financial market model to include a review of the simulation results and the multifractal spectra they generate. In Chapter 5 we expand the zero-intelligence model to incorporate positive-intelligence traders,

and compare and contrast the simulation results with those of the zero-intelligence model, as well as the empirical data from Chapter 3. We conclude in Chapter 6 with a discussion of results and possible avenues of future research built on this work.

Chapter 2

Multifractal Analysis

2.1 Introduction

2.1.1 Fractals

In order to discuss multifractal analysis, some preliminary discussion of fractals in general is warranted. The definition of a fractal is somewhat ambiguous. Mandelbrot originally defined fractals as objects whose Hausdorff dimension strictly exceeds their topological dimension [57]. Other researchers, such as Addison, used a more general definition: fractals are objects which appear self-similar under varying degrees of magnification — that is, each small part of the object resembles the whole in some way [5]. In general, it is the Hausdorff dimension of an object deviating from the object’s topological dimension that mathematically defines a fractal. The literature is rich with examples of fractals, some naturally occurring and others mathematical creations, that could be studied from all manner of perspectives. However, this dissertation is concerned primarily with measuring or quantifying empirical data. We will therefore restrict our discussion of fractals to their application in measuring exceedingly rough objects and time series data. For an excellent introduction to fractals, see Addison’s *Fractals and Chaos* [5].

From the perspective of measuring or quantifying an object, let us first consider an object in Euclidean space with a known measure and known topological dimension — namely, the unit square in two-dimensional Euclidean space, \mathbb{R}^2 . The square is two-dimensional and has area (two-dimensional Lebesgue measure) one. One way to measure such an object is to cover it with sufficiently “small” neighborhoods in \mathbb{R}^2 that have known areas and then sum up the areas of the small neighborhoods required to cover the whole object. To start, we could cover the square with another square having side of length $r = 1$. This would exactly cover the unit square, so our sum total of covering squares, $N(r)$, would be one. We can then calculate the area of the unit square as the area of our basic neighborhood times the number of neighborhoods required: $A = r^2 N(r) = 1$. Alternatively we may use a basic neighborhood having side of length $r = \frac{1}{2}$. In this case, $N(r) = 4$ and thus the area can be measured as $A = r^2 N(r) = (\frac{1}{4})4$. As

we continue in this manner, a pattern becomes obvious (see Table 2.1).

Table 2.1: Scale vs Coverings

$\frac{1}{r}$	$N(r)$
1	1
2	4
4	16
8	64
16	256
...	...
$\frac{1}{r}$	$(\frac{1}{r})^2$

Since the number of required neighborhoods increases by a power of 2 as our scale decreases, we say that the unit square is two-dimensional. We could perform the same analysis for a line or a cube, and we would discover a power law relationship exists for those objects as well. A line scales with exponent 1 and a cube with exponent 3, which is in accordance with our intuition about these objects. Said another way, length follows the power law $L = Cr^{1-D}$, where C is a positive constant and $D = 1$. Volume follows the power law $V = Cr^{3-D}$, where $D = 3$. In practice, the true measure of the object is taken to be the limit as $r \rightarrow 0$. For more complex, nonfractal shapes, the initial measure may differ substantially from the limit, but the convergence to the true measure is guaranteed. In these cases, D is called the topological dimension.

A well-known application of fractals is Mandelbrot's quantification of the coast line of Great Britain [55]. In actuality, Mandelbrot clarified the work of Lewis Fry Richardson and showed it could be used to measure the length of exceedingly rough objects. Richardson had plotted various measurements of various coastlines in relation to the scale r of the measuring device. He found that as the scale r of the measuring device got shorter, the measured length got longer and vice versa. He also showed that this relationship was linear on doubly-logarithmic plots. That is the length, L , followed a power law relationship,

$$L = Cr^{1-D}. \quad (2.1)$$

Given our earlier example, this hardly seems surprising. What was interesting about Richardson's graph — and what Mandelbrot built an entirely new approach to geometry upon — was that Richardson's value of D for Great Britain was roughly 1.25. In fact, Richardson plotted multiple countries' boundary measurements in this way, and none of them produced an integer value for D . We now observe our

previous iteration process breaks down because, in the limit as r approaches zero, L approaches infinity.

Mathematicians have since rigorously proven these relationships and confirmed that the Hausdorff dimension of fractal objects strictly exceeds their topological dimension. This presents us with an issue: the length of the coast of Britain depends on the size of the ruler used to measure the coastline. But in practical terms, this is by no means a problem. If, for example, we want to build a fence around Britain with fence posts 500 meters apart ($r = 0.5$ km), then we would measure the coast to be 7,332 km long. If instead we wanted to line the coast with, say, guard stations 1000 meters apart ($r = 1.0$ km), then we would measure the coast as 6,165 km long. In both cases we would get the “right” answer. That is, as our ruler increases, the measured length decreases because we skip over more and more of the rough nature of the coastline. The real problem arises as our scale (i.e., ruler length) becomes ever smaller. The length of the coastline will diverge to infinity.

The net result for the practitioner is the dimension of an object is now a critical value to have in order to obtain accurate measurements. And our notion of objects being quantified by a single length, area, or volume must also be reevaluated. Geometric objects (and as we shall see, times series) must be quantified with scale-dependent functions of their dimension rather than scalar values. As our ability to measure these objects reaches finer and finer scales, we must relinquish our traditional notion of measure (as it will diverge) and rely more heavily on the fractal dimension itself for quantification.

2.2 Fractal Times Series

2.2.1 The Hurst Exponent and Fractional Brownian Motion

In addition to being too rough for traditional geometry, fractals are self-similar. The increments of a random function $\{X(t) : -\infty < t < \infty\}$ are said to be self-similar with parameter $H \geq 0$ if for any $c > 0$ and t ,

$$X(t + s) - X(t) \stackrel{d}{=} c^{-H} [X(t + cs) - X(t)], \quad (2.2)$$

where the d over the equals sign indicates equal in distribution [61]. Though Mandelbrot pioneered the study of fractals, the presence of self-similarity in certain time series was studied much earlier. A notable study was conducted by Harold Edwin Hurst, who was tasked with constructing levees of suitable height to contain the seemingly unpredictable floods of the Nile river. Since Hurst’s focus was on the maximum and minimum levels of the river, he introduced a new statistic known today as the rescaled range. The rescaled range can be described as the displacement analyzed over different sized time intervals. Formally, for a given set of observations $\{X_i : i \geq 1\}$ that have the partial sum $Y(n) = \sum_{i=1}^n X_i$ for $n \geq 1$ and sample variance $S^2(n) = n^{-1} \sum_{i=1}^n (X_i - n^{-1} Y(n))^2$ for $n \geq 1$, the rescaled range statistic is

$$\frac{R(n)}{S(n)} = \frac{1}{S(n)} \left[\max_{0 \leq t \leq n} \left(Y(t) - \frac{t}{n} Y(n) \right) - \min_{0 \leq t \leq n} \left(Y(t) - \frac{t}{n} Y(n) \right) \right] \text{ for } n \geq 1. \quad (2.3)$$

Hurst found that the Nile flood levels analyzed over different time intervals were self-similar in that their rescaled range statistic exhibited the asymptotic relationship

$$E \left[\frac{R(n)}{S(n)} \right] \sim C n^H \text{ as } n \rightarrow \infty, \quad (2.4)$$

where C is a finite positive constant independent of n and $0 \leq H \leq 1$ [76]. Statisticians of Hurst's day were familiar with stationary models exhibiting sequential ranges asymptotically proportional to the square root of the length n of the observed process (i.e. $H = 0.5$), but Hurst's empirical analysis found the exponent to be $0.5 < H < 1$. Mandelbrot and van Ness later analyzed these relationships as they pertain to time series analysis and showed that the Hurst exponent was integral to the autocorrelation function of the time series. Values of H between 0.5 and 1.0 lead to positive autocorrelation in the increments that decay too slowly for the sum of autocorrelation over all lags to be finite. That is, processes with $0.5 < H < 1$ are long-memory processes, whereas processes with $0 \leq H \leq 0.5$ are said to exhibit short-range dependence [61]. The Hurst exponent also quantifies the inherent roughness exhibited by fractals. It can be shown that the fractal dimension D of the graph of a monofractal time series is related to the Hurst exponent of the underlying process by the relation $H = 2 - D$ [34].

A well-known fractal process exhibiting these properties is Brownian motion. Brownian motion was originally described as the path of a molecule or particle suspended in a fluid, but has been adapted to describe highly irregular time series. Formally, Brownian motion can be described as a continuous time, continuous-state-space Markov process $\{X(t) : t > 0\}$ with variance parameter σ^2 if it has the following properties:

1. For all times t and $s + t$ with $s, t \geq 0$, the increment $X(t + s) - X(t)$ is normally distributed with mean 0 and variance $\sigma^2 s$.
2. For every pair of disjoint time intervals $[t_1, t_2], [t_3, t_4]$, where $t_1 < t_2 \leq t_3 < t_4$, the increments $X(t_2) - X(t_1)$ and $X(t_4) - X(t_3)$ are independent normal random variables with variances $\sigma^2(t_2 - t_1)$ and $\sigma^2(t_4 - t_3)$, respectively.
3. $X(0) = 0$ and $X(t)$ is continuous at $t = 0$.

In addition to the defining properties above, Brownian motion is also known to be self-similar. That is, if we consider pairs of points on the graph of a realization of Brownian motion, then the average magnitude of the vertical displacement between these points is proportional to the magnitude of the

corresponding difference in time raised to the power H [5]. Every sample path of Brownian motion is also known to be continuous and yet nowhere differentiable. So, although we may think of the path of standard Brownian motion (Figure 2.1) as one-dimensional, its roughness is such that it has fractal (Hausdorff) dimension $D = 1.5$ and Hurst exponent $H = 2 - D = 0.5$ [25]. In the context of our earlier example if we were to attempt to measure the length of the path of Brownian motion we would find that $Cr^{1-1.5} = Cr^{-0.5}$, which diverges as $r \rightarrow 0$.

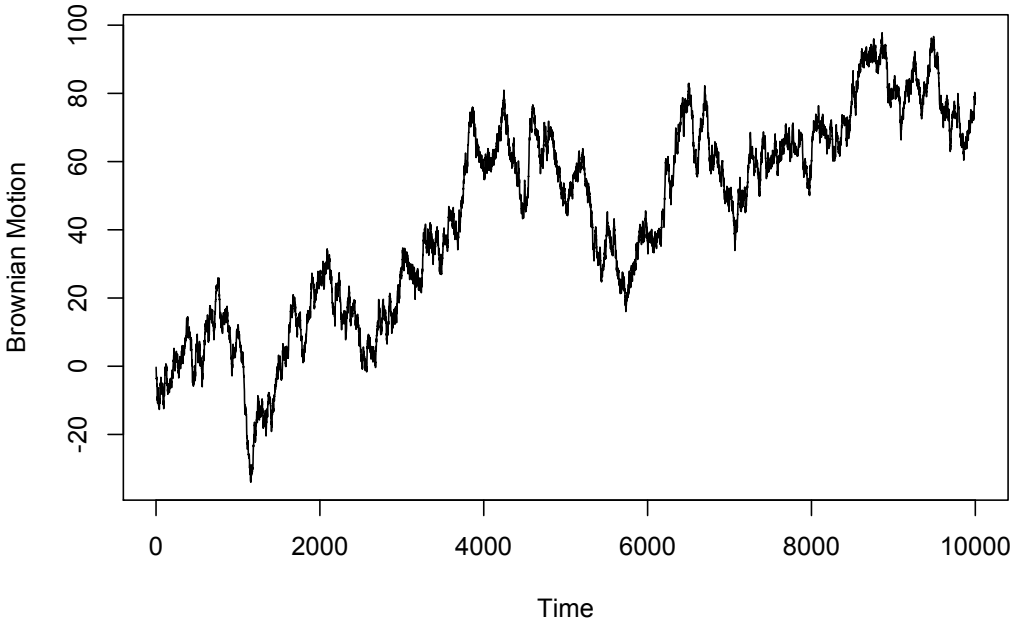


Figure 2.1: An approximation of Brownian motion with 10,000 points

Fractional Brownian motion is the generalization of the concept of standard Brownian motion in that H is no longer restricted to the value 0.5. Different values of H result in time series that are either more or less rough than standard Brownian motion. It can also be shown that H determines the autocorrelation structure of the time series. When $0 < H \leq 0.5$ the series exhibits short-range dependence and has an antipersistent (i.e., rougher) path, while a series with $0.5 < H < 1$ possesses long-range dependence and exhibits a persistent (i.e., smoother) path. The difference in roughness is illustrated in the Figure 2.2. More details on this connection between H and autocorrelation are included in Section 2.5.3.

In the next section we expand on this concept to discuss time series that continue to scale according

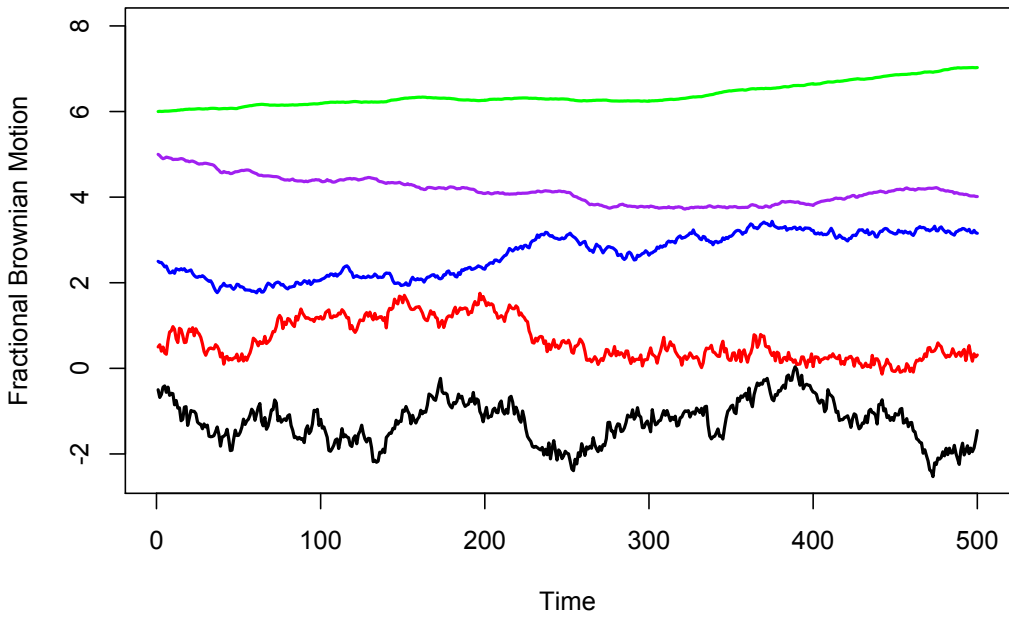


Figure 2.2: Fractional Brownian motion for different values H . From top to bottom $H = 0.8$, $H = 0.7$, $H = 0.5$, $H = 0.3$, and $H = 0.2$

to a power law, but the Hurst exponent is further generalized to be a function $h(q)$. The argument q can take on any real value and functions as a filter for different magnitudes of fluctuation within the series. If different magnitudes of fluctuation are q -dependent, then the series is multifractal rather than monofractal.

2.2.2 The Hölder Exponent and The Multifractal Formalism

Fractals are often introduced in the context of geometric objects; ferns, coastlines, and mathematical creations such as Koch curves. But as we expand our discussion to multifractals, it is convenient to restrict our examples to time series data, as the complexity of a multifractal object would be difficult to visualize.

As noted previously, one way to define a fractal is to say that its Hausdorff measure scales according to a power law — that is, if a fractal object of Hausdorff dimension D is reduced in size by the scale factor $r \in (0, 1)$, then the Hausdorff measure of the reduced object is equal to r^D times the Hausdorff measure of the original object. In the case of a fractal time series, this relationship is captured by the Hurst exponent H . In the case of a monofractal time series, every increment in the time series scales with the same H . A multifractal time series can be defined in a similar way, except the exponent H is no longer a single scalar value, but rather a function of Hölder exponents that vary within the time series. The Hölder exponents are related to a generalized Hurst exponent $h(q)$ — that varies with different order moments q — through the multifractal formalism. The difference between these two descriptive power laws is subtle, but in general the Hurst exponent is a global quantity, while the Hölder exponent is a local quantity [67]. Formally, for some stochastic process $\theta(t)$ with support $[0, T]$, we define the Hölder exponent $\alpha(t)$ at each time $t \in [0, T]$ by the asymptotic relationship

$$\theta(t + s) - \theta(t) = O_p(s^{\alpha(t)}) \text{ for all } t \text{ as } s \rightarrow 0, \quad (2.5)$$

where

$$\alpha(t) = \sup \{ \beta \geq 0 : \theta(t + s) - \theta(t) = O_p(|s|^\beta) \text{ as } s \rightarrow 0 \} \quad (2.6)$$

and in general for continuous-time stochastic processes $\{A(s) : s \in \mathbb{R}\}$ and $\{B(s) : s \in \mathbb{R}\}$, the “big-oh-sub- P ” notation $A(s) = O_P[B(s)]$ as $s \rightarrow 0$ means that given an arbitrarily small $\zeta > 0$, there is a constant $M = M(\zeta)$ and a positive number $\varepsilon = \varepsilon(\zeta)$ such that $\Pr\{|A(s)| \leq M|B(s)|\} \geq 1 - \zeta$ for $|s| < \varepsilon$.

One way to think of a multifractal is as the union of an infinite number of monofractals, each characterized by a single self-similarity exponent α . If for a fixed $q \in \mathbb{R}^1$ we define the set of points

$$\mathcal{T}_q = \left\{ t : \alpha(t) = h(q) + q \frac{dh(q)}{dq} \right\} \quad (2.7)$$

as explained in full detail in Equations (2.9) – (2.13) below, and if we let $\alpha = \alpha_q$ denote the common value of the Hölder exponent $\alpha(t)$ for all $t \in \mathcal{T}_q$, then the multifractal spectrum $f(\alpha)$ evaluated at $\alpha = \alpha_q$ is defined to be the Hausdorff dimension of the set \mathcal{T}_q . These sets are not subintervals in the support

interval $[0, T]$, but are interwoven throughout the interval [58]. As Calvet and Fisher [13] noted, these localized Hölder exponents contribute to the construction of a multifractal time series, but do so at a vanishing frequency. Hence, they never achieve the global property characterized by a Hurst exponent. Although he cited this definition of $f(\alpha)$ as a fractal dimension, Mandelbrot took exception to it, claiming it added a level of “mystery” to the multifractal spectrum $f(\alpha)$ that was unwarranted. The function $f(\alpha)$ can be described in terms familiar to probabilists and engineers and is not a new concept.

Consider a time series $\{\theta(t) : t \in [0, T]\}$ that is multifractal. We can divide the support $[0, T]$ of this process into b^k subintervals, resulting in smaller and smaller increments ($\Delta_k t = T/b^k$) as k approaches infinity, where b is a positive integer greater than one. For each segment, we can then derive the Hölder exponent $\alpha_k(t)$ for each subinterval of the form $[t, t + \Delta_k t]$, where t is a multiple of $\Delta_k t$. Constructing a histogram of the set of observed values of $\alpha_k(t)$, we can infer a probability density, p_k , for the set of Hölder exponents. The density would unfortunately collapse into a single (uninteresting) spike as the dominant Hölder exponent would overshadow all the others. As such, Mandelbrot defined $\rho(\alpha)$ to represent the “renormalized” density of the set $\{\alpha_k(t)\}$ as k approaches infinity. Formally,

$$\rho(\alpha) = -\lim_{k \rightarrow \infty} \frac{\ln p_k(\alpha)}{\ln \Delta_k t}. \quad (2.8)$$

In the special case where $\rho(\alpha) \geq -1$ for all α , we have $f(\alpha) = \rho(\alpha) + 1$ [58]. Recall from our discussion of fractals that the Hausdorff dimension is the best quantification of a fractal object because our traditional concepts of measure will diverge as our measuring device becomes more accurate. Thus, by evaluating the multifractal spectrum $f(\alpha)$ at the point $\alpha = \alpha_q$ associated with the set \mathcal{T}_q of time values for every $q \in \mathbb{R}^1$, we obtain a comprehensive quantification of the local scaling properties of the underlying stochastic process $\{\theta(t) : t \in [0, T]\}$.

Working with $f(\alpha)$ instead of $\rho(\alpha)$ leads to some convenient relationships. To reveal the full significance of these relationships, we must formally define a multifractal stochastic process.

Definition. A stochastic process $\{X(t) : t \in [0, T]\}$ is *multifractal* if it has stationary increments and satisfies

$$E[|X(t)|^q] = c(q)t^{\tau(q)+1} \text{ for all } t \in [0, T], q \in \mathcal{Q}, \quad (2.9)$$

where $T > 0$ and $[0, 1] \subseteq \mathcal{Q}$. The function $\tau(q)$ is called the *scaling function* of the multifractal process [13].

The scaling function is concave (see Proposition 1 of [13]); moreover the multifractal spectrum $f(\alpha)$ of a multifractal stochastic process $\{X(t) : t \in [0, T]\}$ with scaling function $\tau(q)$ for $q \in \mathbb{R}^1$ is given by

$$f(\alpha) = \min_q \{q\alpha - \tau(q)\}, \quad (2.10)$$

which is the Legendre transform of $\tau(q)$ [13]. It can be shown (see Section 2.4.2) that $\tau(q)$ is related to the generalized Hurst exponent, $h(q)$, by

$$\tau(q) = qh(q) - 1 \text{ for } q \in \mathbb{R}^1. \quad (2.11)$$

Let q_0 denote the unique solution of the optimization condition

$$\frac{d}{dq} \left\{ q\alpha - \tau(q) \right\} = 0, \quad (2.12)$$

which is equivalent to

$$\alpha = \alpha_{q_0} = \left. \frac{d\tau(q)}{dq} \right|_{q=q_0}, \quad (2.13)$$

where as usual $\alpha = \alpha_{q_0}$ denotes the common value of the Hölder exponent $\alpha(t)$ for all $t \in \mathcal{T}_{q_0}$.

The function $f(\alpha)$ is the multifractal spectrum, and it stochastically quantifies a multifractal. In general, the multifractal spectrum gives us two important quantifications of a time series: (i) the set of Hölder exponents, $\alpha(t)$, that define how the series scales as we measure on finer intervals; and (ii) the fractal dimension, $f(\alpha)$, of the set of points in time that scale with a particular exponent α . Although $f(\alpha)$ is not a proper probability density, in this renormalization it represents the relative concentration of points in time that exhibit a scaling exponent α . The multifractal spectrum is convex and peaks at the expected value of $\alpha(t)$. If a function is monofractal, like Brownian motion, it has a single exponent defining how it scales for all increments of time and thus its multifractal spectrum is a single point at $\alpha = H$ with $f(\alpha) = 1$. Thus, in the case of standard Brownian motion, we have $f(0.5) = 1$ because standard Brownian motion has Hölder exponent $\alpha(t) = 0.5$ for all $t \geq 0$. That is, the Hölder exponent is the same as the Hurst exponent. This observation naturally raises the question: “For a stochastic process with self-similar increments, what is the relationship between the Hurst exponent and the Hölder exponent for the process?” Combining Equations (2.11) and (2.13), we see that

$$\begin{aligned}
\alpha_{q_0} &= \frac{d}{dq}(qh(q) - 1)|_{q=q_0} \\
&= h(q_0) + q_0 \left(\frac{d}{dq}h(q)|_{q=q_0} \right) \\
&= h(q_0) + q_0 h'(q_0)
\end{aligned} \tag{2.14}$$

and therefore the Hausdorff dimension of the set $\mathcal{T}_{q_0} = \{t : \alpha(t) = \alpha_{q_0}\}$ is

$$\begin{aligned}
f(\alpha_{q_0}) &= q_0 \alpha_{q_0} - \tau(q_0) \\
&= q_0 \alpha_{q_0} - (q_0 h(q_0) - 1) \\
&= q_0^2 h'(q_0) + 1.
\end{aligned} \tag{2.15}$$

Thus we note that when the generalized Hurst exponent $h(q)$ is just a constant H and does not vary with q , then $h'(q_0) = 0$ and $f(\alpha_{q_0}) = 1$, indicating that $\mathcal{T}_{q_0} = [0, T]$. So for monofractal time series, the Hurst exponent equals the Hölder exponent and all points in the support $[0, T]$ exhibit the same self-similarity property. Conversely, a stochastic process with self-similar increments and a constant Hurst exponent H also has a constant Hölder exponent α , and $H = \alpha$.

These various interpretations are collectively referred to as the multifractal formalism and lead to our intuition of the multifractal spectrum. They also lead to methods for extracting the spectrum from empirical data. However, it should be noted here that $f(\alpha)$ cannot always be interpreted as a Hausdorff dimension. It is possible for the renormalized probability density ($\rho(\alpha)$) to yield values less than -1 and thus yield $f(\alpha) < 0$. This leads to a self-contradiction if we always interpret $f(\alpha)$ to be the Hausdorff dimension of the set of points supporting α [15]. But $f(\alpha)$ always stochastically quantifies the multifractal properties of a given time series. As we adapt these concepts to time series analysis, our focus will be to determine the source of the multifractality and thus facilitate standard analysis such as the probability of extreme events and risk estimation. With this in mind, the multifractal formalism is often mentioned in the context of large deviation theory. Since $\rho(\alpha)$ represents a renormalized probability density of Hölder exponents and as previously illustrated $f(\alpha)$ is in fact a differential equation of the scaling function, one can think of $f(\alpha)$ as the rate at which the probability of observing a deviant value of α is decreasing [66]. That is, for higher values of $f(\alpha_q)$ the sample mean for α_q is converging more quickly to the true mean than for lower values $f(\alpha_q)$.

2.3 Multifractal Analysis Background and Literature Review

Analyzing time series data is increasingly critical to modern science. As computers and computing power have increased, so have the volumes of data available. In traditional statistics, each observation is assumed to be independent and identically distributed; and yet collecting successive observations over time introduces an obvious correlation in many applications [71]. Dealing with these correlations has led to autoregressive moving average techniques introduced by Box and Jenkins [10], frequency domain analysis involving the power spectrum [8], Engle's ARCH models of nonconstant variance [21], and stochastic volatility models [36]. Each of these models is focused on bringing the data into a form that can be handled by traditional statistics. If trends and long-term autocorrelation can be identified through these techniques, then these anomalies can be systematically removed so that we are left with stationary observations. At that point, tractable, proven analysis can be performed and the standard confidence intervals and forecasts can be calculated. But as the systems analyzed have become more complex, involving a greater number of random variables interacting at increasing frequency, our models too have required added complexity to the point that trying to reduce the data to stationarity becomes overwhelming. Financial data, in particular, has been argued to possess long-term correlation in returns that manifests as volatility clustering, as well as dramatic day-to-day swings that depart notably from normality. The stock market crash of 1929 and the sudden drop of the Dow Jones in 1987 are both examples of deviations so far from the average as to completely invalidate any hypothesis that a thin-tailed distribution describing these observations is at work [60].

Handling short-term memory in time series is typically addressed by autoregressive techniques. In a typical time series analysis, one postulates the current value of a process, X_t , may have linear dependence on past values of the process, $X_{t-1}, X_{t-2}, \dots, X_{t-p}$ out to some finite lag p . Thus the following autoregressive model of order p can be explored:

$$X_t = \mu_X + \sum_{i=1}^p \varphi_i (X_{t-i} - \mu_X) + \varepsilon_t, \quad (2.16)$$

where the $\{\varepsilon_t\}$ are considered to be i.i.d. random variables with mean zero and variance σ^2 , often called white noise. White noise is most commonly modeled as having a Gaussian distribution.

Another option to consider is modeling the current value X_t as a moving average of past values of the ε_t terms out to some finite lag q ,

$$X_t = \sum_{i=0}^q \theta_i \varepsilon_{t-i}, \text{ where } \theta_0 = 1, \quad (2.17)$$

and again the $\{\varepsilon_t\}$ are i.i.d. Gaussian random variables. In both cases, the researcher seeks the optimal parameters φ_i and θ_i (often employing the method of moments and the Yule-Walker equations [71]) that minimizes the error between predicted and observed points in the process. Going a step further, the two models can be combined into a mixed autoregressive–moving average (ARMA) model,

$$X_t = \mu_X + \sum_{i=1}^p \varphi_i (X_{t-i} - \mu_X) + \sum_{i=0}^q \theta_i \varepsilon_{t-i}, \quad (2.18)$$

which is usually referred to as an ARMA(p, q) process.

Since the ARMA model assumes a constant mean in the data, Box and Jenkins updated this approach with an integration or differencing operator [10]. If the data contain some relatively constant trend or drift, taking the difference (or series of differences) of the observed data points can transform the set into a stationary series. This creates a data set for which traditional statistics can be applied; and once the results are calculated, the inverse transformation gives predictions about the process.

For certain types of time series, this model and its variations are extremely effective, and hence they are widely used. The suggested technique for applying these models is to hold the variance constant and find the smallest values for p and q , i.e., short-term memory of past values and past randomness. Unfortunately financial data and other time series often exhibit periodic trends, long-term memory, and nonconstant variance. Employing these standard transformations on such a data set does not reduce the series to a process governed by Gaussian white noise; and as a result, the standard techniques are less reliable. One approach to handling periodic trends is to add a seasonal component to the ARMA model. The general concept is to condition the process on a periodic lag parameter d in addition to p and q . The obvious question then becomes how do we determine the appropriate periodic lag length d ? These issues in certain time series give rise to additional models and techniques.

For some time series, the trends are more complex than a simple constant drift. Time series data collected from processes that have a seasonal or otherwise repeating cycle will exhibit a never-ending sequence of peaks and valleys. Given that processes in general can be expressed as linear combinations of sines and cosines, a technique known as spectral analysis was developed to analyze these ongoing periodic fluctuations. This amounts to transforming the data from the time domain into the frequency domain, and Fourier transforms are the standard approach [8].

Shumway and Stoffer present spectral analysis in terms of the spectral density [71]. If $\{X_t : t = 1, 2, \dots\}$ is a covariance stationary process with mean μ_X and covariance function

$$\gamma(h) = \text{Cov}(X_t, X_{t+h}) = E[(X_t - \mu_X)(X_{t+h} - \mu_X)] \text{ for } h = 0, \pm 1, \pm 2, \dots, \quad (2.19)$$

and if $\sum_{h=-\infty}^{\infty} |\gamma(h)| < \infty$ (which is the condition for short-range dependence), then the spectral density

of the process, $f(\omega)$, can be represented as the Fourier transform pair:

$$f(\omega) = \sum_{h=-\infty}^{\infty} \gamma(h) e^{-2\pi i \omega h} \text{ for } -\frac{1}{2} \leq \omega \leq \frac{1}{2}, \text{ where } i = \sqrt{-1}, \quad (2.20)$$

and

$$\gamma(h) = \int_{-\frac{1}{2}}^{\frac{1}{2}} f(\omega) e^{2\pi i \omega h} d\omega \text{ for } h = 0, \pm 1, \pm 2, \dots . \quad (2.21)$$

Plotting the spectral density, $f(\omega)$, against ω illustrates which frequencies (expressed in cycles per unit time) are present in the process $\{X_t\}$. For example, many businesses operate on a cycle of length 3 months (i.e., on a quarterly basis) so that the spectral density of their stock might peak at a frequency of $\omega = 1/3$ cycles per month. Many types of weather data, on the other hand, exhibit a cyclic effect with a cycle length of 12 months so that the associated spectral density has a peak at the frequency $\omega = 1/12$ cycles per month. Note the spectral density is a population-based concept rather than a sample-based concept. In practice the discrete Fourier transform is employed, but the approach is the same.

Spectral analysis enables us to extract the periodic effects in data that may cause it to deviate from stationarity. But again, the model is a linear function of sines and cosines, and we are back to the standard statistical techniques for estimating the parameters of that function. We have transformed the data into the frequency domain, but within that domain we seek transformations that lead to a stationary data set.

The issue of nonconstant variance is addressed by a family of models known as autoregressive conditionally heteroscedastic (ARCH) models introduced by Robert Engle [21]. The impetus for Engle's research was the empirical observation that certain times in financial history were observed to have been riskier than others, i.e., the magnitude of returns was substantially larger than the recent past suggested they would be. Moreover, these periods of increased risk seemed to occur in clusters in that large fluctuations were quickly followed by similarly large fluctuations (not necessarily in the same direction). A direct result was that forecasts based on such a time series varied wildly at different points in time. The basic outline for ARCH(p) models is defined below.

If the latest observation X_t of the designated process at time $t > p$ is conditioned on the information $\psi_{t-1} = \{X_u - \mu_u : u = 1, 2, \dots, t-1\}$ available up to time $t-1$, then

$$X_t | \psi_{t-1} \sim N(\mu_t, \sigma_t^2), \quad (2.22)$$

where

$$\sigma_t^2 = h(\varepsilon_{t-1}, \varepsilon_{t-2}, \dots, \varepsilon_{t-p}, \alpha) \quad (2.23)$$

and

$$\varepsilon_u = X_u - \mu_u \text{ for } u = 1, 2, \dots, t-1, \quad (2.24)$$

where the function $h()$ with parameters $\alpha = \{\alpha_k : k = 0, 1, \dots, p\}$ is defined as

$$h(\varepsilon_{t-1}, \varepsilon_{t-2}, \dots, \varepsilon_{t-p}, \alpha) = \alpha_0 + \sum_{k=1}^p \alpha_k \varepsilon_{t-k}^2, \quad (2.25)$$

so that given the history $\{X_u - \mu_u : u = 1, 2, \dots, t-1\}$ of the process up to time $t-1$, the conditional distribution of X_t is normal with mean μ_t and variance

$$\sigma_t^2 = \alpha_0 + \sum_{k=1}^p \alpha_k (X_{t-k} - \mu_{t-k})^2. \quad (2.26)$$

Note that from Equation 2.26 and the variance decomposition formula, it follows that the unconditional variance of X_t is given by

$$\text{var}[X_t] = \frac{\alpha_0}{1 - \sum_{k=1}^p \alpha_k}; \quad (2.27)$$

thus the unconditional marginal variance is constant in the ARCH models. As such, the intent is simply to account for the interim fluctuations, and one interpretation is that these models simply behave the way we need them to rather than giving insight into the true operations underlying the process [21]. Nonetheless, these models are effective at decreasing the error in forecasts of processes that exhibit volatility clustering because the conditional variance is constantly updated to reflect recent trends.

Because of the changes in the conditional variance, ARCH models successfully recreate the empirical observation of volatility clustering, but still fail to imitate the heavy tails in returns. Attempts have been made to adapt ARCH processes using heavy-tailed distributions, but earlier work had addressed the issue of heavy tails directly. In 1963, Mandelbrot published a widely cited article on the analysis of heavy-tailed returns in the cotton commodities market [54]. Building on the work of Paul Lévy, he presented the *stable Paretian* distribution as the underlying distribution of price changes rather than the Gaussian distribution. Stable distributions are defined by the property that summing any two random variables governed by

the same stable distribution results in a random variable that is also governed by that same distribution though perhaps differing in scale or location, i.e., stability implies stable under addition.

Formally, a random variable X is stable if for independent copies of itself, say X_1 and X_2 , the following equation holds:

$$a_1 X_1 + a_2 X_2 \stackrel{d}{=} bX + c, \quad (2.28)$$

where a_1 , a_2 , and b are positive constants, c is an appropriate real constant, and the notation $\stackrel{d}{=}$ denotes equivalence in distribution. The Gaussian distribution is one such distribution, and this stability property is the backbone of the well-known central limit theorem. But Mandelbrot noted the Paretian distribution was the generalization of this property if the requirement of finite moments was relaxed. If U is a Paretian random variable with location parameter δ , scale parameter γ , “skewness” parameter β , and “peakedness” parameter α , then the cumulant generating function of U (i.e., the logarithm of the characteristic function of U) has the form

$$\psi(q) = \ln \{E[e^{iqU}]\} = i\delta q - \gamma|q|^\alpha [1 + i\beta \operatorname{sgn}(q)\Theta(q, \alpha)] \text{ for } -\infty < q < \infty, \quad (2.29)$$

where $i = \sqrt{-1}$,

$$\operatorname{sgn}(q) = \begin{cases} -1, & \text{if } q < 0, \\ 0, & \text{if } q = 0, \\ 1, & \text{if } q > 0, \end{cases} \quad (2.30)$$

and

$$\Theta(q, \alpha) = \begin{cases} \tan(\alpha\pi/2), & \text{if } \alpha \neq 1, \\ (2/\pi) \ln(|q|), & \text{if } \alpha = 1. \end{cases} \quad (2.31)$$

Note that at least in principle, the probability density function of U can be obtained from the inversion formula for characteristic functions,

$$f_U(u) = \frac{1}{2\pi} \int_{-\infty}^{\infty} \exp \{ -iuq + \psi(q) \} dq \text{ for } -\infty < u < \infty; \quad (2.32)$$

see Theorem 3 on page 277 of Gnedenko [31].

Mandelbrot showed that cotton prices from 1900 to 1950 were indeed stable under this distribution

and differed only by γ when examined at different time scales. He illustrated that under certain conditions, if s random variables from the Paretian distribution were added together, they would differ only by $\gamma = s^\alpha$. Although Mandelbrot's stated purpose in this research was simply to replace the Gaussian distribution in price variation models with a heavy-tailed distribution, the concept of examining power law behavior at different time scales combined with his later work in fractal geometry gave way to a new kind of measure altogether — namely, multifractal measures.

Much of the early multifractal research comes from the study of turbulence. Turbulence is known to be self-similar in that large eddies tend to give rise to smaller eddies until the kinetic energy is dissipated. One of Andrey Komolgorov's theories related the kinetic energy of eddies to their scale via a power law. Mandelbrot addressed some of the empirical contradictions of Komolgorov's theory and in so doing introduced the concept of multifractals [56]. The concepts were quickly adapted by mathematicians for general purposes, and the presence of multifractals in empirical observations continued to capture the interest of various practitioners in physics [30], biomedical fields [38], geology [75], and economics [6].

In a series of papers, Calvet, Fisher, and Mandelbrot introduced the multifractal model of asset returns (MMAR) as a direct replacement for the generalized ARCH (GARCH) models [13]. Building on the multifractal formalism presented earlier, MMAR represents a simple compound process that has a closed-form multifractal spectrum. Remarkably — given the authors note it is built on the simplest of assumptions — MMAR manages to produce volatility clustering, heavy tails, and long memory in returns.

Formally, if the price of an asset at time t is $P(t)$ for $t \in [0, T]$ and $T < \infty$, then the associated log-price process is given by

$$X(t) = \ln P(t) - \ln P(0) \text{ for } t \in [0, T]. \quad (2.33)$$

The log-price process is then modeled as a compound process

$$X(t) = B[\theta(t)] \text{ for } t \in [0, T], \quad (2.34)$$

where $B(t)$ is Brownian motion and $\theta(t)$ is a stochastic process termed *trading time*. Trading time is the cumulative distribution function (c.d.f.) of a random multifractal measure, and the processes $B(t)$ and $\theta(t)$ are assumed to be independent.

One commonly used approach is to construct $\theta(t)$ with a multiplicative cascade, where the distribution of the multipliers (or masses) in the cascade are generated from a known probability distribution. Different choices for the distribution of these multipliers result in different multifractal spectra for the compound process $X(t)$, some of which have closed-form expressions. Calvet and Fisher analyzed the Deutsche

mark/US dollar exchange rate and found that for a bounded range of time scales, the data exhibited a spectrum of Hölder exponents. Since the empirical spectrum was quadratic in shape, they chose a distribution for the multipliers in the multiplicative construction of $\theta(t)$ (the lognormal) that would combine with $B(t)$ to give a quadratic multifractal spectrum. Using the closed form, they could adjust the parameters until the spectra were roughly matched and then simulate a time series using these parameters combined with Monte Carlo techniques. They also produced simulated time series from GARCH and FIGARCH models and compared the scaling behavior of these simulated time series with the actual exchange rate series. Though all three produced volatility clustering, the MMAR better represented the multifractal nature of the empirical data. They also noted that the multifractal spectrum is quite sensitive to the “generating mechanism” of trading time. This means a wide variety of spectra can be constructed when searching for a suitable fit to empirical data.

Other works, particularly in the physics literature, have focused on discovering the source of multifractality in empirical data. This body of work started with simpler monofractals such as Brownian motion where the intent was to detect and quantify long-term linear correlation in a time series. Building on the work done in hydrology by Hurst, researchers set about trying to find the best methods for measuring and interpreting the rescaled range statistic and the resulting Hurst exponent, H (see for example [73] and [76]). One successful method for measuring H called detrended fluctuation analysis (DFA) was introduced by Peng et al. [64] in the context of DNA analysis. Using a coding scheme for DNA nucleotides, Peng et al. discovered long memory in the strains of DNA by measuring H . Extending this idea to multifractals, Kantelhardt et al. constructed example time series using either long-term correlated random variables governed by thin-tailed distributions or uncorrelated random variables using heavy-tailed distributions [42]. They found that heavy tails could generate a “bi fractal” time series exhibiting q -dependent generalized Hurst exponents $h(q)$ above a certain threshold value q^* , but a constant h below that threshold. Conversely, their examples built from long-term correlated random variables produced multifractals where $h(q)$ was q -dependent for all q . They concluded that multifractals could arise from either long memory, heavy-tailed distributions, or a combination of the two.

In order to distinguish between these two different sources of multifractality, Kantelhardt and others propose shuffling the increments of a time series randomly and comparing the multifractal properties of the shuffled series to those of the original series. Since multifractal analysis focuses on the scaling properties of fluctuations in the time series, the shuffling of increments will alter the sequential time-dependence of these fluctuations. If the fluctuations are correlated, then shuffling should change the resulting multifractal spectrum. On the other hand, if the increments are governed only by independent, identically distributed random variables from a heavy-tailed distribution, then shuffling should have no effect on the multifractal spectrum. That is, the relative frequency of large, small, positive, and negative increments in a given segment of time should not be changed by random shuffling if the increments are i.i.d. random variables. As a result, the average displacement at a given scale (over a large enough sample population) should remain unchanged. Kantelhardt et al. found this heuristic to accurately differentiate

between correlation and heavy tails in the simulated time series they constructed.

One possible practical application for this empirical result is the detection of nonlinear correlation in data sets. There are various ways of detecting linear correlation that are simpler than multifractal analysis. Monofractal analysis, for example, is considerably easier to implement because it assumes that only one exponent governs the scaling properties of the time series, the Hurst exponent. This is equivalent to only analyzing the generalized Hurst exponent at the value $q = 2$. If the resulting $h(2) = 0.5$, then the increments of the process are assumed to have zero linear correlation. But this is not to say that they are independent. It can be shown that nonlinear correlation fills the gap between zero linear correlation and independence [79]. But detecting and exploiting nonlinear correlation remains a difficult task. Bogachev et al. [9] performed multifractal analysis on financial time series exhibiting zero linear correlation, but were also believed to possess some degree of nonlinear correlation. Their study focused on extreme event probabilities in the data set, and thus differentiating between heavy-tails versus long-term correlation was critical. They showed analytically that nonlinear correlation in the original series could lead to linear correlation in the time intervals between extreme events. Then using simulated time series deliberately constructed to have zero linear correlation, but dependent increments, they confirmed (at least empirically) the shuffling procedure coupled with multifractal analysis would detect the nonlinear correlation. Applying these assumptions to real financial time series, they derived methods for improved risk estimation [9].

This presentation of various time series models may read like a progression towards a single model, but in practice all the above models should be considered. Different data exhibit different properties, and the careful practitioner should choose the correct tool for the job at hand. For example, Shumway and Stoffer [71] suggest analyzing both the autocorrelation function and the partial autocorrelation function when presented with data that may have autoregressive or moving average properties. They give a nice heuristic for choosing the appropriate model based on the behavior of these two functions, but the heuristic is limited to ARMA models and is not intended to be applied to data with, say, periodic trends. Similarly, when the data exhibit volatility clustering, a self-similar or self-affine structure, or heavy tails resulting in outliers more frequent than a Gaussian distribution would suggest, the idea that a multifractal process may govern the time series should be considered. This raises the issue of extracting the multifractal properties from a given time series.

Three techniques have been shown to be effective with varying degrees of accuracy. The first is a simple direct approach called the “method of moments” [28]. The basic algorithm is to partition the data values along the vertical axis in the interval from the minimum to the maximum values observed into bins of size s , and compute the q^{th} moment of the relative frequencies in each bin. This process is repeated for a range of q -values and s -values. If the doubly-logarithmic plot of these moments against the scale s is linear, then the generalized Hurst exponent $h(q)$ can be inferred and $\tau(q)$ can be extracted. Then iterating over possible values of α and finding the Legendre transform of $\tau(q)$ (ignoring negative values) yields an approximation of $f(\alpha)$. The method of moments has the advantage of being easy to program

and computationally fast. However, the statistical accuracy of the results leaves something to be desired.

The second approach is the wavelet transform modulus maxima (WTMM) method introduced by Mallat and Hwang [53]. The basic idea is to apply a wavelet transform to the data set and analyze the q^{th} moments of the local maxima of the transform. This process is repeated at different scales s , and the relationship between the q^{th} moments and s is analyzed again on doubly-logarithmic plots. If the resulting plots are linear, then $\tau(q)$ can be estimated. Employing the Legendre transform yields $f(\alpha)$.

The WTMM method leads to statistically significant results and has the added benefit of illustrating the time-location of the singularities. Where Fourier transforms show us only the frequency domain, wavelets allow us to visualize both the time and frequency domains simultaneously [12]. However, the price of this increased performance is computational complexity. First, the appropriate wavelet must be selected so that it is orthogonal to the trend in the data. Second, if the absolute value of the local maxima are close to zero, then they can disrupt the calculation of the moments. These small values must therefore be eliminated before finalizing the analysis [42]. Nonetheless, the WTMM method is one of the most widely used methods for finding the multifractal spectrum.

The third approach is multifractal detrended fluctuation analysis (MF-DFA) introduced by Kantelhardt et al. [42]. MF-DFA is a generalization of DFA originally introduced by Peng et al. [64]. As mentioned, the motivation behind DFA was to detect long-range correlations in strains of DNA, but it only analyzed the Hurst exponent at $q = 2$. The generalization to MF-DFA involves computing the Hurst exponent for a range of values q . When q is positive with a large magnitude (say between 5 and 10), the large fluctuations in the data will be accentuated and the small fluctuations will be diminished. Conversely, when q is negative with a large magnitude, the small fluctuations will be accentuated and the large fluctuations diminished. Thus, long memory in different size fluctuations (e.g. volatility clustering) can be detected.

The basic MF-DFA algorithm involves partitioning a cumulative sum of increments into segments of length s , fitting a polynomial to each segment, and then computing the average root mean square error of all the segments. This process is repeated for many values s , and the resulting averages are plotted against s in doubly-logarithmic scale. This is analogous to analyzing how the separation of points scales with time to derive the Hurst exponent. Iteratively applying this process to a range of q^{th} -root mean square error terms involving the residuals within each segment and plotting the results on doubly-logarithmic scale yields a function of power laws rather than a single value.

Kantelhardt et al. compared the multifractal spectra extracted using MF-DFA with those extracted with the WTMM method. The results slightly favored MF-DFA, and MF-DFA has the added benefit of being easy to implement and computationally fast. However, care must be taken in the implementation to avoid misleading results. In the next section we describe MF-DFA in much greater detail to include methods for parameter selection.

2.4 Multifractal Detrended Fluctuation Analysis

2.4.1 The Algorithm

The MF-DFA algorithm, as presented by Kantelhardt et al., has five steps, the first three of which are the same as DFA [42]. However, a critical distinction regarding the format of the data may eliminate the first step (see Section 2.4.2). In this formulation we also incorporate the final step of calculating $f(\alpha)$ from $\tau(q)$, for a total of six steps.

- *Step 1:* Ensure the data set $\{Y(n) : n = 1, \dots, N\}$ of length N is an “aggregated” data set as opposed to a “disaggregated” set. An example of a disaggregated set would be daily price increments (i.e., returns) of an asset, while an aggregated set would be the actual daily price (i.e., the accumulated daily price increments). If the data is a disaggregated set, then we must convert it to an aggregated set via a cumulative sum

$$Y(n) = \sum_{k=1}^n (x_k - \bar{x}) \text{ for } n = 1, \dots, N, \quad (2.35)$$

where x_k denotes the k^{th} individual observation of the designated process and $\bar{x} = (1/N) \sum_{k=1}^N x_k$ denotes the sample mean of the process.

- *Step 2:* For a given positive integer s such that $20 \leq s \leq N/10$, divide the aggregated data set $\{Y(n) : n = 1, \dots, N\}$ into $N_s = \lfloor N/s \rfloor$ nonoverlapping segments of length s . Since N may not be a multiple of s , repeat the procedure starting at the other end of the data set. Creating $2N_s$ segments ensures every data point is considered.
- *Step 3:* For $v = 1, \dots, N_s$, the v^{th} segment of the observed cumulative sum values consists of the subseries $\{Y[(v-1)s + i] : i = 1, \dots, s\}$; similarly for $v = N_s + 1, \dots, 2N_s$, the v^{th} segment consists of the subseries $\{Y[N - (v - N_s)s + i] : i = 1, \dots, s\}$. For the v^{th} segment ($v = 1, \dots, 2N_s$) and a predetermined value of m , fit a degree- m polynomial $y_v(i)$ to the observed cumulative sum values in that segment. Calculate the maximum likelihood estimator of the corresponding residual variance in segment v ,

$$F^2(v, s) = \frac{1}{s} \sum_{i=1}^s [Y[(v-1)s + i] - y_v(i)]^2 \text{ for } v = 1, \dots, N_s, \quad (2.36)$$

and

$$F^2(v, s) = \frac{1}{s} \sum_{i=1}^s [Y[N - (v - N_s)s + i] - y_v(i)]^2 \text{ for } v = N_s + 1, \dots, 2N_s. \quad (2.37)$$

- *Step 4:* For a given value s and a predetermined range of values q in a set \mathcal{Q} , calculate the q^{th} -order fluctuation function from the $F^2(v, s)$ values,

$$F_q(s) = \left(\frac{1}{2N_s} \sum_{v=1}^{2N_s} [F^2(v, s)]^{q/2} \right)^{1/q}, \quad (2.38)$$

where in general q can take any real value. For $q = 0$, use

$$F_0(s) = \exp \left\{ \frac{1}{4N_s} \sum_{v=1}^{2N_s} \ln[F^2(v, s)] \right\}. \quad (2.39)$$

Repeat steps 2 to 4 for a predetermined range of time scales s .

- *Step 5:* For each selected value of q in a set \mathcal{Q} including negative and positive values as well as zero, perform a linear regression of $\ln(F_q(s))$ on $\ln(s)$ for selected values of s ; and from the slope $h(q)$ of the fitted linear function, calculate $\tau(q)$ via the following relationship:

$$\tau(q) = qh(q) - 1 \text{ for } q \in \mathcal{Q}. \quad (2.40)$$

- *Step 6:* From the estimators of $\tau(q)$ and for each $q_0 \in \mathcal{Q}$ estimate the derivative

$$\alpha_0 = \left. \frac{d\tau(q)}{dq} \right|_{q=q_0}; \quad (2.41)$$

finally use the multifractal formalism to extract the multifractal spectrum,

$$f(\alpha_0) = q_0\alpha_0 - \tau(q_0). \quad (2.42)$$

The above algorithm is very straightforward, and with modern regression software currently available the more complicated steps are already automated. However, there are some important aspects of the algorithm that are often glossed over. Most notably deciding if Step 1 should be performed or not, the determination of the polynomial degree m , the determination of the appropriate range of s and q values, and the numerical implications of taking the derivative of $\tau(q)$ in the final step given a finite set of discrete values rather than a closed-form function. These issues are all addressed in Section 2.4.2 along with an explanation of the relationship between the generalized Hurst exponent $h(q)$ and the scaling function $\tau(q)$.

2.4.2 Important Notes on Parameter Selection

As noted earlier, the MF-DFA algorithm is relatively easy to achieve with modern software, but the careful practitioner will notice a few questions arise during implementation. This section addresses the more obvious of those questions to facilitate implementation.

Form of the Data: Aggregated versus Disaggregated

When Peng et al. [64] first proposed DFA, they did so in the context of DNA nucleotides. In order to convert the DNA sequence into a data set resembling a time series, they first defined an indicator function such that purines in the nucleotide sequence were assigned the value -1 and pyrimidines were assigned the value $+1$. They then defined the “DNA walk” as the displacement after n steps. This is constructed by a cumulative sum of the indicator functions. The ± 1 values represent a disaggregated structure (that is, the one-step increments of the designated stochastic process), while the cumulative sum converts the disaggregated structure into an aggregated structure (that is, the designated stochastic process itself). Kantelhardt et al. [42] report this cumulative sum as Step 1 of the MF-DFA algorithm. However, if the data is already aggregated (such as the daily closing price of an asset), then this step should be eliminated.

Determining the Range of Scales and the Polynomial Fit

Before undertaking the MF-DFA algorithm, we must determine the polynomial degree m for fitting the various segments of data and the range of scale values s . In general the amount of data and the apparent trends within the overall set determine these parameters, so it is convenient to define suggested guidelines for selection that can be incorporated during software development.

Kantelhardt et al. note that for large scales ($s \geq N/4$), the polynomial regression in Step 3 of MF-DFA will be performed on too few data points, and thus the $F^2(v, s)$ values become unreliable. Similarly, for $s \leq 10$, there will be too few segments producing $F^2(v, s)$ values for computing the average $F_q(s)$, making it unreliable. These general guidelines indicate that we must have $10 \leq s \leq N/4$. However, such a range could potentially be very broad for data sets with large N . In practice we find

that s_{\min} and s_{\max} often require substantial manipulation. True fractals possess infinite detail that will never be captured by a finite data set and thus, empirical multifractality exists only on finite scales. Any implementation of MF-DFA should allow the user to manipulate s_{\min} and s_{\max} as well as the increment size Δ_s used to iterate from s_{\min} to s_{\max} . We present the following guidelines as a good starting point, but always consider the real time interval represented by the data before blindly implementing these heuristics.

$$s_{\min} = \max\{20, N/100\}, \quad (2.43)$$

$$s_{\max} = \min\{20s_{\min}, N/10\}, \quad (2.44)$$

and

$$\Delta_s = \frac{s_{\max} - s_{\min}}{100}. \quad (2.45)$$

These ranges ensure that enough data points are available for the polynomial regression and enough $F^2(v, s)$ values are available for computing the $F_q(s)$ values. The increment Δ_s is designed to provide exactly 100 points for the doubly-logarithmic linear regression of Step 5. Note that for high-frequency financial data with over half a million data points in a one-year time span, we found that $s_{\min} = 1$ day and $s_{\max} = 20$ days (i.e. one month of trading days) typically worked well. The minimum s_{\min} also suggests an upper bound of 18 for the degree of polynomial m (note that $s \geq m + 2$ is required in order to perform the regression). In practice, this bound is not likely to be needed (see below), but it gives a convenient terminating condition for software implementation.

The overall concept of MF-DFA is to extract the power law behavior that manifests as the slope $h(q)$ in doubly-logarithmic plots of the fluctuation function versus the scale over a range of scales. However, strong trends in the data can give an artificial result; and thus the selection of the degree of the polynomial to fit during MF-DFA is critical. If the fitted polynomial $y_v(i)$ of degree m in each segment v does not adequately represent the trend in each segment, then the plot of $\ln(F_q(s))$ versus $\ln(s)$ in Step 5 of MF-DFA will display a noticeable departure from linearity in the form of a sharp upward bend (or “dogleg”) that resembles a crossover from one Hurst exponent to another in the designated time series [41]. Recall that the Hurst exponent is a global property and thus should not change for a given value q . This artificial crossover would cause the doubly-logarithmic linear regression in Step 5 of MF-DFA to yield a poor fit. The artificial crossover is eliminated, however, if the degree m equals or exceeds the degree of the inherent trend in the data, which suggests a convenient algorithm for avoiding this

pitfall. Though there are many tests one could perform to detect these trends, we find the one outlined below is easy to implement and yields reliable results rapidly and automatically. This procedure as been adapted from Kuhl et al., who implemented it in the context of multiresolution analysis for modeling and simulation of nonstationary arrival processes exhibiting nested periodic effects as well as a long-term trend in the underlying arrival rate [44].

For $q = 2$ only and δ set to an acceptable degree of error (say, $\delta = 0.01$):

- *Step 1:* Perform Steps 2 thru 5 of the MF-DFA algorithm for the range of scales s as determined above with $m = 1$.
- *Step 2:* Calculate the error sum of squares (SSE_1) and the total sum of squares (SST_1) from the linear regression of $\ln(F_q(s))$ on $\ln(s)$ in Step 5 of MF-DFA, and form the ratio

$$G = \frac{SSE_1}{SST_1}. \quad (2.46)$$

- *Step 3:* If $G \leq \delta$ then the linear regression of $\ln(F_q(s))$ on $\ln(s)$ using a degree-1 polynomial provides an adequate fit; deliver the current value of m and stop. If $G > \delta$, then set $m = m + 1$ and proceed to Step 4.
- *Step 4:* Form the mean square error from the previous linear regression

$$MSE_{m-1} = \frac{SSE_{m-1}}{J}, \quad (2.47)$$

where SSE_{m-1} is the error sum of squares for fitting a polynomial of degree $m - 1$ to the J data points

$$\{(\ln(s_j), \ln[F_q(s_j)]): j = 1, \dots, J\}. \quad (2.48)$$

With the updated value m perform the Steps 2 thru 5 of MF-DFA again.

- *Step 5:* From the linear regression of Step 5 of MF-DFA, form the new mean square error MSE_m and form the likelihood ratio test statistic

$$\chi^2_{\text{test}} = -J \ln \left(\frac{MSE_m}{MSE_{m-1}} \right). \quad (2.49)$$

If the polynomial of degree $m - 1$ is the correct model for the data set (2.48), then this ratio is chi-square distributed with 1 degree of freedom. Therefore, (2.49) is used to test the null hypothesis that the underlying statistical model for the data set (2.48) is a polynomial of degree $m - 1$ versus the alternative hypothesis that the degree of the polynomial is at least m .

- *Step 6:* Under the null hypothesis, if $\chi_{\text{test}}^2 \leq \chi_{1-\alpha,1}^2$ then m is the best degree polynomial to fit to the segments; stop. If $\chi_{\text{test}}^2 > \chi_{1-\alpha,1}^2$, then set $m = m + 1$ and return to Step 4.

It should be noted that when implementing these procedures, there is always the potential for errors being introduced through the finite precision inherent in modern computers. Specifically, if the $F_q(s)$ fluctuations are close to zero, their logarithm will approach negative infinity. These results can introduce error into the calculation of the multifractal spectrum. Overfitting the polynomial regression should thus be avoided. This is handled first by ensuring a large enough value of s_{\min} and second by minimizing m as much as possible. It is our contention that the above procedures generally avoid this pitfall under the assumptions that the data set is large enough and is inherently multifractal. Complex data sets that do not scale as a power law will give unreliable results.

Relationship of the generalized Hurst exponent $h(q)$ with $\tau(q)$

In Step 5 of MF-DFA, we introduced a relationship between the slope, $h(q)$, of our doubly-logarithmic plot of $F_q(s)$ versus s and the scaling function $\tau(q)$ without explanation. This relationship is derived from the multifractal formalism and the concept of a box probability. In the box counting approach to the multifractal formalism, the number of points falling in a specific interval is measured as the size of that interval changes. If this change follows a power law relation, then the set is a fractal and we can extract the multifractal spectrum. The following relationship between $\tau(q)$ and $h(q)$ is adapted from Kantelhardt et al. as follows [42].

Without loss of generality we assume N is a multiple of s and there is no inherent trend in the data to be removed. Then defining $p_s(v)$ as the box probability of the v^{th} segment at scale s and the partition function as Z_q , we see that the multifractal formalism gives the following scale relationship:

$$Z_q(s) = \sum_{v=1}^{N/s} |p_s(v)|^q \sim s^{\tau(q)}. \quad (2.50)$$

The box probability, $p_s(v)$, can be estimated by a cumulative sum of points in the v^{th} segment at scale s . Recall from Step 1 of MF-DFA that we perform this cumulative sum on the disaggregated data such that

$$p_s(v) = \sum_{k=(v-1)s+1}^{vs} (x_k - \bar{x}) = Y(vs) - Y((v-1)s) \text{ for } v = 1, \dots, N/s, \quad (2.51)$$

where here for simplicity we assume that $0 \leq x_k \leq 1$ and $\sum_{k=1}^N x_k = 1$. If we assume there is no trend in the data to be removed, then the calculation of the variance in Step 3 of MF-DFA simplifies to

$$F^2(v, s) = [Y(vs) - Y((v-1)s)]^2 \text{ for } v = 1, \dots, N/s; \quad (2.52)$$

and thus the q^{th} -fluctuation function becomes

$$F_q(s) = \left(\frac{1}{N_s} \sum_{v=1}^{N_s} [Y(vs) - Y((v-1)s)]^q \right)^{1/q} \sim s^{h(q)}. \quad (2.53)$$

Note that we can rearrange Equation (2.53) to restate the relationship with $h(q)$ as

$$\sum_{v=1}^{N_s} |Y(vs) - Y((v-1)s)|^q \sim s^{qh(q)-1}. \quad (2.54)$$

Then the exponents of s on the right-hand sides of Equation (2.54) and Equation (2.50) give us the relationship

$$\tau(q) = qh(q) - 1 \text{ for } q \in \mathcal{Q}. \quad (2.55)$$

Equation (2.55) holds for disaggregated data that has been converted to an aggregated set. Kantelhardt et al. note the slope $h(q)$ becomes unreliable for scaling exponents close to zero. In such cases, they suggest a modified MF-DFA, where the aggregated data set is put through another cumulative sum, i.e. a double cumulative sum of the disaggregated data. In this case, the polynomial degree m used to fit each segment of the data should be at least two [42].

Recall also that a particular value α_0 is the derivative of $\tau(q)$ with respect to q evaluated at $q = q_0$ and is defined as the Hölder exponent. That is, while $h(q)$ is a global property over the entire data set for a given value q , each α is a local property contributing to the construction of the time series at a vanishing frequency. If the data set is monofractal, then $h(q) = H$ at all points in the time series, and we have $\alpha = \frac{d}{dq}\tau(q) = h(q) + q\frac{d}{dq}h(q) = H$ for all values of q .

Numerical Approximations

The last issue we address with MF-DFA is the obvious error introduced by taking numerical approximations to derivatives in the calculation of each α . In the implementation of MF-DFA, the most convenient approach to finding $\alpha(t)$ is to iterate over a range of q -values centered at zero for uniform increments Δq . Then the values for $\alpha(t)$ are approximated by

$$\alpha_0 \approx \frac{\tau(q_0 + \Delta q) - \tau(q_0)}{\Delta q} \text{ for each } q_0 \in \mathcal{Q}. \quad (2.56)$$

It has been noted that for large magnitudes of $|q|$, the error in the multifractal spectrum tails becomes large [45]. In our implementation we choose $\Delta q = 0.1$; and we iterate between $q = -5$ and $q = 5$, which is within the suggested range for q and yields $\mathcal{Q} = \{-5 + j(0.1) : j = 0, 1, \dots, 100\}$. Choosing $\Delta q = 0.1$ allows for a sufficient quantity of $h(q)$ values to minimize the discretization error in Equation (2.56). However, care should be taken for the particular data set in question. Ideally, the range for q and Δq should be parameters that the user can manipulate easily when running MF-DFA.

2.5 Software Implementation and Testing

2.5.1 Java Application

In order to accommodate the flexibility and computational requirements needed to implement MF-DFA, we decided to program the application in Java. Java's object-oriented approach and extensive API meant that many aspects of the application could simply be inherited from parent objects, enabling us to focus on the details of the algorithm rather than the intricate functionality of the interface. Java also facilitates portability, so the final application can be deployed as a web applet or easily emailed to other users. These advantages of Java led to a faster implementation and a flexible finished product.

The main disadvantage to Java is computational speed. When working with large high-frequency data sets, we may perform hundreds of polynomial regression analyses in rapid succession. For linear regression this is straightforward and relatively fast. For higher degree-polynomials, the process involves matrix decomposition that is computationally intense. Data sets with over a million points and second (or higher) degree polynomial trends can take upwards of two hours depending on available computing power and the settings for s_{\min} , s_{\max} and Δs . Nevertheless, Java proved to be a good choice for implementation and allowed us the flexibility to integrate MF-DFA with our other simulation applications.

The Java application consists broadly of three parts: functionality for manipulating empirical data sets or generating simulated data sets, functionality for performing and storing the results of MF-DFA, and an overall graphical user interface (GUI) that coordinates these functions. Manipulating data is a key aspect to MF-DFA and can sometimes be a tedious task in software development. Our application

implements XYSeries objects from the JFree Chart [3] library for storing and plotting time series. We also incorporated two algorithms for generating simulated data. One generates Brownian motion through Monte Carlo sampling of a standard Normal random variable, and the other implements a binomial multiplicative cascade. This functionality allowed us to generate test data with known, closed-form multifractal spectra. We also added the Fisher-Yates shuffling algorithm to facilitate testing the source of multifractality in a given time series [27]. The algorithm creates a new time series from original data that has the components randomly shuffled.

The algorithm for implementing MF-DFA is outlined in Section 2.4.1. To that basic structure we added the algorithm for selecting the degree m for the polynomial regression, progress monitoring, and cancellation functions for terminating long runs. The output of the MF-DFA implementation is an object called “multifractal spectrum” that contains the original data set, α and $f(\alpha)$, and the relevant interim results – such as the fluctuation function values, the range of q values, and the range of scales s used in the algorithm – that lead to α and $f(\alpha)$. For polynomial regression, we employed the JAMA Java Matrix Package [2]. This basic linear algebra library contains various methods for solving matrix equations. For both computational speed and robust application, we chose QR decomposition as the basis for polynomial regression with $m > 1$.

The GUI portion of the application essentially coordinates the other two functions and allows the user to upload time series from a file and export results to files. The JFree Chart functionality used for storing the time series is also linked to various plotting options that allow for visual inspection of the time series and results. The interface gives point-and-click functionality to uploading, shuffling, plotting, and exporting data. It also displays default suggestions for s_{\min} , s_{\max} , Δs , and the range of q -values while also allowing the user to customize these parameters. The application checks the data for trends to decide on the appropriate degree polynomial to fit to the time series by default, but also allows the user to override this option. Once the results are calculated, the GUI will plot both the multifractal spectrum and the generalized Hurst exponents, $h(q)$, for inspection. This allows the user to decide if the appropriate trend was removed and determine whether the data is in fact multifractal in the range specified. The results can be saved or exported or the user can return to the parameters interface to make changes and run the analysis again. Java’s Swing library was employed for the GUI programming, and we borrowed some of the plotting features from the MASON package, originally written by Sean Luke [52].

2.5.2 Testing on Known Multifractals

As mentioned, the MF-DFA application contains functions for generating known fractal and multifractal time series. However, recall that fractals possess infinite detail such that examining finer and finer scales only reveals more and more detail or roughness. Clearly a computer simulation of a finite number of points imposes a limit on the amount of detail that can be captured experimentally. As such, we have found that simulated monofractals produce small multifractal spectra with $f(\alpha)$ values all between

roughly 0.8 and 1.0 clustered around the expected value of α rather than the single point predicted by theory. Recall also that multifractal analysis in general is the search for long memory in a time series as characterized by the generalized Hurst exponent, $h(q)$. Although the detection of long memory in a time series is relatively straightforward, quantifying the degree of self-similarity is notoriously difficult. Beran notes that applying Hurst's rescaled range approach to subsets of the Nile river minima time series confirms that H differs substantially from 0.5, but yields results ranging from around $H = 0.8$ up to $H = 1.17$ [7]. This makes statistical inference about the true value of H difficult at best. The net result for the practitioner is that MF-DFA can determine if the data is self-similar and whether that self-similarity results from a broad spectrum of q -dependent generalized Hurst exponents or from a narrower spectrum indicating monofractality. MF-DFA can also indicate the relative size of the generalized Hurst exponents in the data and thus can detect long memory. However, when these values are in the neighborhood of 0.5, it is not possible to make a statement about long memory with statistical significance. Mandelbrot was able to show the nonuniversality of the multifractal spectrum, so the true value of multifractal analysis on finite-length time series is the comparison of one multifractal spectrum to another. If the spectra produced by two different time series exhibit the same properties, then we can infer that the underlying mechanisms driving the two processes – that is, heavy-tailed probability distributions or some degree of long memory or both – are the same.

2.5.3 Brownian Motion

A relatively easy monofractal process to simulate approximately is standard Brownian motion. Given that the one-time-unit increments of standard Brownian motion are normally distributed with mean zero and variance one, we can simply generate a series of random variables from the Normal distribution, and their cumulative sum yields an approximation to Brownian motion. In the case of standard Brownian motion, we would expect the simulated time series not to exhibit q -dependence in the generalized Hurst exponent $h(q)$ and therefore all Hölder exponents would be the same at point ($\alpha = 0.5, f(\alpha) = 1$). Figure 2.3 shows 2^{16} data points of simulated standard Brownian motion, and Figure 2.4 shows the multifractal spectrum obtained via MF-DFA. The results in Figure 2.4 are all clustered around the theoretical point. The interpretation of this multifractal spectrum is that the finite time series exhibits Hölder exponents in the neighborhood of 0.5. In this case the expected value of α is approximately 0.48.

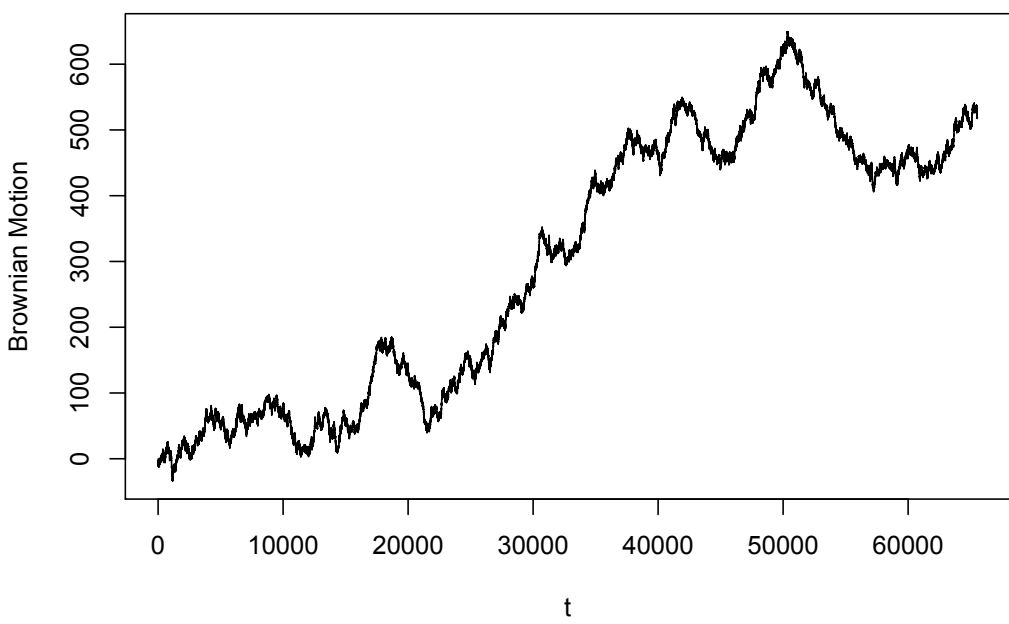


Figure 2.3: An approximation of standard Brownian motion: 2^{16} points

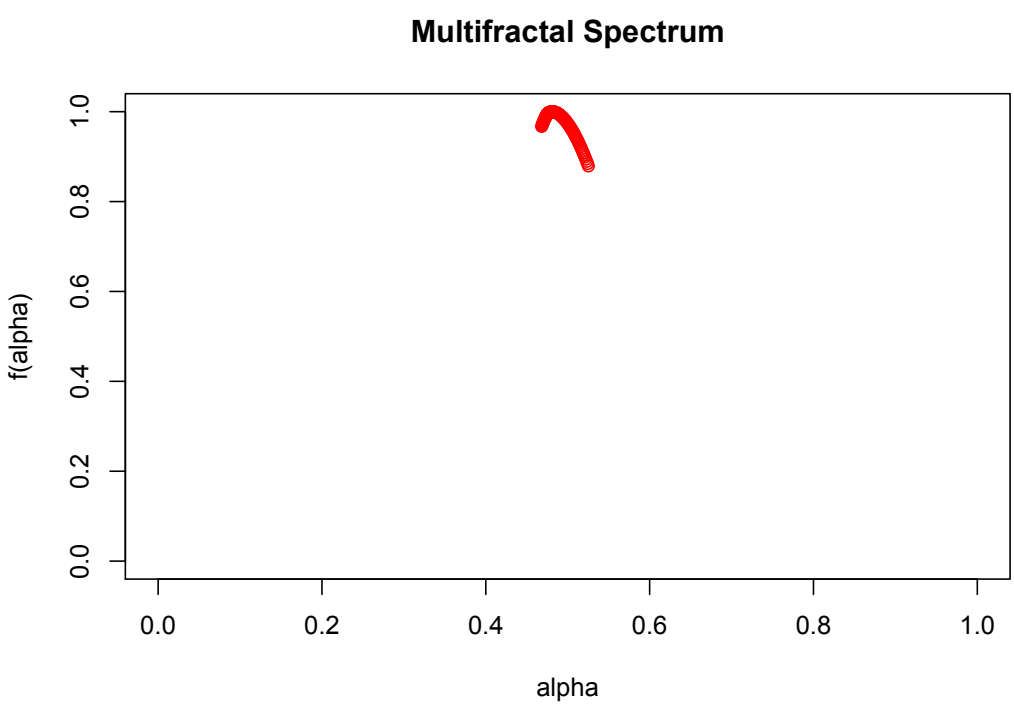


Figure 2.4: The multifractal spectrum of simulated standard Brownian motion

Though the multifractal spectrum is a convenient way of visualizing the multifractal properties of a time series, it is simply a measure of how the generalized Hurst exponent $h(q)$ is changing with q . It is therefore often useful to analyze the q^{th} -fluctuation plot, where $h(q)$ is represented by the slopes of the regression lines at different values q over the range of scales s . Figure 2.5 gives a sample of the regression lines used to calculate the multifractal spectrum of the simulated standard Brownian motion.

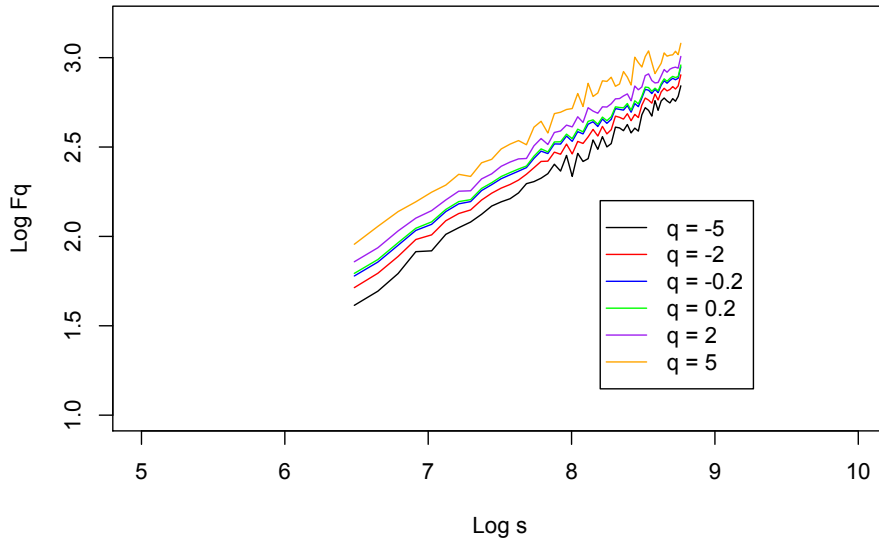


Figure 2.5: MF-DFA results for Brownian motion: $\ln(F_q(s))$ vs. $\ln(s)$ for the range of q -values

Generalized fractional Brownian motion $\{B_H(t) : t \geq 0\}$ is described by Taqqu et al. as a Gaussian process with mean zero and variance t^{2H} [73]. It can be shown that the fractional Brownian motion disaggregated process $\{X_i : i = 1, 2, \dots\}$ defined by the increments

$$X_i = B_H(i) - B_H(i-1) \text{ for } i = 1, 2, \dots \quad (2.57)$$

has an autocovariance function, $\gamma(h)$, given by:

$$\gamma(h) = \text{Cov}(X_i, X_{i+h}) = \frac{1}{2} \left((h+1)^{2H} - 2h^{2H} + |h-1|^{2H} \right) \text{ for } h = 0, 1, \dots \quad (2.58)$$

What is important to note about $\gamma(h)$ is the behavior as the lag h approaches infinity. In particular,

provided that $\frac{1}{2} < H < 1$, we have

$$\gamma(h) \sim 2H(2H - 1)h^{2H-2} \text{ as } h \rightarrow \infty, \quad (2.59)$$

which means that the process (2.57) exhibits long-range dependence. On the other hand

$$\left. \begin{array}{l} \lim_{h \rightarrow \infty} \gamma(h) = 0 \\ 0 < \sum_{h=0}^{\infty} |\gamma(h)| < \infty \end{array} \right\} \text{ if } 0 \leq H \leq \frac{1}{2}, \quad (2.60)$$

which establishes that the generalized fractional Brownian motion disaggregated process (2.57) exhibits short-range dependence when $H \in [0, \frac{1}{2}]$. Note that when $H = \frac{1}{2}$, we have standard Brownian motion so that the process $\{X_i : i = 1, 2, \dots\}$ is uncorrelated.

Using a package called “fArma” in R, we were able to generate fractional Brownian motion with $H = 0.6$ and $H = 0.8$. The two plots of fractional Brownian motion are shown in Figure 2.6, separated arbitrarily for visual clarity.

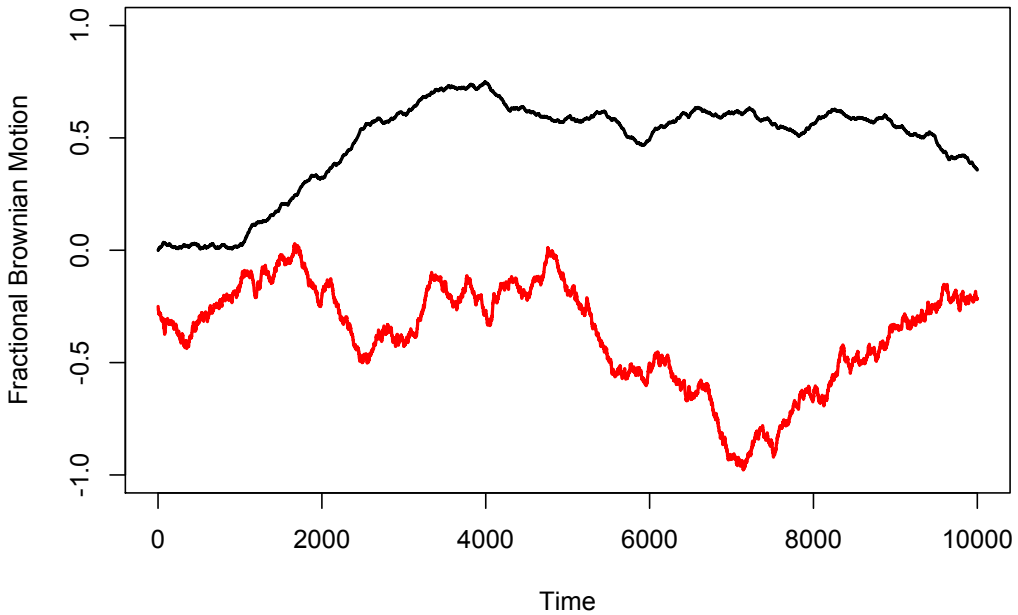


Figure 2.6: Fractional Brownian motion with $H = 0.8$ (top) and $H = 0.6$ (bottom)

The parameter H in fractional Brownian motion is the same at all scales, meaning such a time series is a monofractal. As such, we would expect a simulated time series to exhibit a multifractal spectrum with a single point at $(\alpha = H, f(\alpha) = 1)$. The results of MF-DFA run on the two fractional Brownian motion time series are shown in Figure 2.7. Again, the finite series exhibit some q -dependence in the generalized Hurst exponents, but the Hölder exponents are clustered around the value H as we would expect.

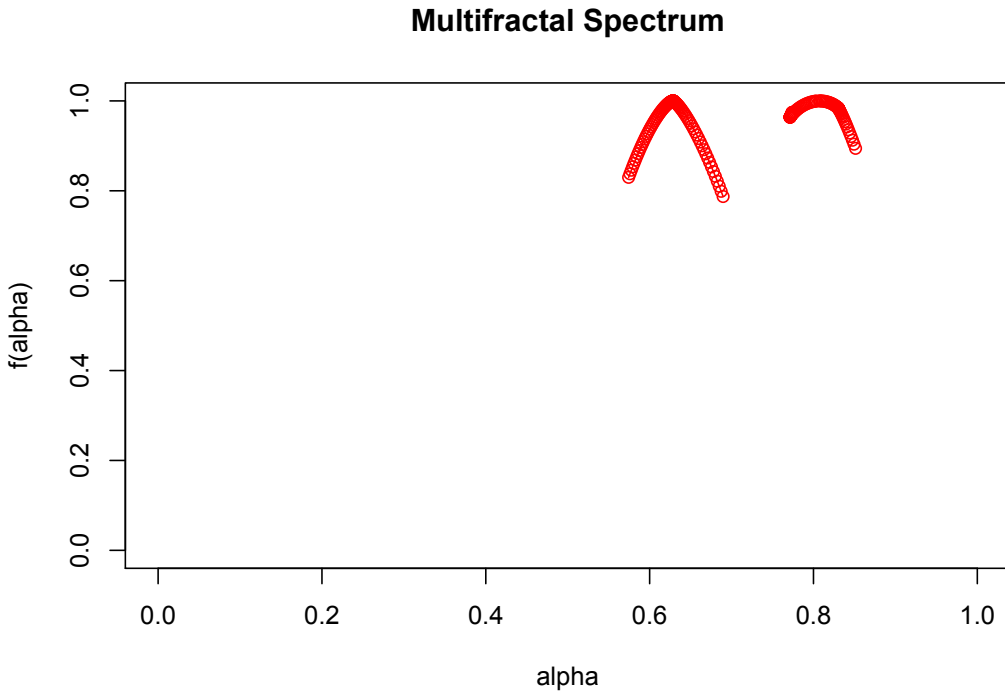


Figure 2.7: Multifractal spectra of fractional Brownian motion with $H = 0.6$ and $H = 0.8$

As noted, in the case of fractional Brownian motion, the value $H > 0.5$ indicates a long-range dependence in the increments of the series, whereas in the case of standard Brownian motion the increments are independent identically distributed random variables. Employing Kantelhardt's technique of shuffling the increments should therefore produce a change in the fractional Brownian motion multifractal spectrum, but no change in the standard Brownian motion spectrum. Figure 2.8 shows the results of MF-DFA run on the shuffled standard Brownian motion compared with the spectrum of the original series. Although there is a change in the standard Brownian motion shuffled multifractal spectrum, it is still clustered around the theoretical $\alpha = 0.5$.

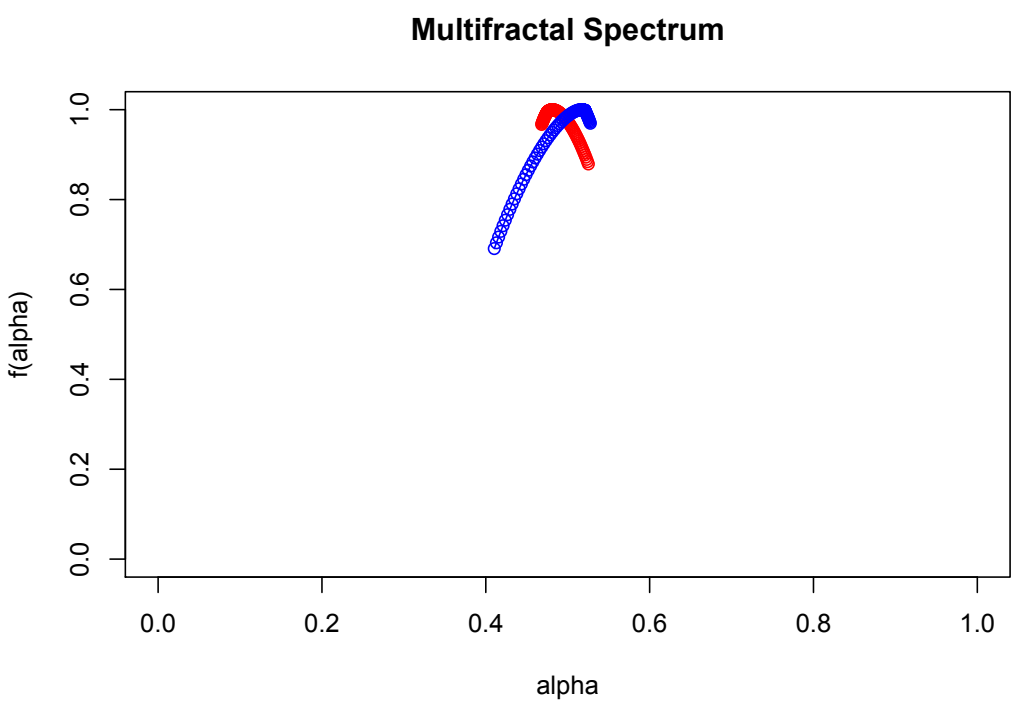


Figure 2.8: Multifractal spectra of standard Brownian motion: original in red, shuffled in blue

Similarly, Figures 2.9 and 2.10 show the same comparison for the fractional Brownian motion with $H = 0.6$ and $H = 0.8$. In these cases, the shuffled multifractal spectra exhibit a clear departure from the region of $\alpha = 0.6$ (Figure 2.9) and $\alpha = 0.8$ (Figure 2.10).

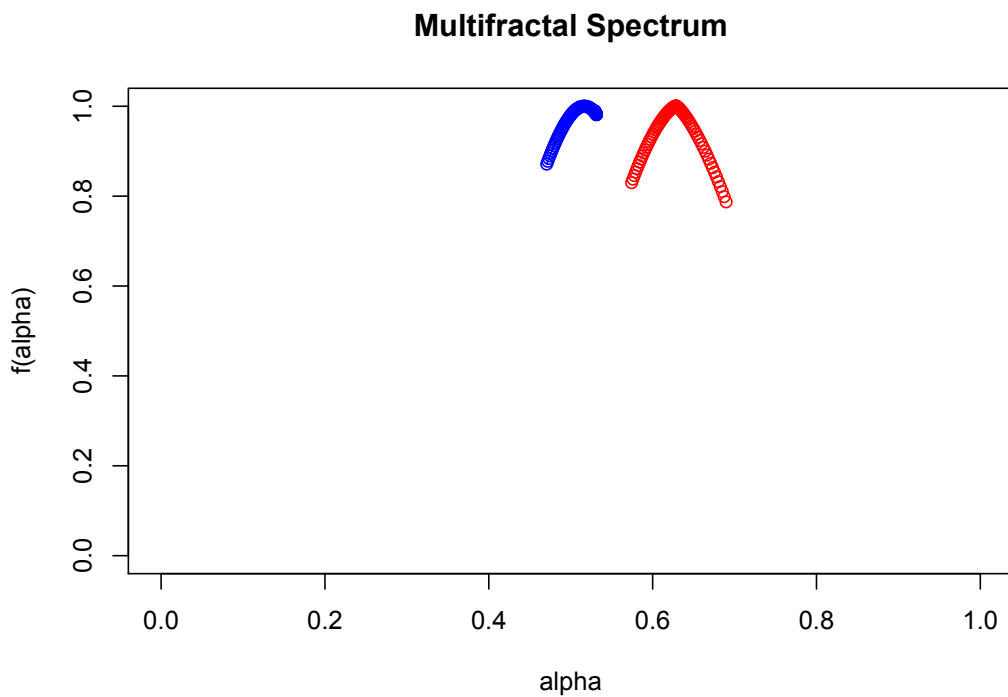


Figure 2.9: Multifractal spectra of fractional Brownian motion ($H = 0.6$): original in red, shuffled in blue

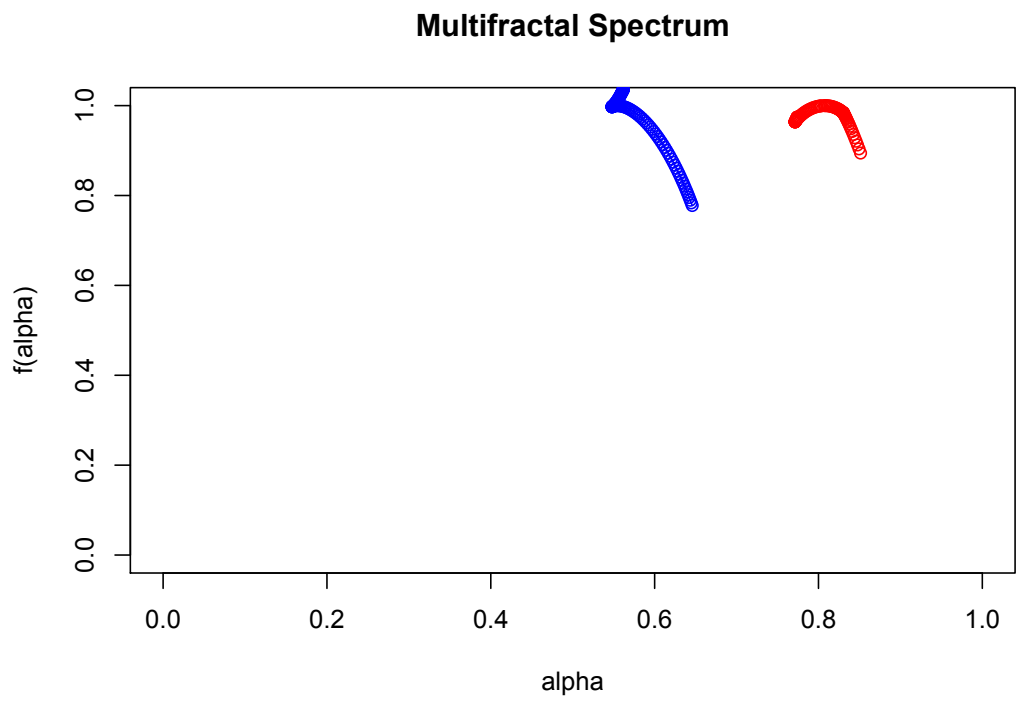


Figure 2.10: Multifractal spectra of fractional Brownian motion ($H = 0.8$): original in red, shuffled in blue

2.5.4 Multifractal Binomial Measure

A common example when presenting multifractals is the multifractal binomial measure. The measure is constructed by an iterative process that can be easily programmed in modern software. The basic idea is to continually divide segments of the unit interval in half and at each iteration assign a positive mass or weight m_0 to the left half and weight m_1 to the right half such that $m_0 + m_1 = 1$ and $m_0 \neq 0.5$. It can be shown that in the limit as the number of iterations of the generation procedure tends to infinity, this iterative process creates increasing heterogeneity in the allocation of weight and is thus a continuous, but nowhere differentiable probability measure [13]. Figures 2.11 and 2.12 illustrate this property for 2^{16} points generated with $m_0 = 0.25$. Appendix A gives the mathematical derivation of the binomial measure and our algorithm for simulating the measure.

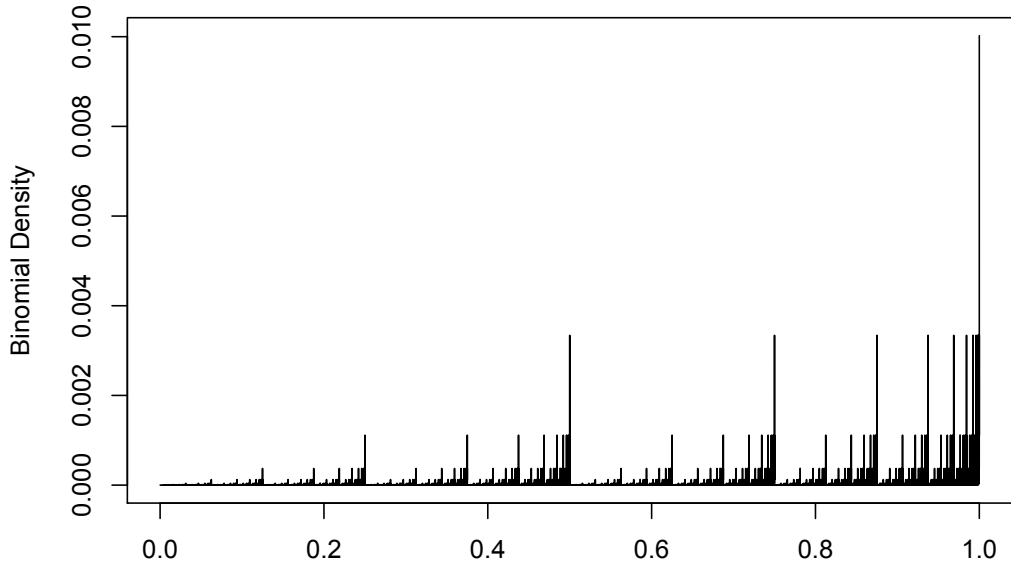


Figure 2.11: The density of 2^{16} points of the multifractal binomial measure

Close examination of the figures reveals a self-similar structure as we would expect with any fractal. However, the binomial measure is a multifractal and therefore should exhibit a broader multifractal spectrum than our simulated Brownian motion of the previous section. Due to the simple nature of the construction of the binomial measure, we can derive a closed-form expression for that spectrum.

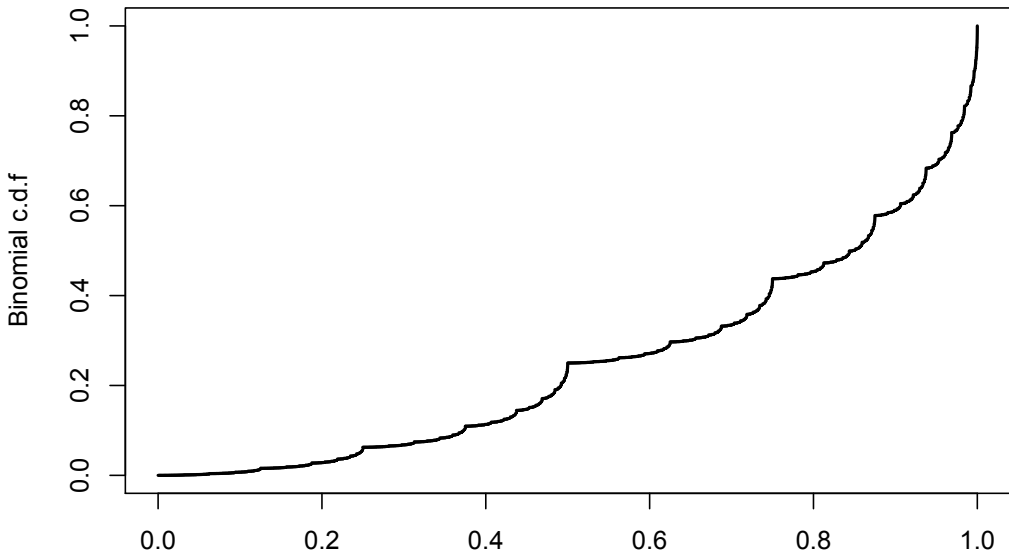


Figure 2.12: The cumulative multifractal binomial measure

Specifically $\alpha(t)$ can take any value between $-\log_2(m_0)$ and $-\log_2(m_1)$. The expected value of $\alpha(t)$ is given by $-0.5 \log_2(m_0 m_1)$, which is where the multifractal spectrum should peak. Figure 2.13 shows the results of running MF-DFA on the points shown in Figure 2.12. For $m_0 = 0.25$, $\alpha(t)$ should range from 0.41 to 2.0 and peak around 1.20. This is in close agreement to the multifractal spectrum produced by MF-DFA.

Note in Figure 2.11 how the increments tend to cluster together in a predictable pattern. The pattern gets ever larger as we move from left to right, but the smallest parts of the pattern are always on the left followed by a crescendo of increments as we move right. If we were to shuffle these increments, we would clearly alter the displacement of their cumulative sum in a given interval and therefore alter the average displacement over all intervals of that size in the series. We would therefore expect the multifractal spectrum to change if the increments of the series were shuffled. Figure 2.14 illustrates the impact of shuffling a multifractal that is driven by long term dependence. There is a notable change in the multifractal spectrum as it reverts to a set of Hölder exponents clustered around 0.5.

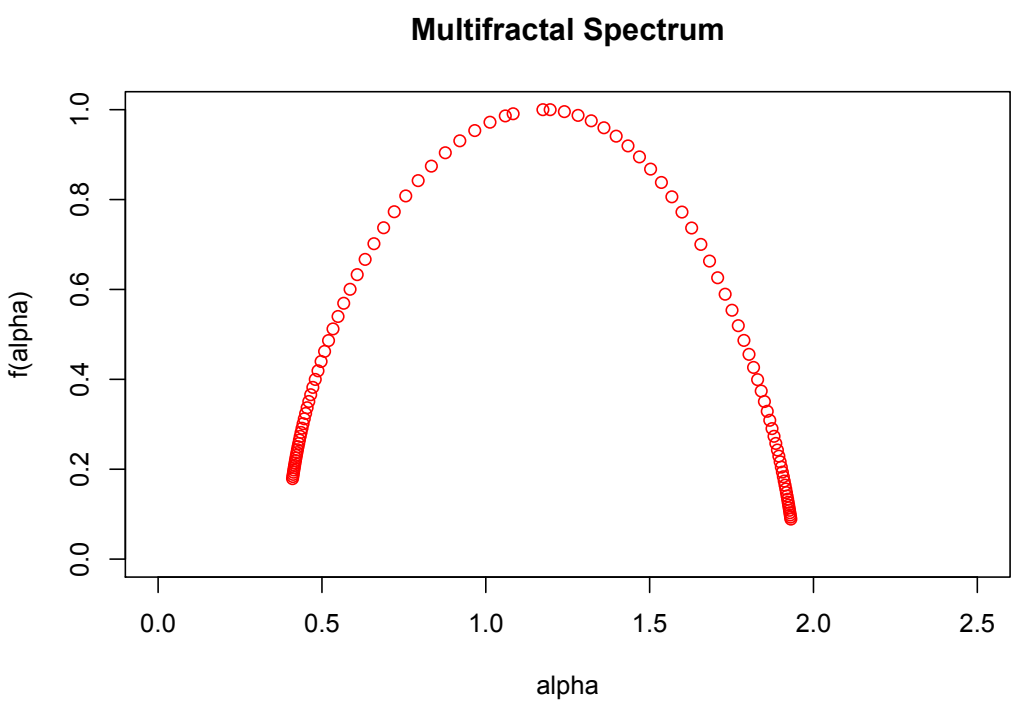


Figure 2.13: The multifractal spectrum of the binomial measure with $m_0 = 0.25$

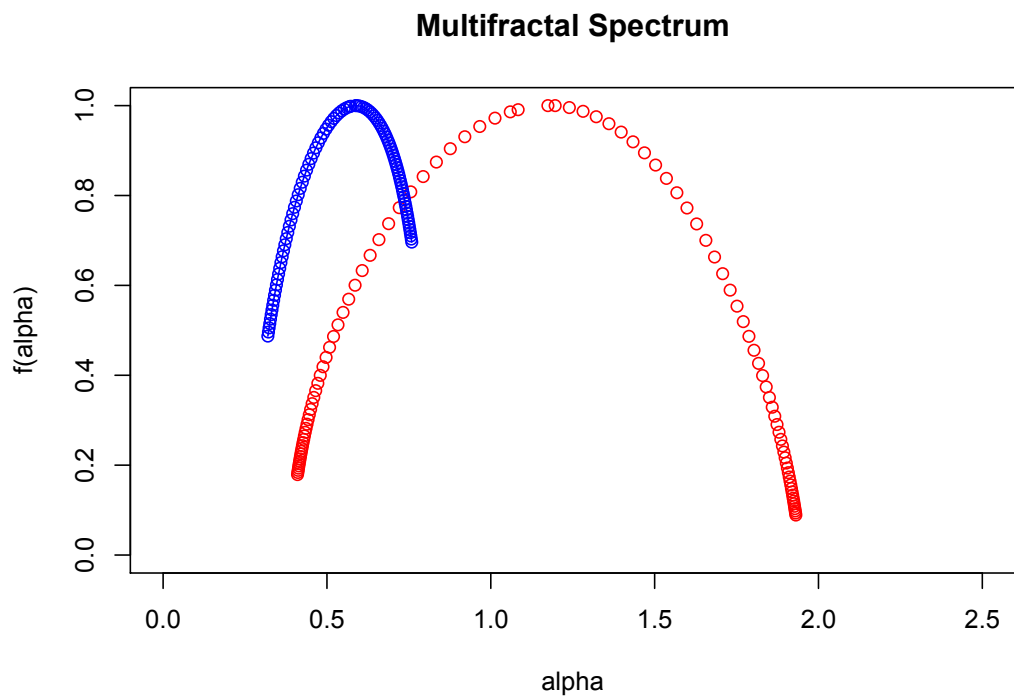


Figure 2.14: The multifractal spectrum of the binomial measure (red) and the resulting spectrum from the shuffled series (blue).

In the preceding example, we constructed a deterministic multifractal process such that each iteration always applied mass m_0 to the left half of an interval and mass $1 - m_0$ to the right half. On the other hand, if we select the mass to apply to the left half (m_0 or $1 - m_0$) randomly at each iteration and its complement is applied to right half, we obtain a stochastic multifractal process. Stochastic multifractal processes are used to model trading time in Calvet and Fisher's MMAR presented earlier. Such processes no longer possess the well-organized self-similarity seen in Figure 2.11, but rather exhibit a statistical self-similarity. For example, compare Figure 2.11 with the random multifractal binomial measure shown in Figure 2.15. Although the deterministic multifractal process of Figure 2.11 differs considerably in appearance from the stochastic multifractal process of Figure 2.15, they were constructed with the same masses $m_0 = 0.25$ and $1 - m_0 = 0.75$. As a result, their underlying multifractal spectra should be the same. The results of running MF-DFA on the c.d.f of both the deterministic binomial measure and the stochastic binomial measure are presented in Figure 2.16.

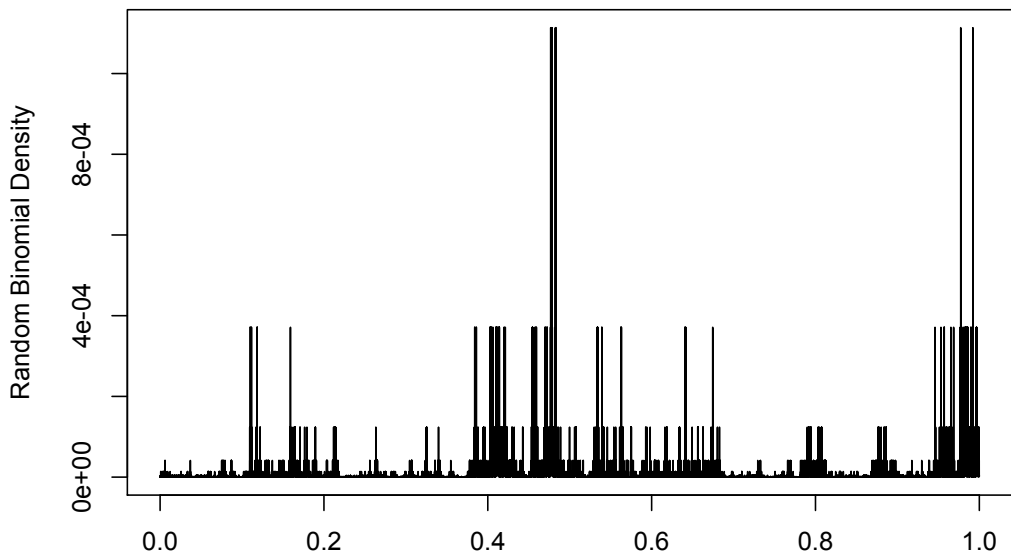


Figure 2.15: The density of 2^{16} points of a random multifractal binomial measure

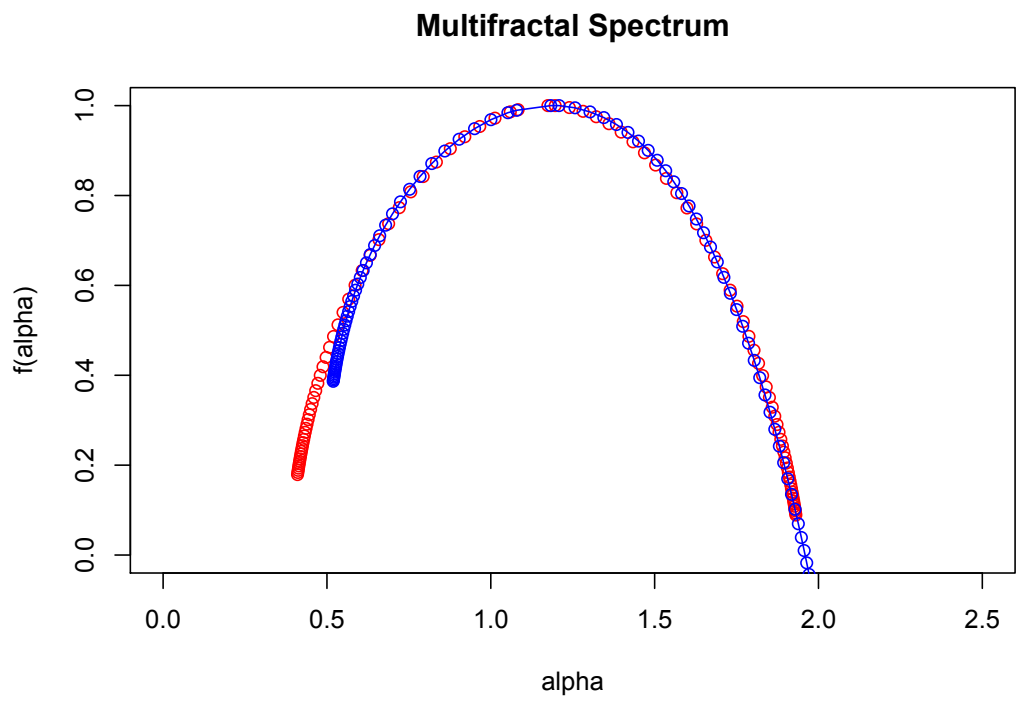


Figure 2.16: The multifractal spectrum of the deterministic binomial measure (red) and stochastic binomial measure (blue)

The above examples illustrate the value of multifractal analysis. The path of Brownian motion shown in Figure 2.3 appears considerably more erratic than that of the binomial measure in Figure 2.12. But the underlying process of Brownian motion scales as a single exponent H at every point, while the binomial measure displays a spectrum of exponents across sets of points that are interwoven along the unit interval and possess a fractal dimension anywhere between zero and one. Thus the relative complexity of the two processes is not immediately evident through comparison of their paths, but plotting their multifractal spectra together (see Figure 2.17) illustrates the difference more readily. Additionally, the deterministic binomial density shown in Figure 2.11 appears quite different in structure than the stochastic binomial density shown in Figure 2.15, yet multifractal analysis reveals that their underlying construction (i.e., m_0) is the same.

We conclude that our implementation of MF-DFA functions as it was intended and allows us to gain some insight into the mechanisms creating a particular time series as compared to another. If a series is dominated by long memory then we can employ the shuffling heuristic paired with MF-DFA to detect the time dependence. And when two time series appear to behave similarly, we can illuminate their true similarities (or lack of) by plotting their multifractal spectra together.

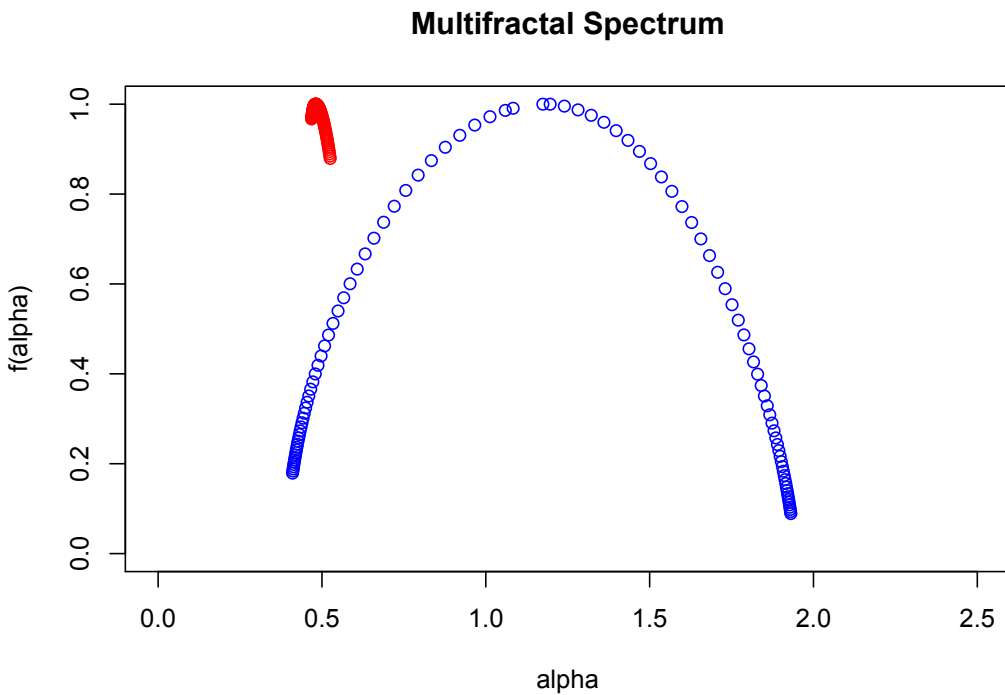


Figure 2.17: The multifractal spectra of the binomial measure (blue) and standard Brownian motion (red)

2.6 Summary

In this chapter we introduced the concept of fractals to quantify objects and time series that are too rough or irregular to measure using traditional analysis. In the case of a monofractal time series, the value of the process scales at all points in time according to a single scaling exponent H known as the Hurst exponent, whereas in the case of a multifractal time series, different sets of interwoven points in time scale according to a spectrum of exponents $\alpha(t)$ known as Hölder exponents. In either case, the scaling exponents and the corresponding Hausdorff dimension of the set of supporting points \mathcal{T}_q — known as the multifractal spectrum $f(\alpha)$ — stochastically quantify the time series. MF-DFA as described above is a proven method for extracting the multifractal spectrum from time series data. We implemented this algorithm in a robust software application that allows the user to manipulate the various parameters to facilitate inference about the multifractal properties of a given data set. The application was tested on known multifractal time series and the results were in agreement with theoretical predictions. In the next section we apply MF-DFA to high-frequency (i.e., fine scale) data sets from the New York Stock Exchange.

Chapter 3

Applications of MF-DFA to Empirical Data

3.1 Introduction

In this chapter we apply MF-DFA to a high-frequency data set from the New York Stock Exchange. North Carolina State University's Department of Economics has access to stock exchange data on very fine scales provided by Wharton Research Data Services (WRDS) [4]. WRDS was established in 1993 to assist research faculty at the University of Pennsylvania. Part of the function of WRDS has been to compile trade and quote (TAQ) data from various exchanges into a database to facilitate fine-scale analysis. In the sections that follow we conduct an in-depth analysis of the multifractal properties of General Electric's (GE) stock price extracted from the WRDS database for the period 2000 to 2003.

Stock price data is often stored and presented with a number of adjustments. The purpose for these adjustments is to provide analysts with a more accurate representation of the firm's true value by accounting for various corporate actions. For example, stock splits are a way of increasing the number of shares of a stock while keeping the market capitalization constant. So although a three-to-one split would cause the share price to immediately drop by one third, all shareholders would simultaneously have their quantity of shares increased by a factor of three. Such a drastic change in the stock price could be misconstrued as a decline in the firm's value, even though many splits occur because the company is doing well and projecting growth. Splits and dividends (or other distributions) by the company are often taken into account for this reason, and the reported price is thus not exactly what a trader might have observed on a particular day. However, the TAQ data from WRDS are raw quotes and trades as they happen and therefore do not incorporate such adjustments. In general, this is how we would like to analyze the data from a multifractal perspective, as it illustrates the true fluctuations in the price path on a given time scale. But stock splits constitute a notable exception. The splits are typically announced in advance and occur after the market has closed. The sudden drop in price is misinterpreted by multifractal

analysis as a fluctuation that does not have a power law relationship to any other fluctuation within the series. Drops due to splits typically cause the output of MF-DFA to indicate a blip or jump in the multifractal spectrum. However, when the split is accounted for, the multifractal spectrum appears smooth and concave. Taking this empirical observation into account, we adjust the TAQ data for splits, but not for other corporate actions such as dividends.

As previously mentioned, time series analysis is often a subjective task that is informed by exploratory analysis. Visual inspection of the data and its various transforms along with a number of heuristics are employed. Unfortunately, the models suggested by these heuristics may still fail to yield an adequate representation of the underlying process. Thus, caution must be exercised when drawing conclusions from such subjective analysis. The general approach is to seek a weakly stationary data set — that is, a time series where each realization has the same mean, and the autocovariance function depends only on the size of the lag l and not the particular time-location within the series. Once transformed into a stationary series (if necessary), the autocovariance is modeled by one of the many techniques discussed in the previous chapter. The researcher may employ the autocorrelation and partial autocorrelation functions to determine the parameters of an ARMA(p, q) model or analyze the periodogram to detect the parameters of seasonal trends. Similarly, if the volatility appears nonconstant then the researcher may attempt to fit a GARCH model to capture the changes in conditional variance.

In Section 3.2 we start by presenting the GE data set and its basic properties. In Section 3.3 we describe the traditional methods of exploratory time series analysis that we employ and why we felt they were appropriate for this particular data set. We then conduct multifractal analysis on the original data and on simulations from the fitted models established by our analysis. We close in Section 3.4 with a brief discussion of our findings and avenues for future applications of MF-DFA.

3.2 The General Electric Data

Our choice of GE as the asset for analysis was arbitrary. GE is a diverse conglomerate with a long history dating back to Thomas Edison before the turn of the twentieth century [1]. The company is primarily known as a manufacturer — with divisions in energy, technology infrastructure, and household and industrial products — but they also engage in capital finance. GE is publicly traded on the New York Stock Exchange and is a component of the Dow Jones Industrial Average and the S&P 500.

The adjusted daily closing price going back to 1962 is freely available from various online sources (see Figure 3.1). To put the TAQ data set in perspective, the daily closing price from 1962 to 2012 consists of 12,786 data points, while the TAQ data from 2000 to 2003 (delimited by the vertical dashed lines in Figure 3.1) consists of 4,273,056 data points. The TAQ data for the period 2000 to 2003 is shown in Figure 3.2.

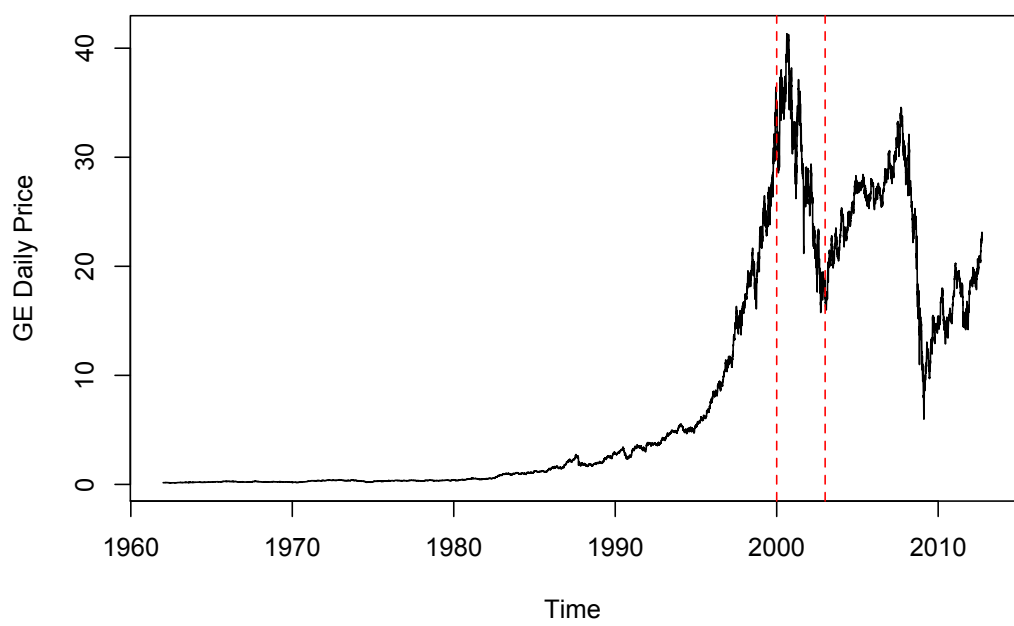


Figure 3.1: The adjusted daily closing price for GE from the period 1962 to 2012

On May 8, 2000, GE issued a three-to-one split of their shares; and the price dropped from \$156.38 to \$52.13 from the market closing on Friday, May 5, 2000, to the first trade on Monday, May 8, 2000. To adjust the price for this split, we divided by 3 each observation up to May 5, 2000. The date of the split is shown by the vertical dashed line in Figure 3.2. Any other adjustments that may have been incorporated in the data set shown in Figure 3.1 are not incorporated in the TAQ data. For the years 2000, 2002, and 2003, there were 252 trading days throughout the year. In 2001, the September 11th terrorist attacks occurred and resulted in four less trading days for that year for a total of 248 days. Trading volume increased steadily during the period from 2000 to 2003. For the 252 trading days of 2000, there were on average 3,233 trades per day. By 2003 this number had increased to roughly 5,327 trades per day. See Table 3.1 for a complete description of the TAQ time series.

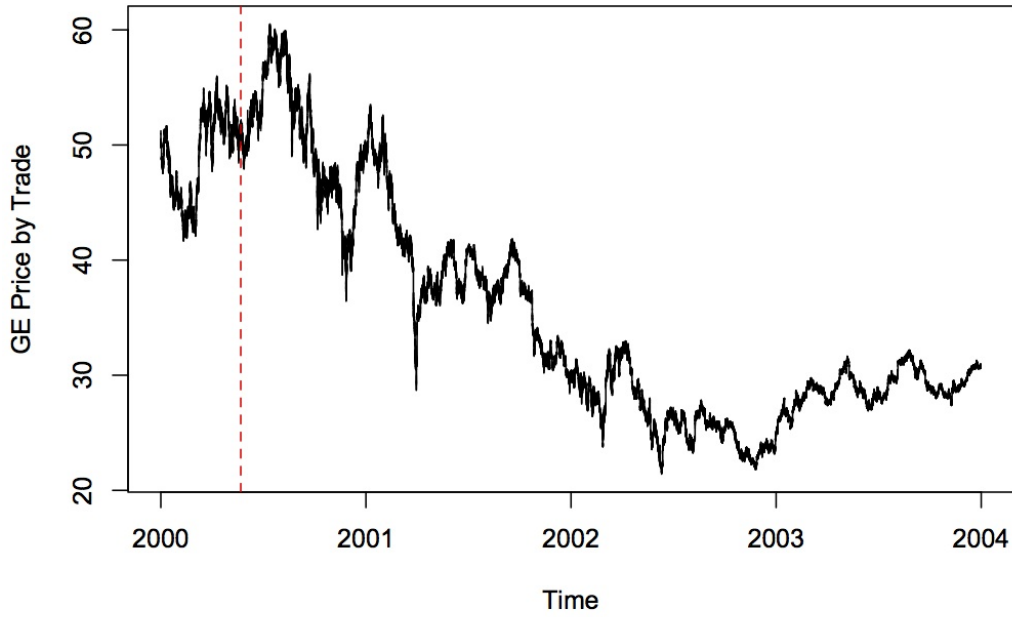


Figure 3.2: The fine-scale TAQ price for GE from the period 2000 to 2003

Table 3.1: GE TAQ Data: 2000 to 2003

Year	Trades	Trading Days	Average Trades per Day	Splits
2000	814,728	252	3,233	May 8 th – 3:1
2001	808,669	248	3,261	None
2002	1,307,249	252	5,188	None
2003	1,342,410	252	5,327	None

3.3 Methods and Results

3.3.1 Traditional Time Series Analysis

The first step in our analysis of GE was a simple visual inspection of the time series and its first difference. Figure 3.2 presented in the previous section shows the typical rough nature of financial data and what appears to be a strong downward trend from a high of \$60.50 until it levels out around \$30.00. There are also a couple of large changes in price that stand out, indicating the possibility of heavy tails in the underlying stochastic process. The plot of the first difference, Figure 3.3, gives a clearer picture of the size of the changes in the price and the volatility within the series. By visual inspection alone, we can see the volatility does not appear to be constant. The first difference does appear to have stabilized the mean, however, bringing the data closer to a stationary series.

When working with financial data, it is customary to investigate the log-returns. This practice functions as a normalization process that converts multiple assets to the same scale. The hope is that the transformed series $y(t) = \Delta \ln(P(t))$ will define a stationary stochastic process with more tractable dependency structure. We applied this transformation to the GE TAQ data, but as can be seen in Figure 3.4 the data continue to exhibit nonconstant variance and large jumps.

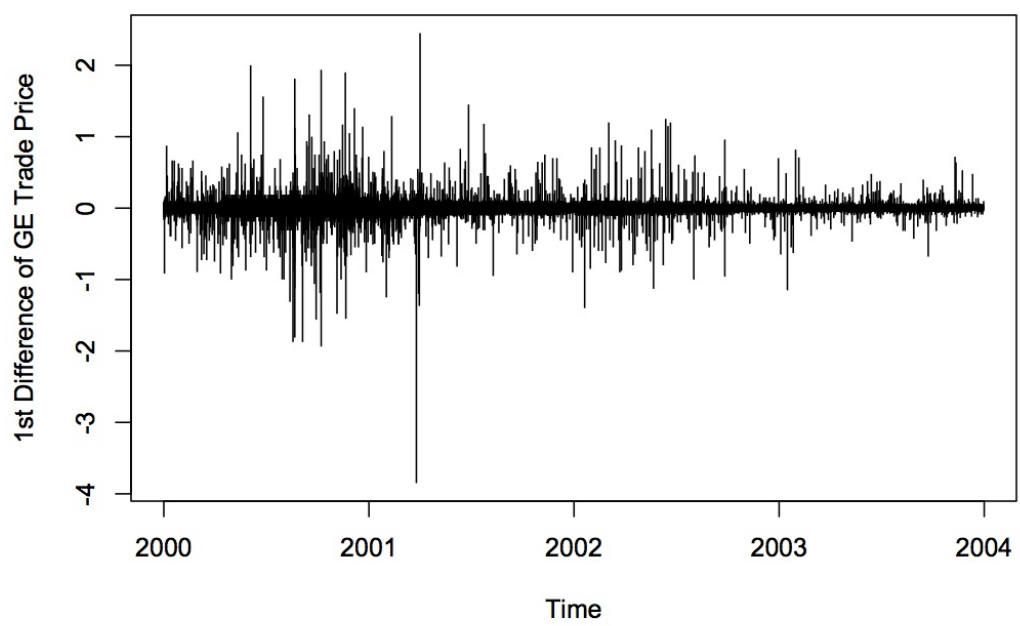


Figure 3.3: The first difference of the GE TAQ data

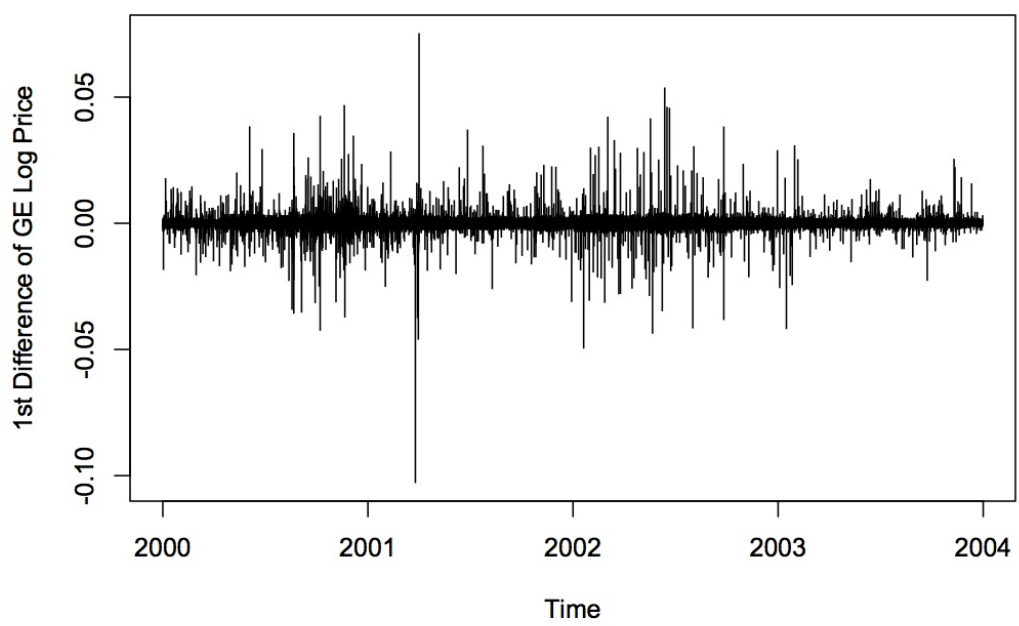


Figure 3.4: The first difference of the log-price GE TAQ data

The results of this simple visual analysis suggest that the data exhibit a time dependence in the mean that can be removed by detrending and a nonconstant variance that is not removed by taking log-returns. A reasonable choice for a model of this process might therefore be a GARCH model or an ARMA+GARCH model, but for illustrative purposes we also analyzed the autocorrelation function (ACF) and partial autocorrelation function (PACF) of the original data. As mentioned earlier, a useful heuristic for determining the parameters of an ARMA(p, q) model is to analyze these two functions together. A sharp drop off in the ACF at lag l suggests a moving average model of order $q = l$, while a sharp drop off at lag l in the PACF suggests an autoregressive model of order $p = l$. Figure 3.5 shows the ACF trailing off well beyond a lag of 60, while the PACF drops off around lag $l = 4$.

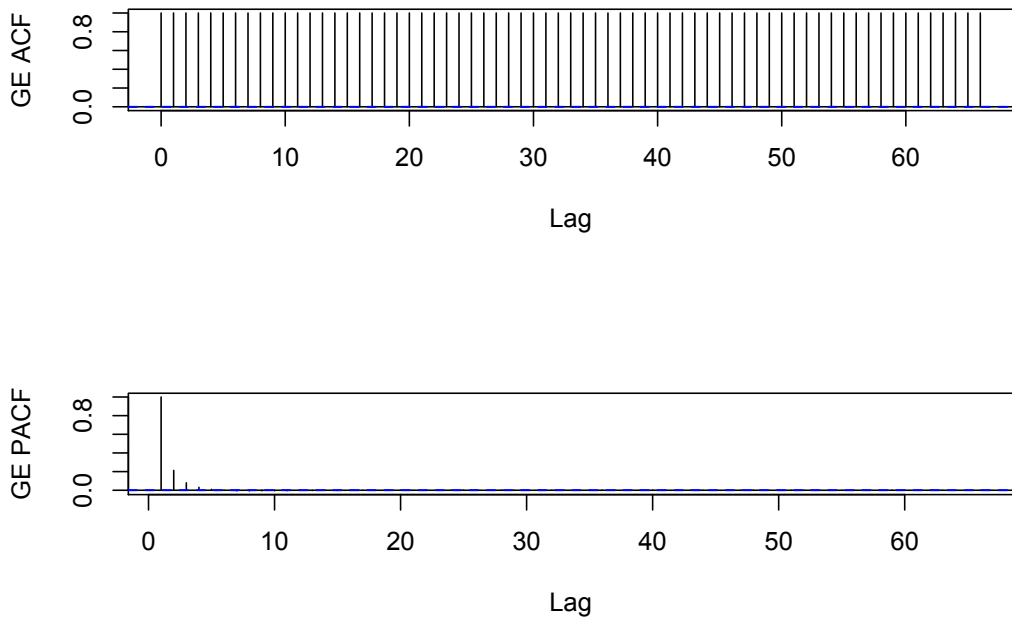


Figure 3.5: The autocorrelation function (top) and partial autocorrelation function (bottom) of the GE TAQ data

The ACF suggests the series is nonstationary, as it decays so slowly that the plot out to lag $l = 70$ does not appear to have begun to decay at all. However, the PACF reveals that much of the autocorrelation at longer lags is simply due to the autocorrelation at the shorter lags being carried over through the time series. The PACF filters out this “carry-over” correlation and thus reveals a much shorter memory. This

result strongly suggests an AR(p) model would be appropriate for this particular series where $p \leq 4$.

When fitting ARMA(p, q) models, it is good practice to minimize the values of p and q to avoid overfitting the data, which could lead to false confidence in the model. One technical heuristic for ensuring the correct values were chosen is to analyze the Akaike Information Criterion (AIC) of possible models, incrementing the values of the parameters systematically. Table 3.2 illustrates this process for fitting AR(p) models to the GE data for $p = 0, \dots, 4$. The AIC analysis shows a drastic improvement in the model fit from AR(0) to AR(1), but additional gains for AR(2) to AR(4) are dropping off rapidly, which suggests that $p = 4$ is certainly high enough for this autoregressive model and perhaps even too high.

Table 3.2: GE TAQ Data: Akaike Information Criterion for AR(p), $p = 0, 1, \dots, 4$

Parameter p	AIC(p)	100[Δ AIC(p)]%
$p = 0$	31,842,229	
$p = 1$	-20,953,846	-165.81%
$p = 2$	-21,209,901	-1.22%
$p = 3$	-21,252,219	-0.20%
$p = 4$	-21,260,093	-0.037%

The results of the above exploratory analysis illustrate the challenge of time series analysis, particularly in the field of finance. Our initial visual inspection suggests a nonconstant variance may be governing the underlying process and thus points to a GARCH model. But the heuristic for determining an ARMA model — coupled with a quick analysis of the change in AIC — suggests an AR(4) would be an appropriate description of the price path. In actuality, neither model proved to be a good fit for the GE TAQ data. The results of the AR(4) model suggested GE's price from 2000 to 2003 was described by

$$X_t = 0.731X_{t-1} + 0.159X_{t-2} + 0.068X_{t-3} + 0.043X_{t-4} + \varepsilon_t. \quad (3.1)$$

However, the Box-Ljung test on the residuals out to lag $h = 20$ indicates a p -value of less than 2.2×10^{-16} and therefore overwhelmingly rejects the null hypothesis that the residuals are i.i.d. random variables. The residuals from the AR(4) fit are plotted in Figure 3.6. Note the nonconstant variance of the residual plot and the occasional large deviations. To further illustrate the inadequacy of this model, we formed a Q-Q plot of the residuals. Figure 3.7 shows that while many of the quantiles fall in line with the assumption of normality, the tails of the residuals depart notably from those of the Gaussian.

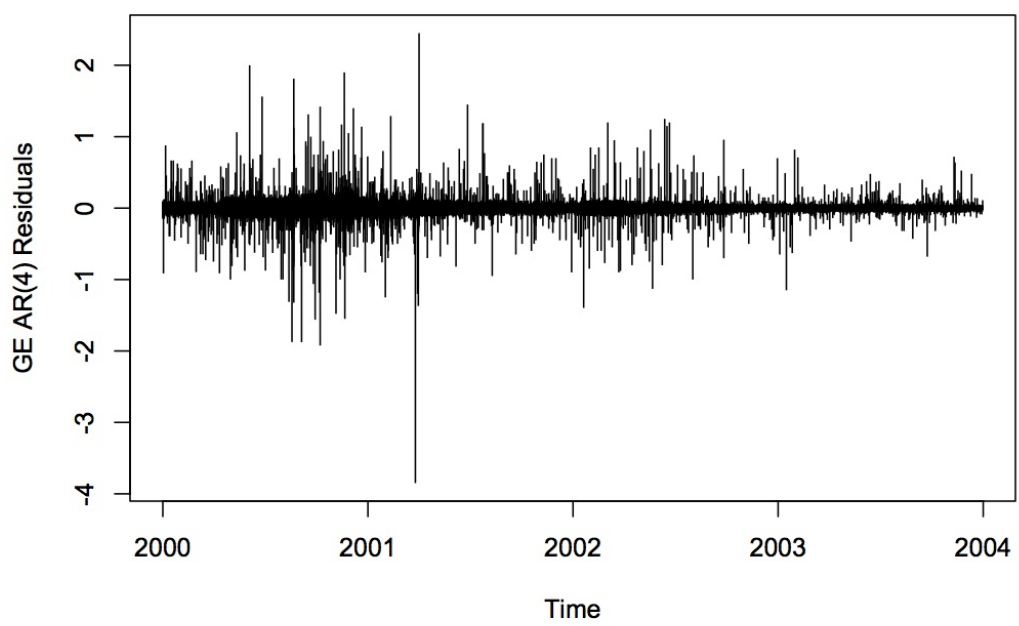


Figure 3.6: A time series plot of the residuals of the AR(4) model fit to the GE TAQ data

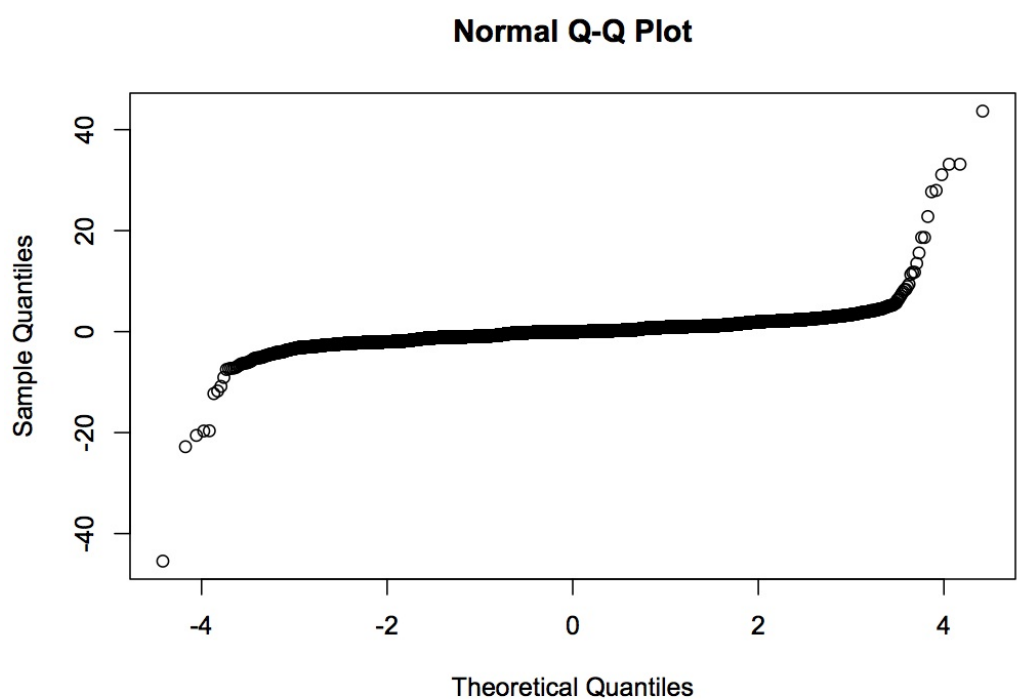


Figure 3.7: A Q-Q plot of the residuals of the AR(4) model fit to the GE TAQ data

The above conclusions are confirmed by the Pearson χ^2 goodness-of-fit test that resulted in a p -value $< 2.2 \times 10^{-16}$, indicating sufficient evidence exists to reject the null hypothesis that the residuals are i.i.d. normal random variables. Figure 3.8 shows a histogram (normalized to a density) of the residuals, revealing a leptokurtic distribution with very long tails. Note the minimum standardized residual is -191 and the maximum is 121 , while the mean is approximately 0 . The sample skewness and kurtosis of the residuals were -1.32 and 691.21 , respectively.

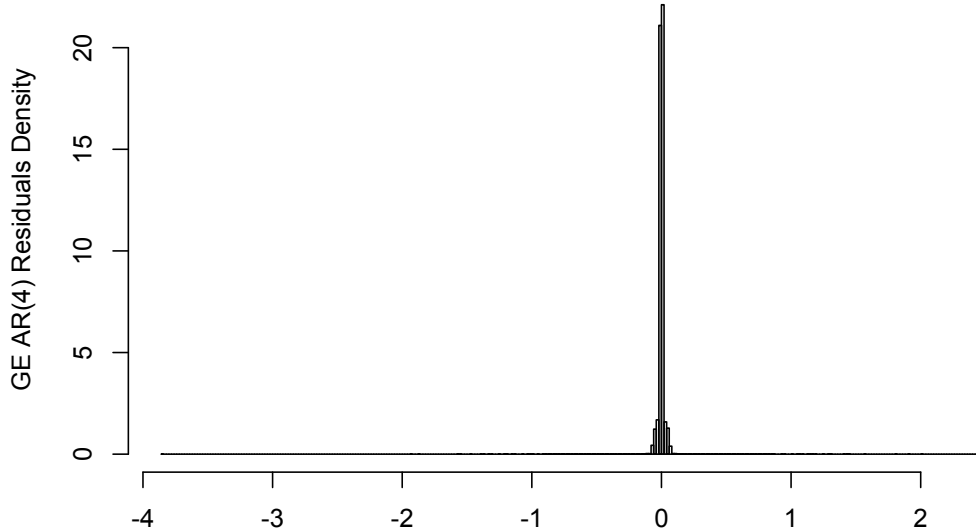


Figure 3.8: A histogram of the residuals of the AR(4) model fit to the GE TAQ data

Finally, analyzing the autocorrelation structure in the residuals of the AR(4) model (see Figure 3.9) reveals substantial partial autocorrelation, which again underscores its inability to capture the true nature of the GE data. Note how the PACF exhibits significant autocorrelation in the residuals well beyond lag $l = 40$.

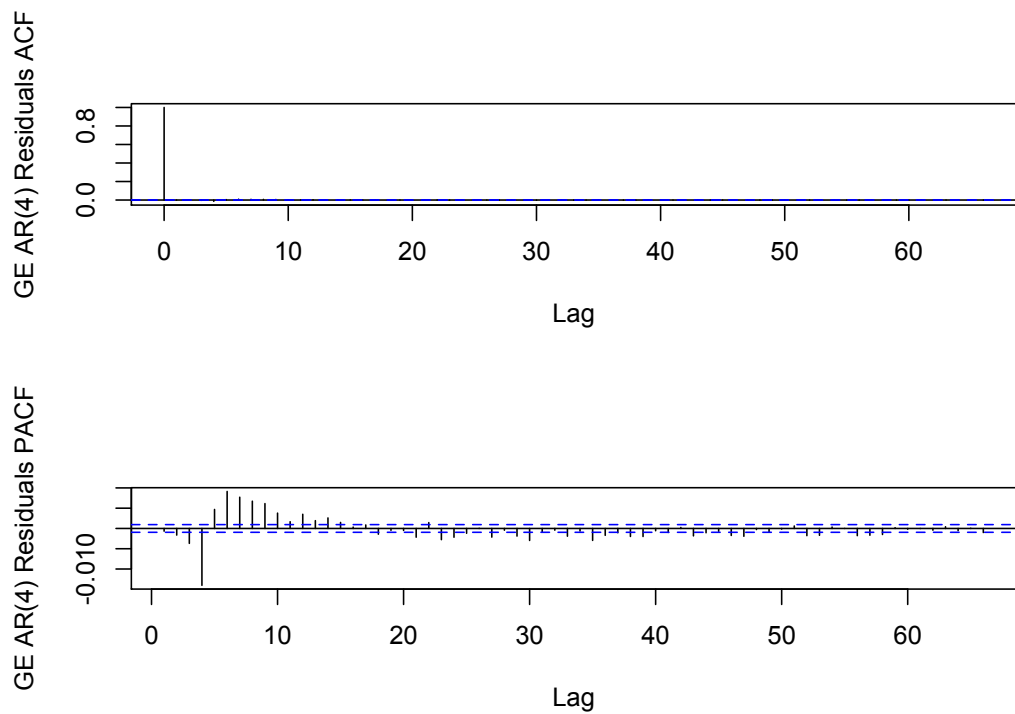


Figure 3.9: The ACF and PACF of the residuals of the AR(4) model fit to the GE TAQ data

The lack of fit from the AR(4) model is perhaps not surprising since we noted in our visual inspection that the data exhibited a nonconstant variance, suggesting a GARCH model or an AR+GARCH model might be more appropriate. But fitting a GARCH(1,1) model to the GE TAQ data produced similar results. Using the “fGarch” package in R, we see the results of fitting a GARCH(1,1) model to the GE TAQ data suggest the price from 2000 to 2003 had a conditional variance given by

$$\sigma_t^2 = 90.66 + 0.92\epsilon_{t-1}^2 + 2.98 \times 10^{-10} \sigma_{t-1}^2. \quad (3.2)$$

The p -value from the Box-Ljung test on the residuals of this model was again on the order of 10^{-16} , indicating a rejection of the null hypothesis that the residuals were i.i.d. random variables. Plotting the residuals from the GARCH(1,1) fit reinforces the Box-Ljung result, as there is an obvious drift and perhaps periodic nature evident in the trace of their path (see Figure 3.10).

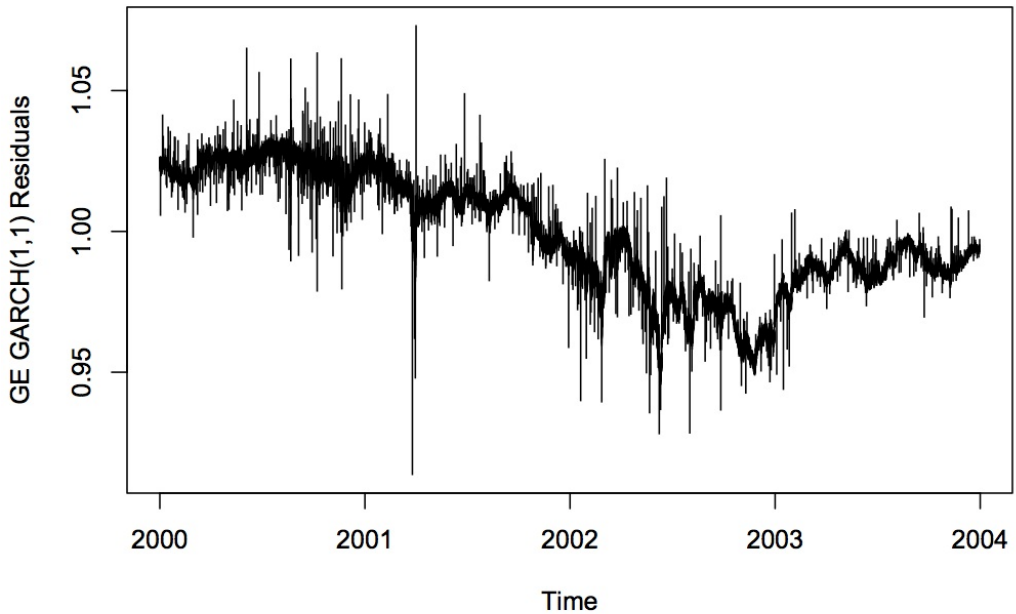


Figure 3.10: A time series plot of the residuals of the GARCH(1,1) model fit to the GE TAQ data

Examination of the histogram of the residuals from the GARCH(1,1) model also reveals a very different structure than the excessively peaked distribution of the AR(4) model. The skewness and kurtosis of the GARCH(1,1) residuals were -0.19 and 1.94 respectively. Figure 3.11 shows a bimodal

distribution for the residuals and thinner tails than we observed with the autoregressive model.

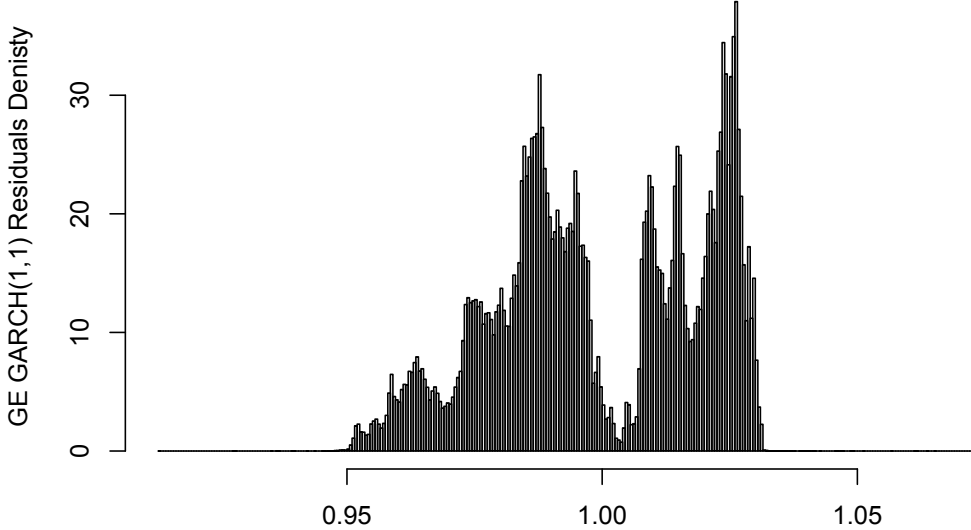


Figure 3.11: A histogram of the residuals of the GARCH(1,1) model fit to the GE TAQ data

Finally, we observe the ACF and PACF of the residuals from the GARCH(1,1) fit. From the results shown in Figure 3.12, we conclude the residuals possess significant partial autocorrelation out to lag $l = 30$, indicating the difference between the model and the true data is far from being simple white noise. Unfortunately, one interpretation of these results is that one model compensates for the problems of the other by introducing problems of its own.

Given the failure of the AR(4) and the GARCH(1,1) models separately, we took the exploratory analysis a step further and attempted to fit the log-returns with an AR(4)+GARCH(1,1) model. Unfortunately, given the size of the data set (and perhaps its complexity) the fGARCH package in R encountered a singularity error and was unable to fit the log-returns with the combined model. We systematically reduced the number of parameters in an attempt to avoid the singularity error, and even scrubbed the data to remove transactions that were made at the same price (i.e., zero returns). However, we were unable to obtain a combined model for log-returns, and thus attempted the combined model on just the log-prices.

We encountered similar difficulty in fitting an AR(4)+GARCH(1,1) model to the log-prices, but we

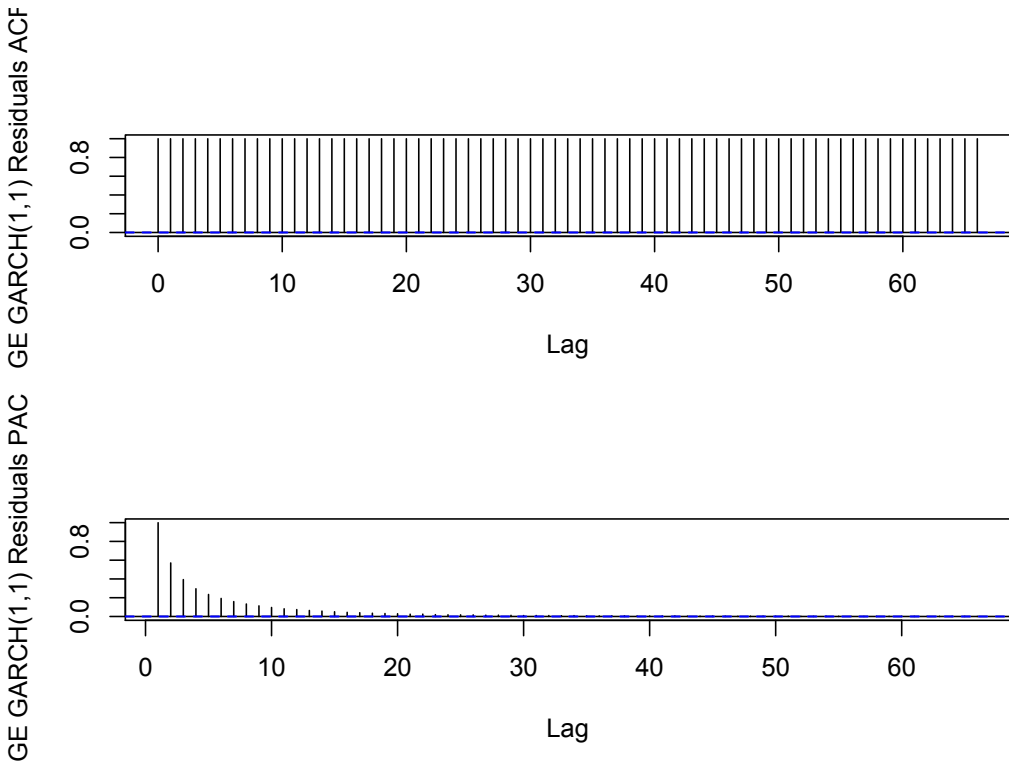


Figure 3.12: The ACF and PACF of the residuals of the GARCH(1,1) model fit to the GE TAQ data

ultimately obtained a model by reducing the parameters to an AR(2)+GARCH(1,1). This model also failed the standard goodness-of-fit tests. The Q-Q plot of the residuals from the combined model is shown in Figure 3.13 and the histogram of the residuals is shown in Figure 3.14. The skewness and kurtosis of the residuals of the combined model were -0.34 and 1.83 respectively.

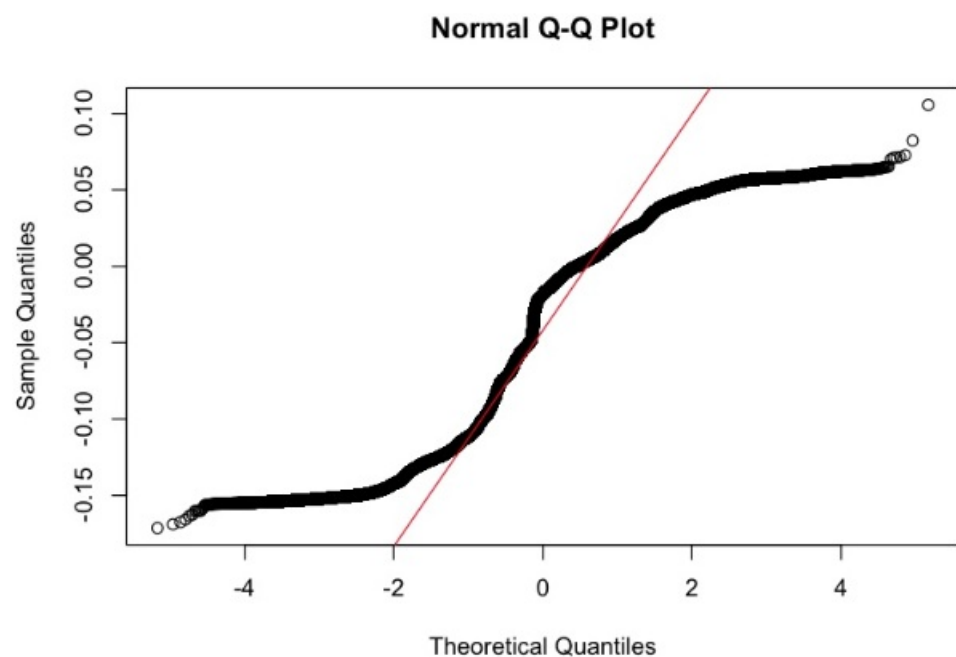


Figure 3.13: The Q-Q plot of the residuals of the AR(2)+GARCH(1,1) model fit to the log GE TAQ data

Log GE: AR(2)+GARCH(1,1)

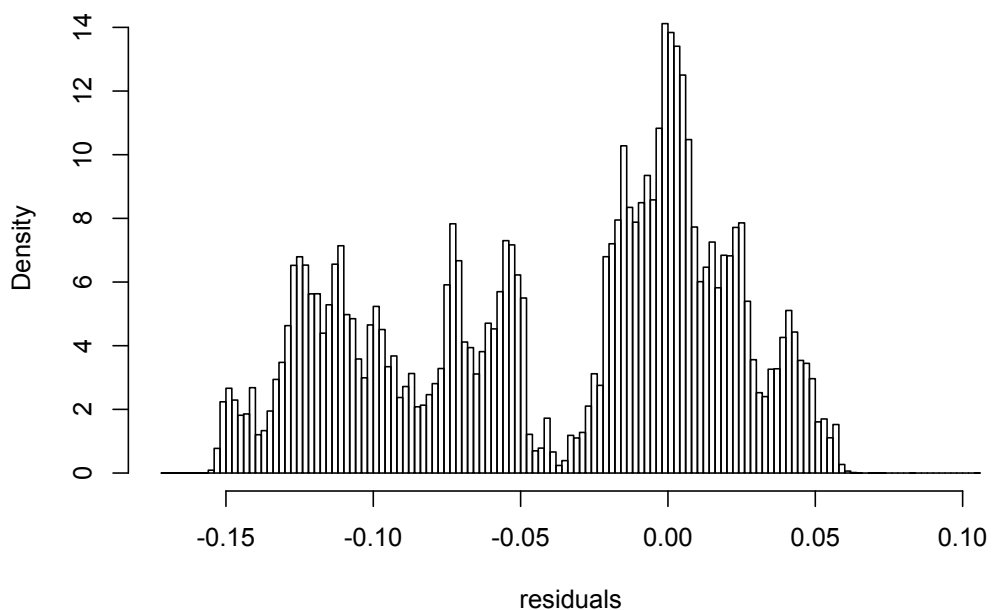


Figure 3.14: The histogram of the residuals of the AR(2)+GARCH(1,1) model fit to the log GE TAQ data

3.3.2 Multifractal Time Series Analysis

In addition to the traditional tests and models, we investigated the scaling properties of the GE data using MF-DFA. One advantage of multifractal analysis is that there is no reason to transform the time series with logarithms or other operations. The intent of multifractal analysis is to analyze the changes in fluctuations over different time scales, and thus the raw (i.e., undifferenced and unlogged) trades or the adjusted daily closing prices are all that is required [28]. The multifractal spectrum exhibited by the GE TAQ data is shown in Figure 3.15. Recall that the GE TAQ data consists of over 4 million data points, and the number of daily trades ranged from 3,000 to roughly 5,000. When performing MF-DFA we set $s_{\min} = 3,000$ and $s_{\max} = 400,000$, with increments of $\Delta s = 7,000$. This amounts to analyzing fluctuations in an interval of about one day all the way up to an interval of about six months in roughly two-day increments. We also allowed the moment order q to range from -5 to 5 . The spectrum peaks around $\alpha = 0.51$, indicating the dominant fluctuations in the process are similar to standard Brownian motion and are uncorrelated, but there is a wide spectrum ranging from $\alpha = 0.30$ to $\alpha = 0.70$. This indicates that large fluctuations, accentuated by positive q -values, tend to be antipersistent, while small fluctuations, accentuated by negative q -values, tend to be persistent and show long memory.

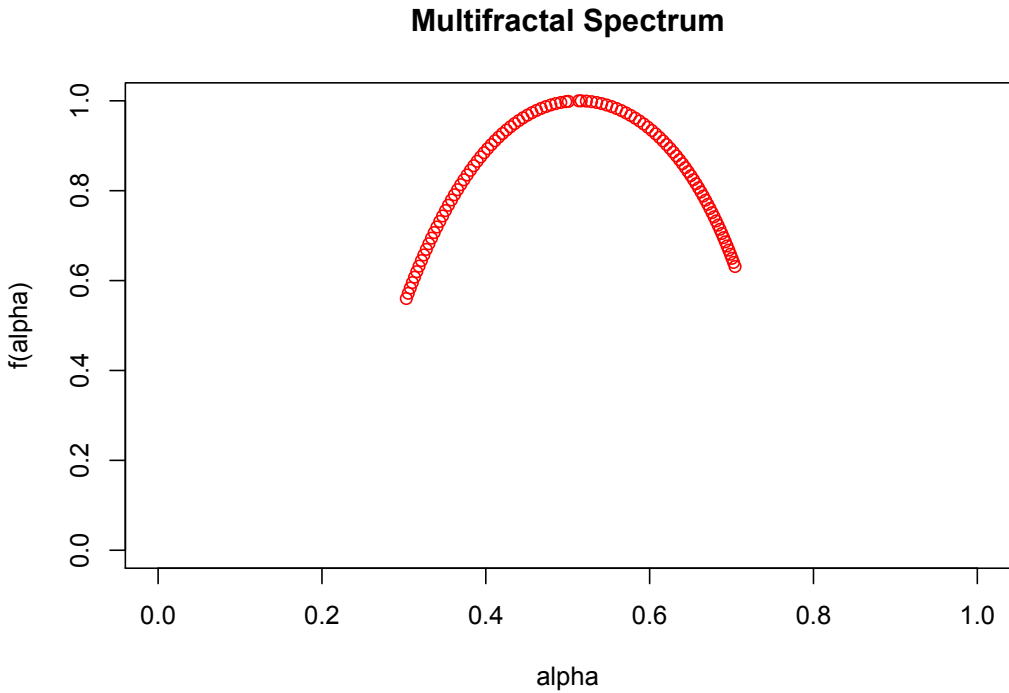


Figure 3.15: The multifractal spectrum of the original GE TAQ data

Employing the heuristic of shuffling the increments of a time series and analyzing the multifractal properties of the shuffled series reinforces our assertion that the small fluctuations exhibit long memory. The multifractal spectrum of the shuffled series is shown in comparison with the original GE TAQ multifractal spectrum in Figure 3.16. There is a notable change in the spectrum, as the shuffled series appears to be more monofractal, with most of its Hölder exponents clustered around $\alpha = 0.5$.

Finally, we simulated time series from the AR(4) model, the GARCH(1,1) model, and the combined AR(2)+GARCH(1,1) model produced by our earlier analysis and used MF-DFA to analyze their multifractal properties. All three models appeared more monofractal than the original GE data they are supposed to represent. The AR(4) model indicates a strong antipersistence, with the majority of Hölder exponents clustered around $\alpha = 0.25$, while the GARCH(1,1) model and the combined model both have Hölder exponents clustered closer to where the GE data multifractal spectrum peaks at $\alpha = 0.49$ (see Figure 3.17). However, they both fail to obtain the breadth of Hölder exponents seen in the GE data.

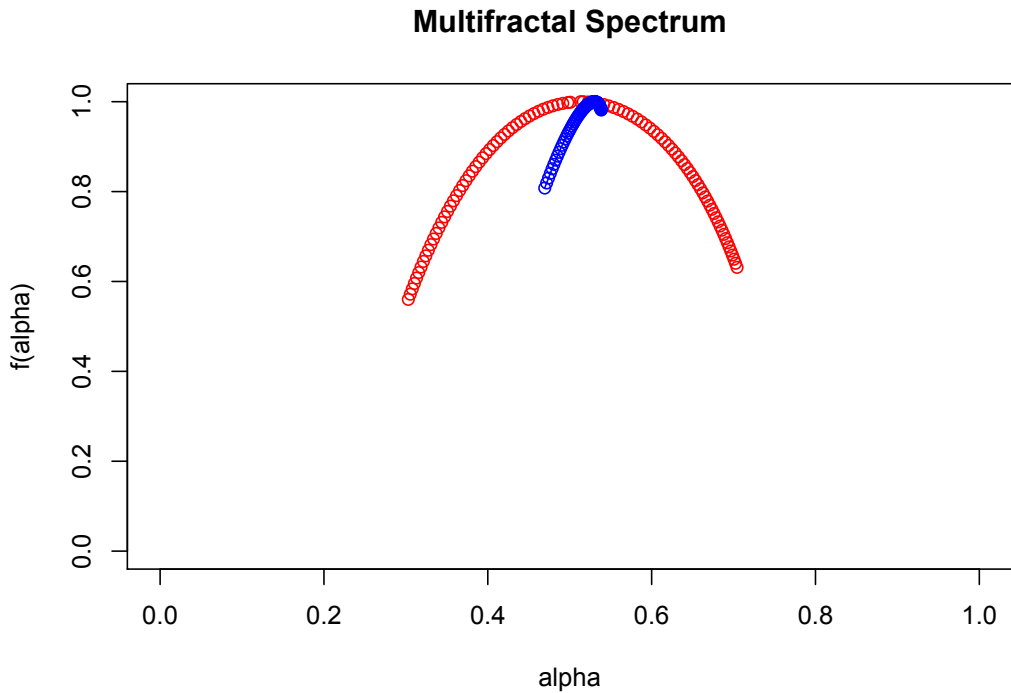


Figure 3.16: The multifractal spectrum of the GE TAQ data (red) and a shuffled version of the series (blue)

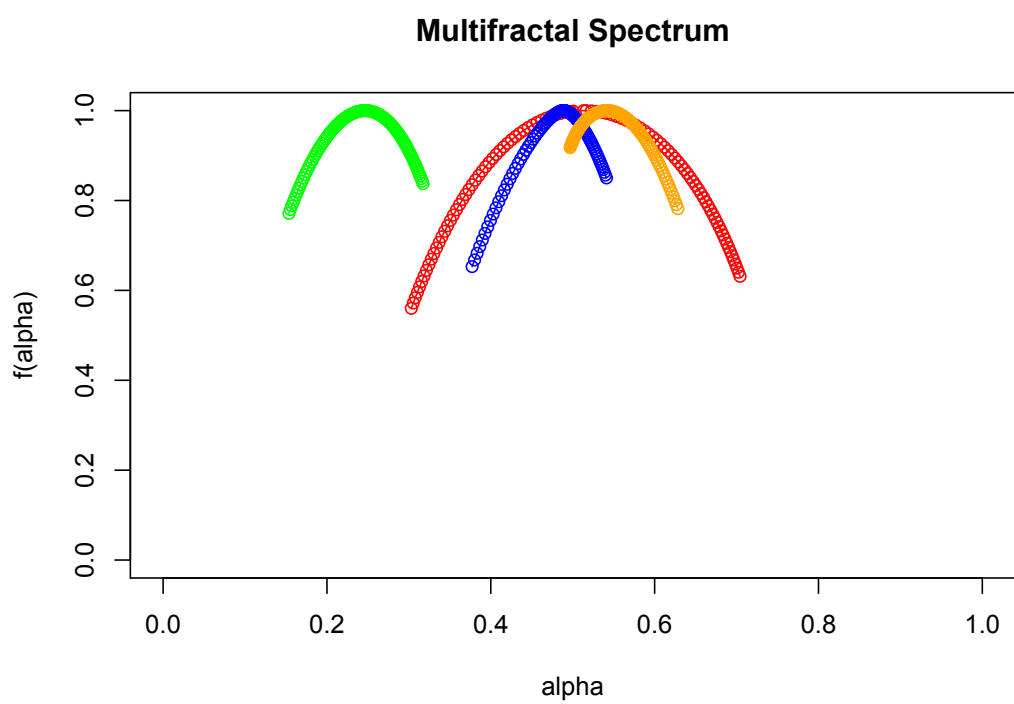


Figure 3.17: The multifractal spectra of the GE TAQ data (red), the simulated AR(4) data (green), the simulated GARCH(1,1) data (blue), and the combined AR(2)+GARCH(1,1) data (orange)

3.4 Discussion

During the twentieth century, economists relied heavily on Brownian motion to construct theoretical models of finance. The advantages of using Brownian motion stem from its foundation in the Gaussian distribution; and with advances in stochastic calculus and differential equations, it became a staple in models of empirical finance. The well-known Black-Scholes model for options pricing is a prime example of this application [23]. The Gaussian is a thin-tailed distribution such that a random variable sampled from it rarely exceeds six standard deviations from the mean. Even an extremely large number of such variables summed together fails to capture the erratic nature of some real processes like prices or log-prices of financial assets. Given that multifractal analysis has the ability to illuminate the underlying difference between a monofractal like Brownian motion and a considerably more diverse construction like the binomial measure, we contend it must find its place in financial theory. The obvious obstacle to this incorporation is the departure from the tractable closed-form mathematics associated with Gaussian measures. However, with advances in computer simulation, it is our belief that the impact of this obstacle can be minimized if not eliminated.

In the preceding analysis, we saw that traditional models applied to very fine-scale raw data tend to underestimate the multifractal properties of financial time series. What is interesting to note is the presence of both antipersistence and long memory in the GE TAQ data. This phenomenon underscores the concept of trading time. Small fluctuations might exhibit long memory, as they represent the normal fluctuations of a stock price on a slow news day. But large fluctuations exhibit antipersistence as groups of investors overreact and overcompensate to information they believe will have a more drastic impact on the asset's price. Although this is a convenient and plausible explanation for the properties we see in the GE TAQ data, it begs the question of whether it can be supported by empirical analysis or not.

The remainder of this dissertation introduces an application of multifractal analysis combined with agent-based simulation intended to investigate the source of multifractality in financial markets. Given that multifractal analysis can differentiate between monofractal and multifractal time series as well as illuminating the similarities (and lack thereof) in the underlying mechanisms driving a stochastic process, we believe MF-DFA can be employed to validate agent-based models of trading time and financial markets.

Chapter 4

Agent-based Modeling and the Zero-Intelligence Financial Market

4.1 Introduction

The fields of industrial engineering and operations research have long relied on discrete-event simulation (DES) as a tool for numerically analyzing a system. Many of the early applications of DES were in manufacturing, where flows through a process were the primary focus. Modelers quickly recognized that many systems exhibited flows analogous to manufacturing processes; and the use of DES expanded to areas such as transportation systems, call centers, hospitals and medical clinics, and military operations [46]. The challenge to the discrete-event modeler is to define the entire system in the context of a finite set of possible events that could change the state of the system. If the occurrence of each event can be reasonably modeled with a given probability distribution, then DES can be applied. The term *discrete-event* stems from the fact that these models only consider the points in time when events occur. This is handled by an event calendar that provides centralized control over the simulated environment [62].

In 1971, Thomas Schelling used a simulation to conduct thought experiments about sociology [69]. An important issue in his day was segregation in the United States. Schelling's simulation was thus an analysis of how intense the demand of members of one group to separate themselves from another needed to be in order to cause widespread segregation within the model. In this case, there were no set processes, flows, or queues. Each member of a group was capable of counting the number of his neighbors from the opposite group. When the quantity of opposite group members hit a preference threshold, the member would move to an area within his acceptable threshold.

Schelling's dynamic model of segregation is thought to be the first agent-based model [62]. The difference between his agent-based model and DES models was that Schelling focused on the individuals in the simulation and how their individual decisions created emergent effects within the context of the

whole model. The inputs did not require complex probability distributions to describe them — they consisted only of the relative quantities of each group and a set of rules or behaviors that each individual would follow. The output, on the other hand, was unexpected and complex in nature due to the number of individual decisions interacting to produce various degrees of segregation. For example, agents with relatively moderate preference thresholds requiring only a small percentage of their neighbors to be the same color can result in substantial segregation within the model.

Since Schelling’s model , the use of agent-based simulation has expanded considerably. Fields such as complexity science, the study of networks from supply chains to Internet traffic, and economics have all found uses for agent-based simulations [62]. Economics in particular has long been concerned with how the behavior of market participants and the structure of procurement processes affects the market at large. Agent-based modeling provides a powerful tool for building systems comprised of different behaviors interacting in a controlled environment, and thus an entire subfield known as agent-based computational economics (ACE) has emerged. Tesfatsion contends that ACE can serve four possible avenues of research [74]:

- empirical understanding of observed market regularities;
- normative understanding of how proposed policies or institutions will perform over time;
- qualitative insight and theory generation; and
- methodological and pedagogical advancement.

In this work, we pursue the first of these avenues by analyzing the construction of multifractal time series through an agent-based model. We begin with a prototype model based on Farmer et al. in which the agents possess “zero intelligence,” and the double auction order book is the driving factor in the market [26]. We adjust the distribution of the size of price offsets used by the agents in the model and analyze the impact on the price path and its multifractal properties.

The remainder of this chapter is organized as follows. In Section 2 we conduct a review of the literature on agent-based computational economics and zero-intelligence financial markets. In Section 3 we describe our zero-intelligence model structure and the behavioral logic of the agents. In Section 4 we present the results of the simulation and of the multifractal analysis of the output. We conclude in Section 5 with a brief discussion and an outline of the proposed avenues for future research.

4.2 Agent-Based Modeling Background and Literature Review

4.2.1 Applications in Economics

In general DES is most useful for systems that progress through time according to random factors that are reasonably represented by a given probability distribution, while the set of processes and relationships

between them remain constant [62]. The classic example is a manufacturing process involving a number of machines and assembly lines. Each station in the process may have any number of permutations handled by different configurations. The stations may experience machine failures, stockouts, long queues, scheduled maintenance, and shift changes. But ultimately the various parts manufactured, stations within the factory, and events that can change the state of each station are countable and finite. Even the most intricate processes of this nature can be reduced to a manageable set of events that can each be modeled by an appropriate probability distribution. The typical marketplace is rarely this deterministic. Fads based on new products, shocks related to world events, scandals involving company leaders, or outright criminal activity can drastically change the processes and relationships governing a market.

Economists originally built models based on the assumption that agents in the market behave rationally in an effort to maximize their expected utility when making decisions involving risk. However, in 1979, Kahneman and Tversky published their initial work on prospect theory [40]. Specifically they documented empirical contradictions to expected utility theory and offered prospect theory to explain their contradictory results. The basic idea of prospect theory is that decision making under risk is a two-step process where the individual first edits the prospects available and then evaluates the edited versions. Often this two-step process leads to contradictions to expected utility theory. Kahneman and Tversky noted that individuals would change their choice if the contradiction became evident, but that many situations did not allow the decision-maker to discover the inconsistency [40]. Since many economic models assume that agents rationally maximize their utility and are homogenous in their behavior, prospect theory had a profound impact on the field.

The typical economic benchmark for competitive market systems is a Walrasian equilibrium which, by the nature of its assumptions, must contain a market-clearing agent [74]. This theoretical agent ensures that demand and prices are optimal under expected value and that the aggregate supply is greater than or equal to aggregate demand. In the real market, this centralized agent does not exist. Instead the pricing process is governed by a decentralized collection of procurement processes created by market participants who randomly enter and exit the marketplace [74]. Tesfatsion notes that the challenge to any modeler trying to capture such a tumultuous environment involves, at a minimum, the issues of asymmetric information, strategic interaction, collusion, coordination failure, and the impact of market protocols enforced differently by different governments in a global economy [74].

Describing a real financial market with analytically solvable equations is likely to be an insurmountable task; and narrowing it down to a countable set of predetermined relationships and events is insufficient. Fortunately, agent-based simulations present us with new possibilities for modeling such environments. Since agent-based models are known to produce emergent effects that were never explicitly programmed by the modeler, some studies test the hypothesis that a Walrasian clearing agent emerges either from market structure, agent behavior, or a combination of the two. Gode and Sunder constructed a zero-intelligence model to determine if a double auction order book could produce “allocative efficiency” similar to Walrasian equilibrium [32]. They concluded that market discipline (i.e., the rules associated

with buying or selling) plays a significant role in producing a Walrasian clearing effect.

Gode and Sunder's model combined participatory agent-based modeling with computer simulation; that is, they used actual people who were instructed to follow a certain set of rules as their "intelligent" traders and computer agents for the zero-intelligence traders. In 2005, Farmer et al. conducted a similar experiment with an agent-based computer simulation [26]. They were able to show that market structure was a dominant factor in the variance of price spread and price diffusion rates of real assets from the London Stock Exchange.

Other studies have focused on the behavior of agents more than the structure of the market. Martin Lettau used boundedly rational agents and genetic learning algorithms to study mutual fund flows [51]. The performance of this model was consistent with Kahneman and Tversky's conclusion that people react asymmetrically to positive and negative returns. These early agent-based models focused on the existing theories (e.g. Walrasian equilibrium and prospect theory) and tried to gain some insight into market mechanisms that lead to results consistent with the theory.

Key aspects of real asset prices remain unexplained by macroeconomic theory. The issues of volatility clustering and heavy-tailed behavior are examples of empirical observations that cannot be explained by isolating a single factor [49]. Agent-based simulations incorporating coevolutionary features — where both unsuccessful agents and unsuccessful strategies are eliminated, while successful agents and strategies survive — have been shown to exhibit volatility clustering and heavy-tailed returns in the price paths they generate [47]. LeBaron notes that the results of his simulation actually overshoot empirical observations by generating too many large moves inside a particular volatility cluster and exhibiting heavier-tailed distributions in the returns [47]. However, this is an enormous improvement given that the biggest critics of early economic models stress how those models routinely underestimate risk [72]. In the next section we discuss the different approaches for implementing coevolutionary features into a simulation.

4.2.2 Behavioral Logic

Learning has been defined as "any relatively permanent change in behavior that occurs as a result of experience" [68]. The topic of learning is most often addressed by the field of psychology in the context of theories like classic conditioning, operant conditioning or reinforcement learning [11]. Brenner narrows the number of theories down to two: reinforcement learning and cognitive learning. In broad terms, reinforcement learning means actions resulting in reward are performed in the future with greater frequency, while actions resulting in punishment are avoided. Cognitive learning refers to a person's ability to reflect on their experiences and the experiences of others, and thus establish a preferred action in the event of a similar situation presenting itself in the future [11].

These theories of learning are typically modeled with some probability distribution for the possible actions the person might take. As time progresses the probabilities for each action are updated based on some reinforcement parameter or utility function. Common models are the Bush-Moesteller model and

the melioration learning model of Vaughan and Herrnstein [11]. These models require a mathematical formulation dependent on the utility function, which in turn leads to the issues and questions raised by prospect theory. Another reinforcement model is Bayesian learning, where conditional probabilities are established *a priori* and then updated after each outcome is known [39].

From the field of biology the concepts of selection, mutation, and evolution have been modeled as systems of differential equations that have been adapted into learning algorithms. Evolution typically involves the survival of fitter agents and the elimination of weaker ones. LeBaron programmed a model where fitness was determined by wealth, and thus periodically one of the least wealthy agents was removed and replaced in his virtual market [47].

Genetic algorithms involve the mutation from one set of economic choices or actions to another. These algorithms in turn have given rise to genetic programming, where the mutation involves formulae or program-like structures rather than simple choices [11]. The agents in LeBaron's model mentioned earlier also possessed a time-limited memory. Certain strategies or rules that had not been used in the last ten periods would be designated for replacement, thereby mutating the strategies in play [47].

Agent-based models provide us with a new approach to modeling complex and dynamic systems. Indeed, Epstein and Axtell suggested that the modeling question may change from “can you build it?” to “can you grow it?” [22] — the implication being that genetic algorithms, artificial intelligence approaches, and modeled learning can result in new processes and relationships that were never explicitly programmed by the modeler. These emergent effects are of critical interest when analyzing an agent-based simulation.

The tool of agent-based modeling is still relatively new; and as such, its place in economics and other well-established fields is not yet completely understood. Nevertheless, the ability of agent-based models to exhibit both stylized facts and empirical anomalies that theories cannot currently explain, underscores their value to researchers and practitioners. This raises the obvious next question of what tools are currently available to facilitate implementation? In the next section, we review a few of the software platforms available and illustrate the reasons behind our selection of MASON for this model [65].

4.2.3 Review of Available Software

The selection of an appropriate software platform is a critical decision in the modeling process. One option for the practitioner is to program the model completely in a programming language such as Java or C++. However, all simulations (including DES and agent-based) require the following capabilities implemented with a high degree of quality [46]:

- a random number generator;
- functions for generating random variates;
- functions for advancing simulated time;

- functions for synchronizing and controlling events;
- functions for collecting output statistics;
- functions for presenting results in graphical or text format; and
- functions for detecting error conditions.

Additional capabilities to consider might be the integration of the simulation into some larger software package and functions for inferring probability distributions from empirical observations. Specific to agent-based simulation platforms are the functions for representing physical space and movement within that space. While DES models typically handle geographic issues by modeling the interevent times, agents often need to be aware of their surroundings and to be capable of moving to different locations at will. Additionally, object-oriented programming is a convenient paradigm for agent-based models. Agents must contain their own logic and behaviors, and thus objects lend themselves naturally to agent representation [62].

A number of “framework and library” platforms have thus emerged to provide researchers with some of these common tools needed for agent-based models [65]. The four most commonly used platforms are Swarm, Repast, NetLogo, and MASON [65]. Each of these platforms has advantages and disadvantages and thus each may be appropriate or inappropriate for a given model. Swarm was one of the first such platforms and is generally well regarded. However, Railsback et al. note that Swarm is difficult to learn and implement quickly due to its foundations in the Objective-C language [65]. NetLogo is typically recommended for novices, as it was originally designed as a teaching tool. Researchers with more experience in simulation and those seeking more control over the programming environment, however, may find NetLogo to be oversimplified. Repast and MASON are newer platforms. Both are built with the Java programming language and exploit the object-oriented paradigm accordingly. All these platforms utilize the Mersenne Twister random number generator and have some functions for analyzing output as well as generating random variates from the commonly used distributions.

When deciding which of these packages to use for this dissertation, we concluded that the driving factors were the issues of computational speed, flexibility, control, and integration with other tools such as MF-DFA. One advantage of MASON is the separation of the simulation from the visual representation of the model. Having these two aspects linked is an artifact of social science endeavors — such as Schelling’s original segregation model— where visualization of agent movements is the primary output. This dissertation is concerned with analyzing the price path of a financial asset, and visualizing the agents is less important. In today’s financial markets, orders are placed remotely, e.g., by computer programs or people interfacing with a web site. Their physical movements are thus less important, even though their relationships to each other are critical.

MASON is ideal for our purposes because it provides the core functions needed to build an agent-based simulation while maintaining a high degree of flexibility in the type and size of model that can

be built. MASON’s foundation in Java means that we can access the wide array of Java libraries to program the MF-DFA algorithm and have the flexibility to integrate MF-DFA directly into the simulation. MASON was intended to be fast, transferable across multiple computing platforms, and efficient enough to support up to a million agents [52]. And many of the criticisms noted by Railsback et al. in 2006 have since been addressed, notably the documentation available and the library of functions for generating random variates [65]. Some of the drawbacks to this selection include the extensive knowledge of Java required to implement the MASON platform and the lack of GUI-oriented design tools familiar to most DES modelers. Although these drawbacks certainly increased the time required to build the initial model, we believe the finished product is higher quality because of the flexibility and control that MASON provides. The next section presents more details on the zero-intelligence models, illustrating a new approach to the rationality problem that builds towards a coevolutionary model.

4.2.4 Zero-Intelligence Financial Markets

As mentioned earlier, Gode and Sunder conducted a study to determine the source of market efficiency and the Walrasian equilibrium. They compared two double auction order book models; the first consisted of graduate students who were instructed to maximize their profits, and the second consisted of computer programs that placed orders at random [32]. They concluded that market discipline — i.e., the double auction order book — was the primary reason for efficiency in markets. Although they cited a number of interesting implications of this finding, the most profound is that market structure may have the ability to override any effects of irrational behavior by agents on a microlevel and thus create a macrolevel Walrasian equilibrium. They conclude by stating that Adam Smith’s invisible hand may be embodied by market structure creating aggregate rationality from individual irrationality, i.e., an emergent effect [32].

Farmer et al. go a step further, attempting to calibrate the zero-intelligence model to the rates of order placement and cancellation observed on the London Stock Exchange. Their study focused on the average spread between bid prices and ask prices, as well as the price diffusion rate, defined as the size and frequency of increments in the random walk governing the price. They describe this approach as a deconstruction of the standard rationality-based problem into two parts; the first is understanding the impact of order flows on a structured market, and the second is explaining why the order flows vary (i.e., agent behavior). By comparing the rates of order placements, they were able to quantify how patient or impatient traders were and then quantify the impact of that level of patience on the market. In general, they reinforce the findings of Gode and Sunder that market efficiency may be largely determined by the rules of the double auction order book, but they add the analysis of changes in volatility due to the relative amount of patience and impatience in the market. These results have far-reaching implications for policy makers trying to control volatility and market practitioners trying to hedge against losses. Farmer et al. note that future research should incorporate more agent intelligence to better represent the correlation and price-dependence of order flows, and eliminate the arbitrage opportunities that are allowed by their

simplified market structure [26].

In the sections that follow we construct an agent-based financial market similar to those described above. Farmer et al. defined price diffusion D by the relationship

$$V(t) = Dt, \quad (4.1)$$

where $V(t)$ is the variance of the random walk of the price at time t . Multifractal analysis investigates this relationship, as well as the moments of order $q \in \mathcal{Q}$ that determine the set of Hölder exponents observed in the process. We first describe the model and the logic governing the agents. We then analyze the model output using traditional time series approaches. Finally we analyze the impact that the distribution underlying the price offsets for a limit order has on the multifractal properties of the price path.

4.3 The Model

4.3.1 Continuous Double Auction Structure

Our model is loosely based on the zero-intelligence model of Farmer et al. [26]. The basic premise for the zero-intelligence models is that market structure, rather than agent behavior, is the dominant factor in price movements. In this case, the market structure is represented by a continuous double auction order book. That is, traders can place either buy or sell orders, and they can place these orders at any time.

Using the terminology from Farmer et al., we define a limit order to be an order placed with a price that does not currently meet the best price being offered [26]. In the case of a buy limit order, this means the current best sell price is higher than the limit order's bid price. In the case of a sell limit order, the opposite is true. Since the limit order terms cannot be immediately met or "crossed," the limit order is placed in a best-price-first queue. Ties in the queue are broken on a first-come-first-serve basis. At time t , the lowest selling price $a(t)$ is the best price in the ask-order queue and the highest buying price $b(t)$ is the best price in the bid-order queue. These values are known as the boundary conditions for new limit orders. At time t , the bid-ask spread $s(t)$ is defined as the difference between the best ask price and the best bid price, $s(t) = a(t) - b(t)$. When new orders arrive, any orders that are crossed are immediately executed, and the bid-order and ask-order queues are reorganized as necessary to ensure the best buying and asking prices are first in their respective queues. Limit orders are placed by "patient" agents who are theoretically willing to wait for the market to meet their price thresholds.

Impatient agents, by contrast, are not willing to wait and therefore place market orders instead of limit orders [26]. Market orders cause an immediate transaction. That is, buy market orders execute at the current best asking price and sell market orders execute at the current best bid price. Market orders thus create an immediate ripple in the price process as they clear the current best price, thereby changing the boundary condition for new limit orders. Market orders and limit orders are one representation of behavior in the zero-intelligence model. Patient agents place only limit orders according to a Poisson

process. Impatient agents place only market orders according to another independent Poisson process. Orders of both types expire according to a third point process whose event times are derived from a Poisson process that is embedded in the order-generating process. The order expiration interevent time is set when the order is created by the patient agent, thereby making it dependent on that agent's limit-order Poisson process. In our simplified double auction order book, all orders consist of one share of a single asset. The limit order price is constructed by offsetting the current best price (ask or bid) by a random variable independently generated from a selected distribution. Offsetting the current best price ensures that $a(t)$ and $b(t)$ create boundary conditions for new limit orders. Figure 4.1 illustrates how the order book queues limit orders as they arrive.

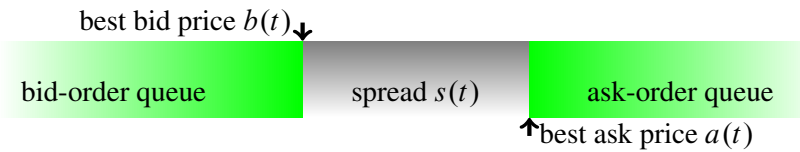


Figure 4.1: Double auction order book bid and ask queues

In our prototype example, we arbitrarily choose to have 50 patient agents and 50 impatient agents. Patient agents have fields for storing the next buy time and the next sell time. Each agent is instantiated and scheduled for time $t = 1$ when the simulation is started. Then each agent generates an exponential interarrival time for its next buy and sell orders, and schedules itself to place these orders accordingly. Each time thereafter when an order is placed, a future order of the same type (buy or sell) is scheduled and the order expiration time is scheduled. Setting the price for new limit orders amounts to generating a random value Δ_p with which to offset the appropriate boundary condition. That is, for sell orders the limit order price is set to $p = b(t) + |\Delta_p|$ and for buy orders the limit order price is set to $p = a(t) - |\Delta_p|$, where the distribution of Δ_p and its impact on the multifractal properties of the price path are the subject of this study. To ensure a level of reality in the price process, limit orders with a negative price are not allowed to enter the the best-price queue. The choice of distribution is predicated on stressing the discipline enforced on the market by the double auction order book. Since limit orders are arranged in the bid-order and ask-order queues according to the best-price-first queuing discipline, the market structure is such that large ask orders and small bid orders are rarely satisfied by incoming market orders. As Farmer et al. note, the prices placed well outside the bid-ask spread will ultimately expire before they are ever cleared. In contrast, those closer to the spread will be cleared more readily as market orders cause shifts in the current best prices [26]. Using a thin-tailed distribution for Δ_p would mean that all limit orders would have a price close to the spread (say, within six standard deviations); and thus the market

discipline would be difficult to distinguish from the general trend of the price offsets.

Figures 4.2 shows our conceptualization of the double auction order book network. The central square is the double auction order book, and the graph of nodes and edges connects the 50 patient traders and 50 impatient traders to the order book. The model was constructed using the MASON agent-based modeling framework [52]. As previously mentioned, the network connections in a financial market are typically virtual in today's world of advanced communications. However, using visual displays like Figure 4.2 gives us access to MASON's built-in *inspectors*, which include tools like time series charts and histograms.

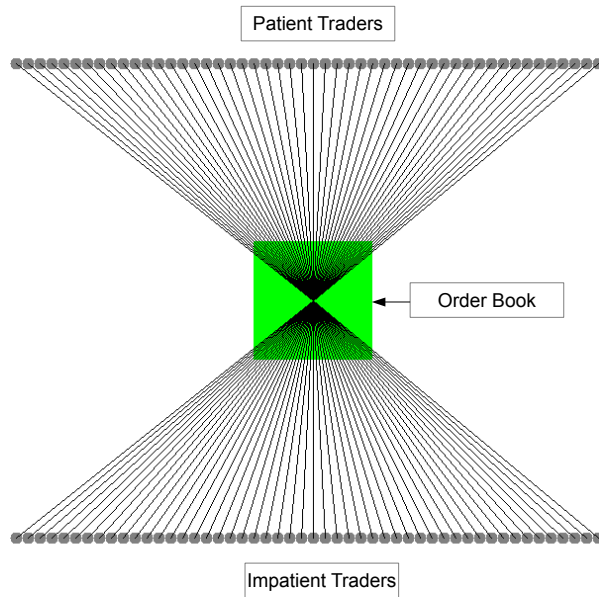


Figure 4.2: Double auction order book with 50 patient agents (top) and 50 impatient agents (bottom)

4.3.2 Experiments

The zero-intelligence model is one of the simplest approaches to artificial stock markets, but it still contains enough parameters to facilitate hundreds of different studies. The impact of each individual rate, the interaction of all the rates, the ratio of patient to impatient agents, the queueing discipline of the order book, and the distribution of order price offsets could all be considered in their own right. Given our interest in multifractals and the fact that multifractal properties are often induced by heavy tails, we narrowed our focus to the distribution of the price offset Δ_p . The basic question under study is whether the market structure paired with different distributions of price offsets in limit orders produces multifractal properties in price paths.

The claim by Farmer et al. is that zero-intelligence models, properly calibrated to empirically observed rates of order placement, produce a good approximation to the price diffusion rate observed in actual price paths [26]. Recall from Equation (4.1) that the diffusion rate D is a measure of how the variance changes with the interval of time. This metric can be derived through detrended fluctuation analysis (DFA) of Peng et al. [64], where the entire time series is assumed to be governed by a single Hurst exponent. However, we showed in the previous chapter that many financial time series exhibit a spectrum of Hölder exponents that give way to more erratic price paths and the possibility of extreme events. Thus, we propose that MF-DFA may be more appropriate for validating an agent-based financial market against empirical data. Farmer et al. also note that a heavy-tailed distribution for Δ_p will accentuate the impact of the double auction order book, while a thin-tailed distribution will mask the market discipline. It is thus of interest to see how the presence of thin or heavy tails in Δ_p will change the multifractal spectrum of the price path.

To investigate the impact of Δ_p on the zero-intelligence model we chose the Pareto distribution and the Normal distribution to drive the offset random variable. The cumulative distribution function of the Pareto is given by

$$F(x) = \begin{cases} 1 - (x_{\min}/x)^c, & \text{for } x \geq x_{\min}, \\ 0, & \text{if } x < x_{\min}, \end{cases} \quad (4.2)$$

where $x_{\min} > 0$. It can be shown that if $0 < c \leq 1$, then the Pareto distribution fails to have a finite mean; and for $c \in [1, 2)$ it fails to have finite variance. Bearing this in mind, we chose $c = 1.1$ for our simulation. This means the offset Δ_p has a finite mean, but an infinite variance—i.e., very heavy tails. In contrast we chose the $\text{Normal}(0, 1)$ distribution for Δ_p to represent the thin-tailed run of the simulation. Since the Gaussian is two-sided, we took the absolute value of the random variate generated to serve as the offset Δ_p ; and in this case the offset Δ_p has a folded normal distribution, which is easily seen to be light-tailed.

In the following experiments with light- and heavy-tailed distributions for Δ_p , we generated time

series $\{x(t) : t = 1, \dots, N\}$ of length $N = 543,883$ for the resulting trading prices. Since we deliberately chose two extreme distributions for the parameter Δ_p , the impact on the price path is profound, as shown in Figures 4.3 and 4.4 below. In the next section we apply the standard time series analysis techniques to these data sets, as well as multifractal analysis.

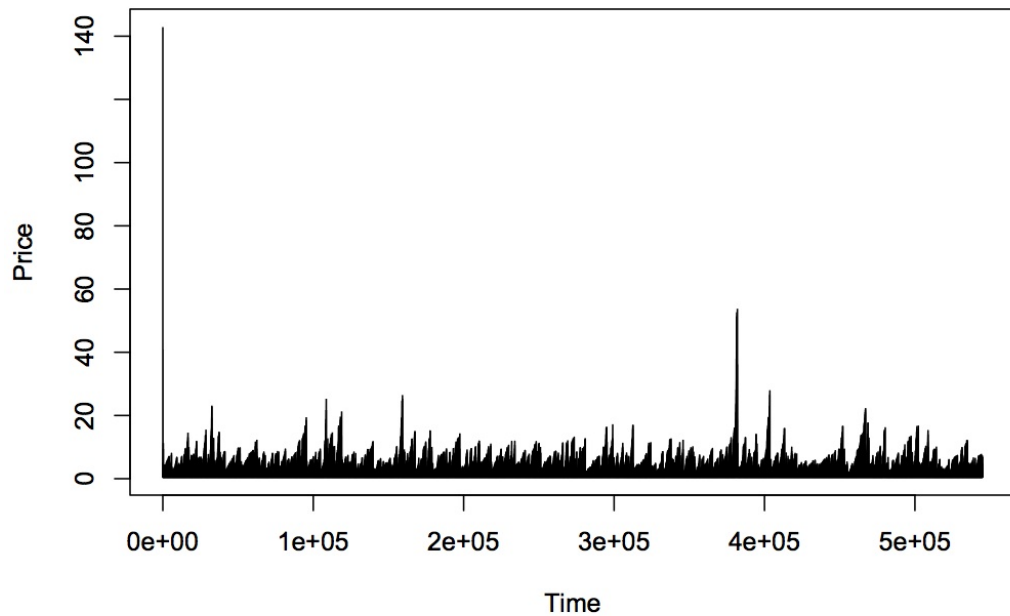


Figure 4.3: Zero-intelligence price with heavy-tailed price offsets Δ_p

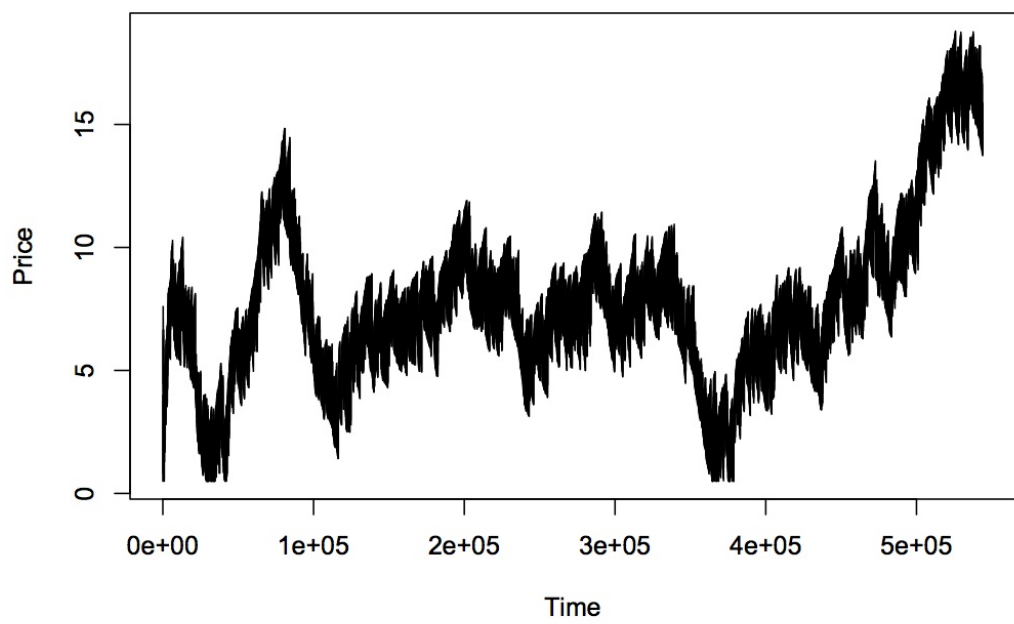


Figure 4.4: Zero-intelligence model with thin-tailed price offsets Δ_p

4.4 Results

4.4.1 The thin-tailed simulation

Acknowledging that these are deliberately extreme results, we seek to assess the ability of agent-based financial markets to reproduce various stylized facts observed in real financial data. Starting with the thin-tailed experiment, we note from Figure 4.4 that the price path could feasibly represent a real asset. There are 543,883 data points ranging from a low of \$0.50 to a high of \$18.79 per share. There are long periods of increase and decline, but on a finer scale there are many small fluctuations. Inspecting the first difference of the series suggests that white noise may be governing the trade-to-trade fluctuations (see Figure 4.5), as the differenced series appears to be weakly stationary.

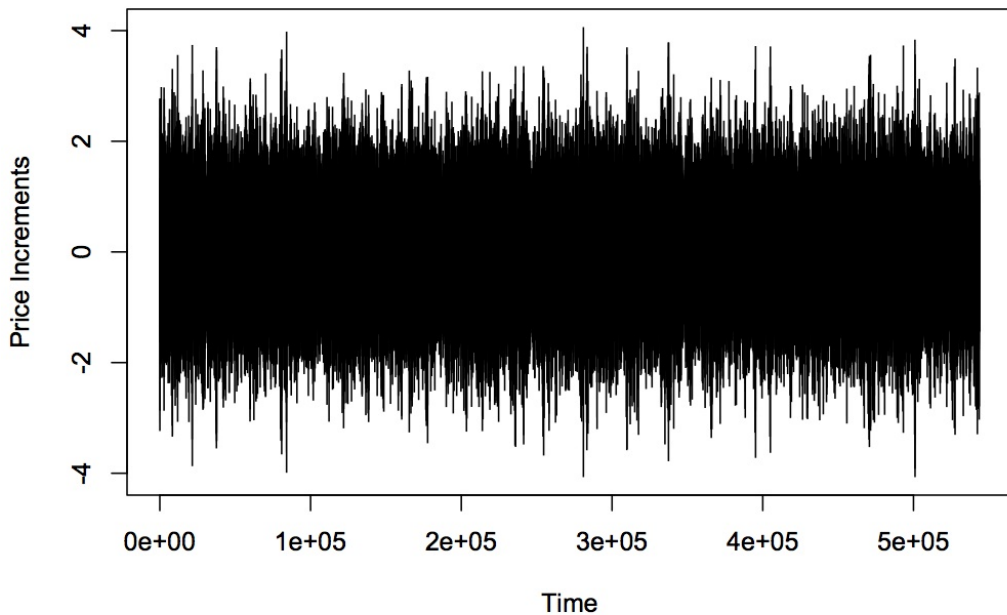


Figure 4.5: The first difference of the thin-tailed simulation

Both the autocorrelation and partial autocorrelation functions of the original series decay very slowly with lag l . Given the first difference appears to be weakly stationary, we analyzed its autocorrelation structure, shown in Figure 4.6. The sharp decline in the ACF coupled with a slow decline in the PACF indicates that a moving average may best describe the transformed data set.

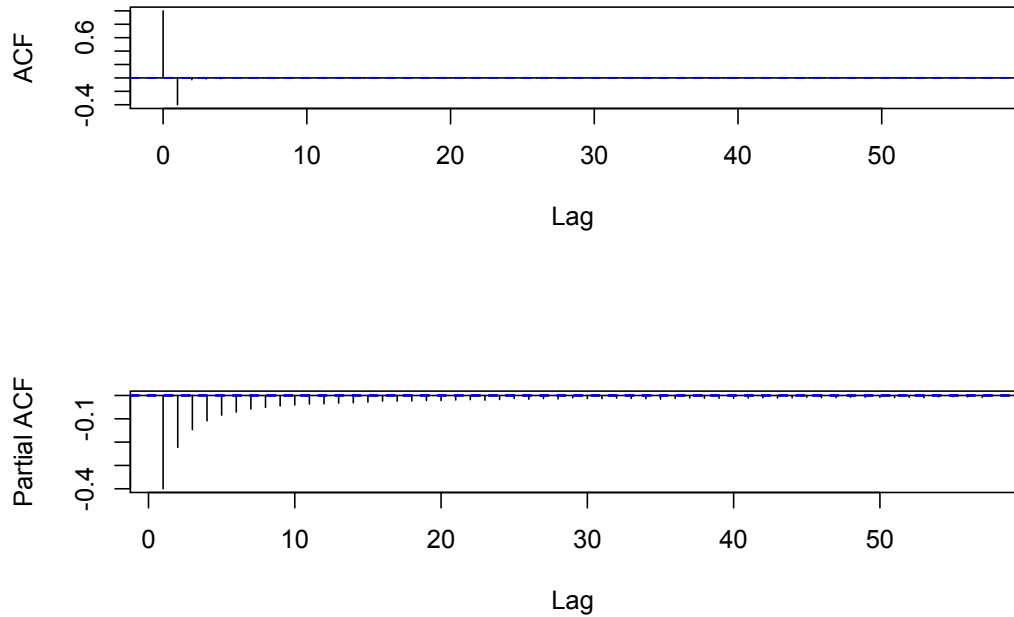


Figure 4.6: The ACF and PACF of the first difference of the thin-tailed simulation

Since the ACF cuts off sharply at lag $l = 2$, we fit a moving average MA(2) model to the first difference of the price path. However, the resulting model was not statistically a good fit for the data. The Box-Ljung-Pierce lack-of-fit test indicates there is not enough evidence to conclude that the residuals are i.i.d. random variables. However, the histogram of the residuals sheds some light on why this might be the case (see Figure 4.7). The structure of the double auction order book is such that the price changes will rarely be exactly zero. From one time step to the next, traders are shifting the bid-ask boundary conditions, thus causing most changes to be around zero, but never exactly zero. This creates the bimodal histogram observed in the residuals.

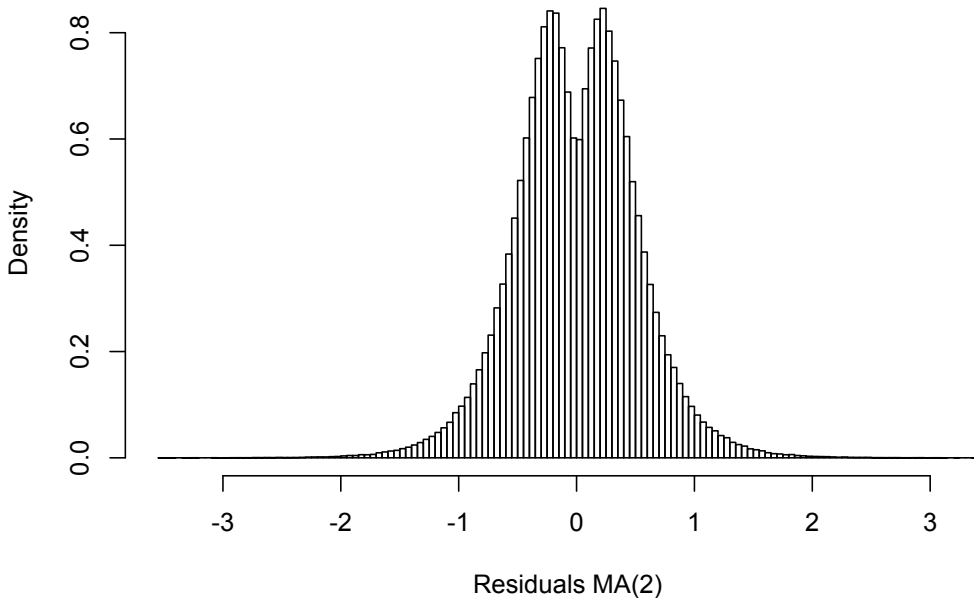


Figure 4.7: Histogram of the residuals from the MA(2) model of the thin-tailed simulation

Finally, we observe the QQ-plot of the residuals in Figure 4.8. The plot deviates enough from the predicted line (shown in red) to conclude the residuals are not standard normal random variables. However, the tails do not seem to be the reason for this deviation. Given that our price distribution for Δ_p is known to be Gaussian, we can conclude that market discipline, along with the other parameters such as order rates, combine to create an erratic price path that is poorly described by autoregressive-moving average techniques.

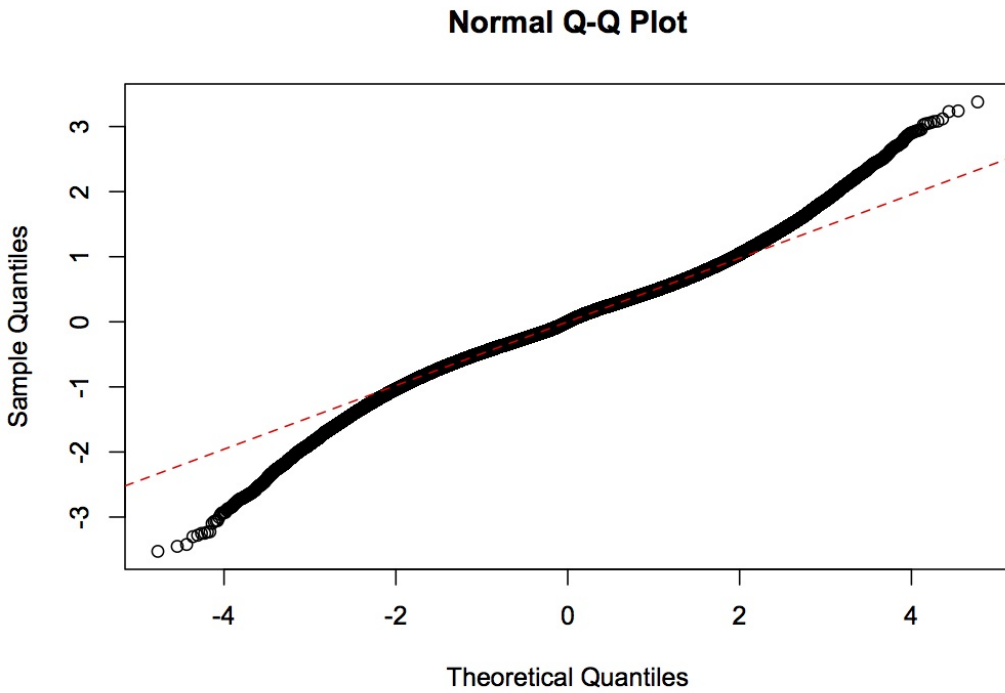


Figure 4.8: QQ-Plot of the residuals from the MA(2) model of the thin-tailed simulation

4.4.2 The heavy-tailed simulation

We proceed in a similar manner for the heavy-tailed simulation. As predicted, we observe wild swings in the price as it ranges from less than a dollar to over \$140. The first difference also reveals clusters of volatility have been induced by the heavy-tailed distribution coupled with the market discipline of the order book (see Figure 4.9). However, the clusters appear to follow a very antipersistent pattern, as large positive changes are quickly followed by large negative changes. This clustering of volatility strongly suggests a GARCH model would be appropriate for this series.

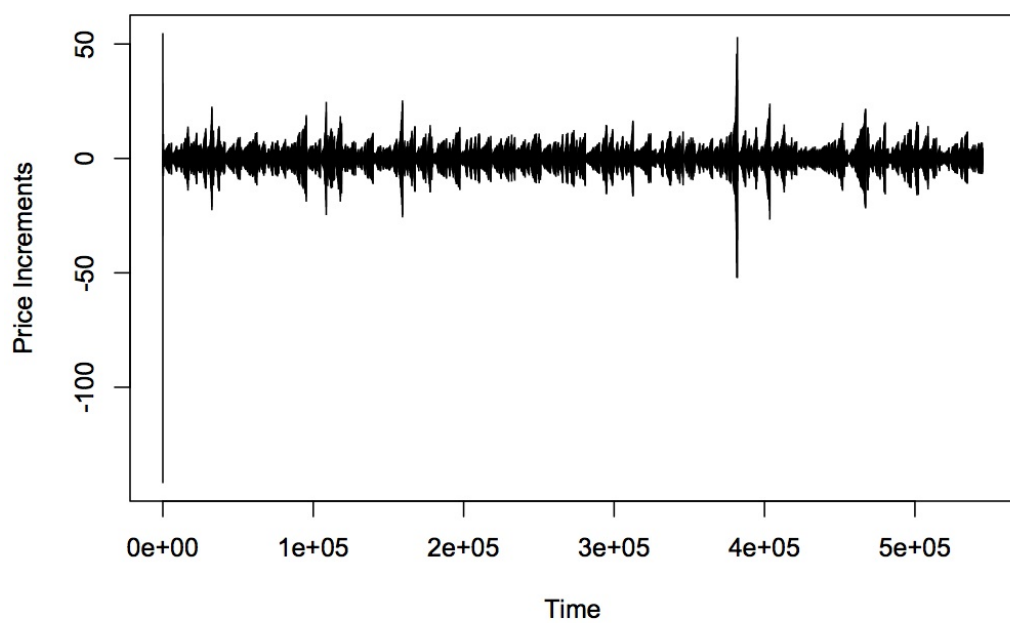


Figure 4.9: The first difference of the heavy-tailed simulation

Next we analyze the autocorrelation structure to determine if our initial thought of fitting a GARCH model is reinforced by long-term correlation. Figure 4.10 shows that although the correlation is small in the ACF, it continues to exceed the minimum level for significance well beyond lag $l = 50$. Similarly, the PACF fails to decay below the significance level at this lag, indicating that finite-order autoregressive-moving average may fail to yield adequate fits for this data set. Pairing that with our observation of volatility clustering, we settle on a GARCH(1,1) model for the data set.

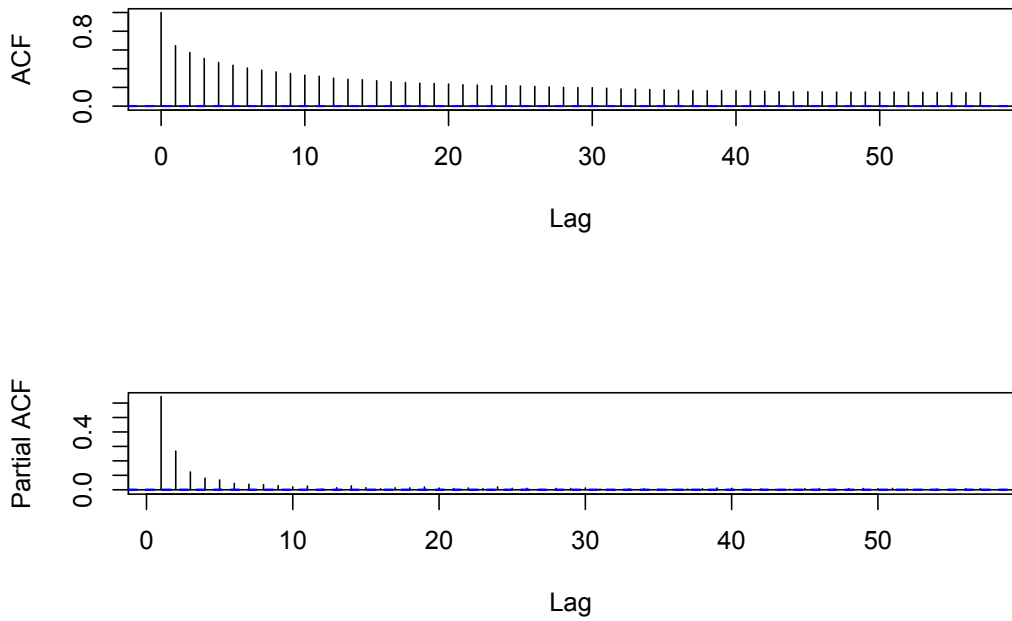


Figure 4.10: The ACF and PACF of the heavy-tailed simulation

The histogram of the residuals of the GARCH(1,1) fit reveals a leptokurtic structure (Figure 4.11). The GARCH(1,1) residuals also result in rejection of the null hypothesis of the Box-Ljung-Pierce test that they are i.i.d random variables. And the QQ-plot reinforces the rejection, revealing a substantial departure from the Gaussian distribution, particularly in the tails (Figure 4.12).

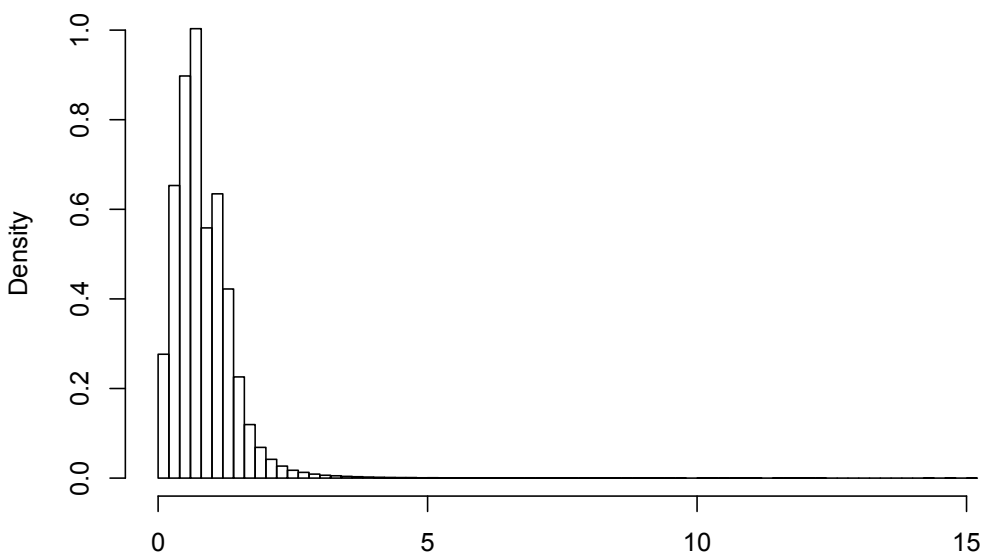


Figure 4.11: The histogram of the residuals from the GARCH(1,1) fit to the heavy-tailed simulation

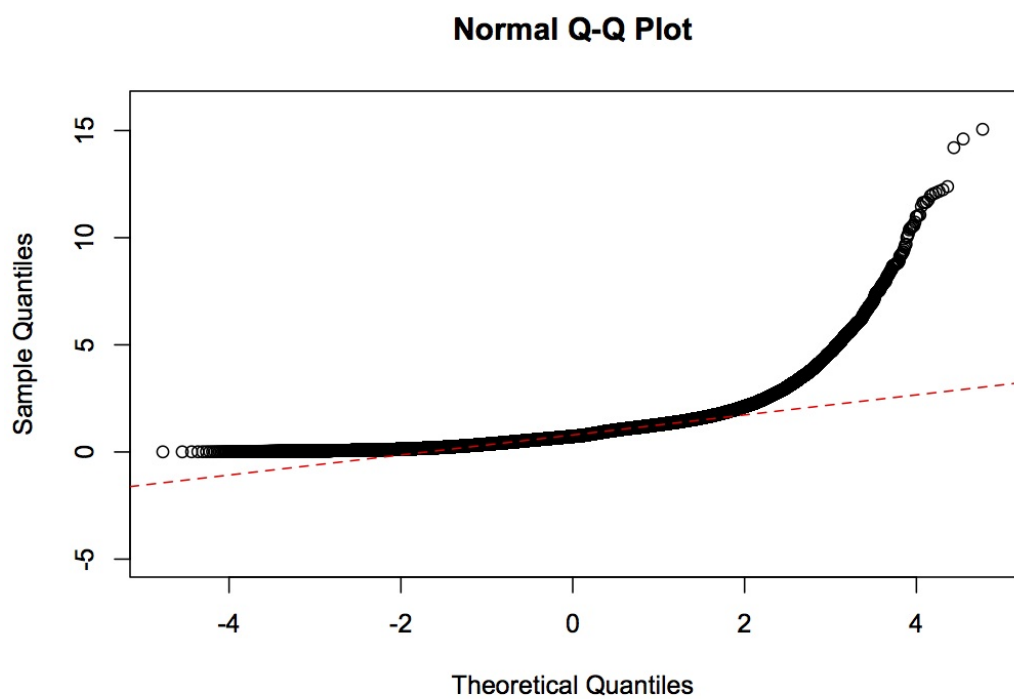


Figure 4.12: The QQ-Plot of the residuals from the GARCH(1,1) fit to the heavy-tailed simulation

The above analysis is admittedly rudimentary, but the intention is to illustrate the difficulty in applying some of the standard, readily available techniques to time series generated by agent-based financial models. One could certainly continue to manipulate the parameters of ARMA or GARCH processes to obtain considerably better fits than those presented here. However, this process would not be straightforward, and the researcher would have to rely on various heuristics that ultimately may reduce to subjective judgement about the process. Additionally, these data sets are generated by a known simulation structure where the ARMA and GARCH assumptions were not incorporated directly, and thus their lack of fit is not entirely unexpected. In the next section we present multifractal analyses of both time series, and show how their multifractal spectra compare to other known multifractals, as well as actual financial data.

4.4.3 Multifractal Results

Visually inspecting the price path from the thin-tailed simulation in Figure 4.4 along with its first difference in Figure 4.5 reveals a stochastic structure similar to Brownian motion. The erratic nature of the price path indicates a continuous function that is likely too rough to be differentiable, but the first difference indicates the increments of the process may simply be white noise. Given the lack of heavy-tailed behavior and the relative stationarity of the first difference, we formulate the hypothesis that the process is monofractal. We can investigate this hypothesis using MF-DFA, which in the case of a monofractal time series should reveal a single scaling exponent at all points in time. The value of the scaling exponent corresponds to the Hurst exponent H and gives us insight into the autocorrelation structure of the series. Figure 4.13 shows the results of running MF-DFA on the thin-tailed simulation data set.

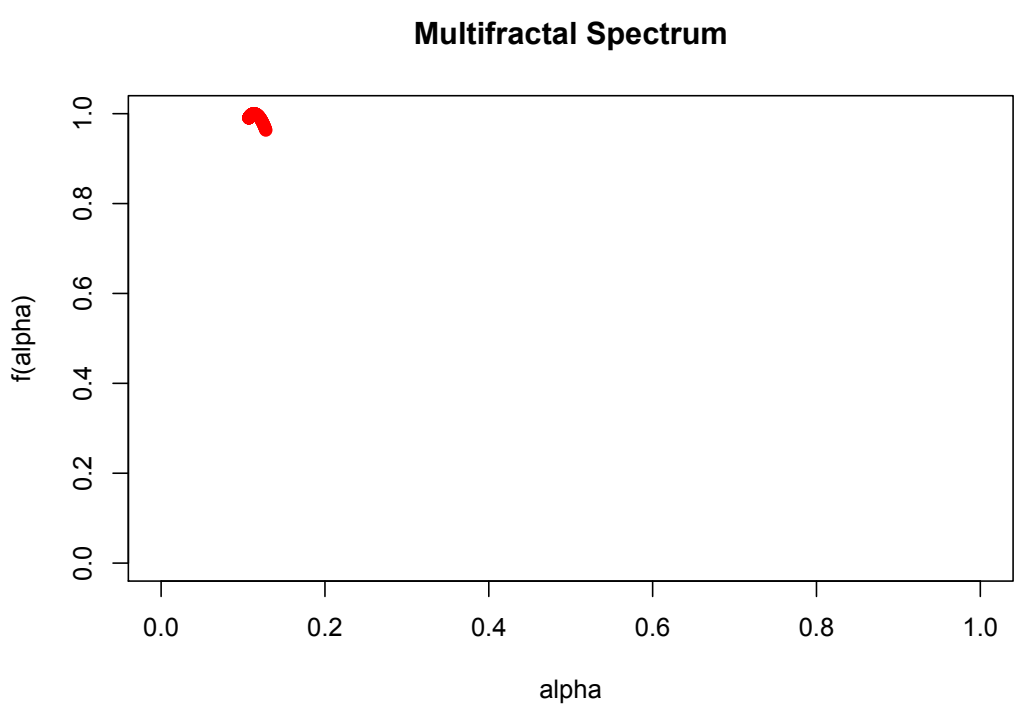


Figure 4.13: The multifractal spectrum from the thin-tailed simulation

The multifractal spectrum confirms that the process is monofractal. Essentially the fluctuations within the process all scale in time according to the same generalized Hurst exponent with an approximate value $\alpha = H = 0.11$. In the context of fluctuation analysis, this indicates the process is similar to fractional Brownian motion. The value of $H < 0.5$ indicates the process has short-range dependence and is antipersistent — that is, positive fluctuations are more likely to be followed by negative fluctuations and vice versa. In the context of time series analysis, this procedure represents a more efficient first step in exploratory analysis. By running MF-DFA on the data set first, we are immediately informed that fractional ARMA is likely to be the most appropriate family of time series models, and short-range dependence along with antipersistence characterize the time series. Recall from Chapter 2 that either heavy tails or long-range dependence in a process will induce multifractal behavior. Recall also that standard Brownian motion is generated by the non-overlapping increments being normal random variables, with their respective variances being proportional to the lengths of the corresponding increments. Since we deliberately set the distribution for Δ_p to be $N(0,1)$, we conclude that MF-DFA properly detects the thin-tailed nature of the simulation since it reveals a monofractal structure. We also conclude that market discipline, in this case, induces an antipersistence in the price path causing a deviation away from standard Brownian motion, since $H = 0.11 < 0.5$.

Next we apply the same procedure to the heavy-tailed price path. Since the simulation parameters were held exactly the same except for the distribution governing the price offset Δ_p , we might expect to see multifractal properties induced by the heavy-tailed distribution while still maintaining the antipersistent nature we concluded was the result of market structure. The results of running MF-DFA on the heavy-tailed simulation output are shown in Figure 4.14.

Multifractal Spectrum

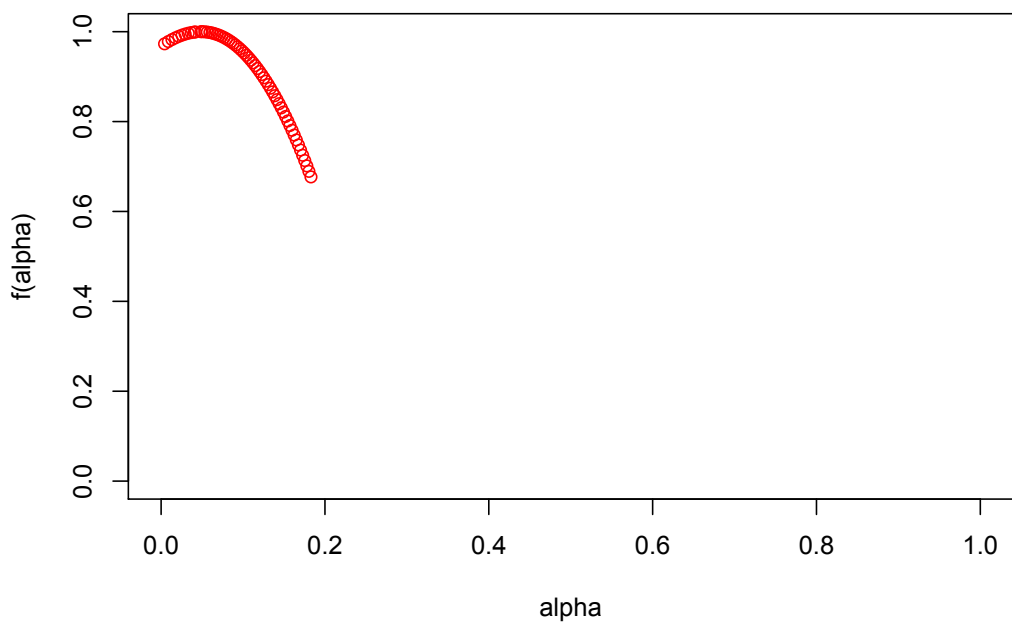


Figure 4.14: The multifractal spectrum from the heavy-tailed simulation

The multifractal spectrum of the heavy-tailed simulation output confirms the data set is indeed multifractal, as expected. The range of Hölder exponents is notably broad, but all values of α appear to be less than or equal to 0.5. Interestingly, the spectrum peaks at roughly $\alpha = 0.05$ and has a strong concentration of Hölder exponents in the neighborhood of the monofractal produced by the same simulation with a thin-tailed price offset (see Figure 4.15).

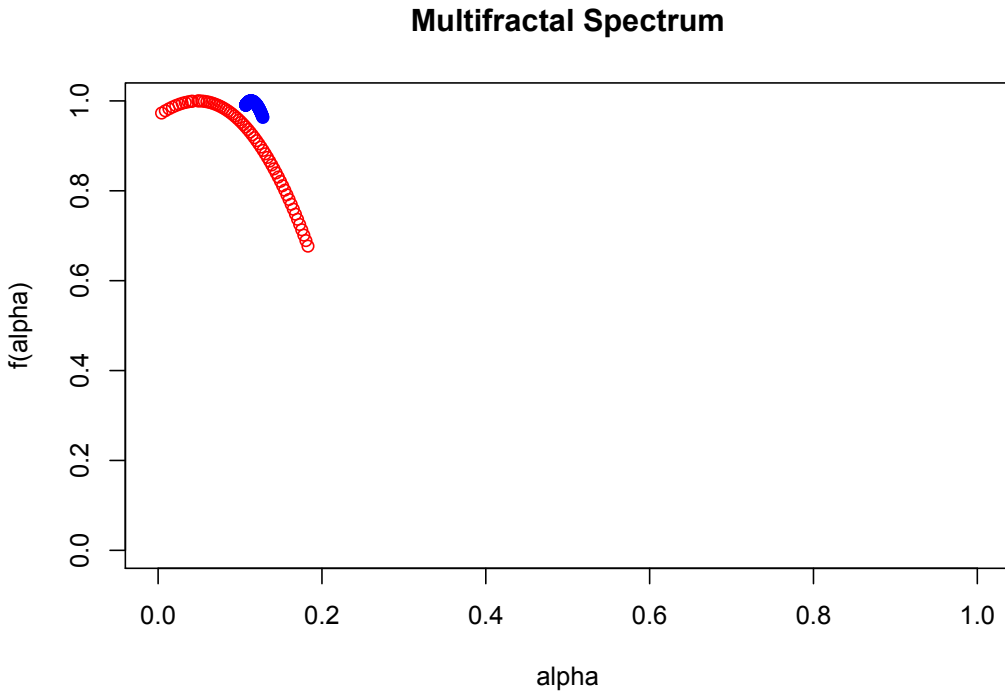


Figure 4.15: The multifractal spectrum from the thin-tailed simulation (blue) compared with that of the heavy-tailed simulation (red)

In summary we have shown that zero-intelligence agent-based financial models have the potential to produce monofractal price paths with Hurst exponents similar to fractional Brownian motion, as well as more complex structures with multifractal properties. In our model, the market discipline determined by the order rates and continuous double auction order book structure appeared to induce an antipersistence that was present regardless of which distribution was used for the price offset Δ_p . This is in keeping with conclusions of Farmer et al. and Gode and Sunder that market structure can produce an aggregate emergent effect that is independent of how irrational the individual participants become [26, 32].

4.5 Discussion

The zero-intelligence output is an indication that a simple set of rules being followed by 100 participants who are driven by relatively simple random factors can produce a complex time series exhibiting volatility clustering and heavy-tailed marginals. These admittedly broad results are in accordance with previously published accounts of zero-intelligence models, to which we add the conclusion that the time series produced can be multifractal. Gode and Sunder suggested that Adam Smith’s invisible hand may in fact result from the market discipline introduced by procurement processes such as the double auction order book [32]. Farmer et al. also concluded that market efficiency could (at least in theory) emerge on the macrolevel regardless of how irrationally the market participants were behaving [26]. Our experiment with the zero-intelligence model appears to reinforce these conclusions. What is interesting to note is the apparent ability of MF-DFA to differentiate between properties within the time series that were induced by market discipline versus those induced by agent behavior. In our experiment, we altered the agent behavior from placing relatively reasonable bid and ask orders to placing extremely unreasonable bid and ask orders. However, both time series exhibited antipersistence with the dominant (i.e. expected) Hölder exponent in the range of $\alpha \in (0.05, 0.11)$. Since the market structure remained unchanged and only the agent behavior was altered, a reasonable hypothesis for investigation is that market structure is revealed by the dominant Hölder exponent in the output while the degree of multifractality (i.e. the breadth of the multifractal spectrum) is determined by agent behavior.

Missing from this analysis are the calibration of rates to an actual asset and the open question of how to induce persistent (i.e. $\alpha > 0.5$) behavior in the multifractal spectrum. Figure 4.16 shows the multifractal spectrum from the heavy-tailed simulation compared with the multifractal spectrum from the GE TAQ data set. By employing the shuffling heuristic, we concluded the GE data set contained both long memory and heavy tails. This is reflected in the multifractal spectrum, as it exhibits both antipersistence in the large fluctuations and persistence in the small fluctuations. But its dominant Hölder exponent is roughly $\alpha = 0.48$, and the breadth of exponents exhibited by the series appears wider than that of the heavy-tailed simulation. The added complexity of long memory appears to combine with heavy tails in the GE data to produce a wider spectrum than heavy tails alone. The next step in this dissertation is investigating what combination of behaviors, learning, and market structure are needed to produce a price path comparable to reality and a multifractal spectrum that is tuned to empirical data.

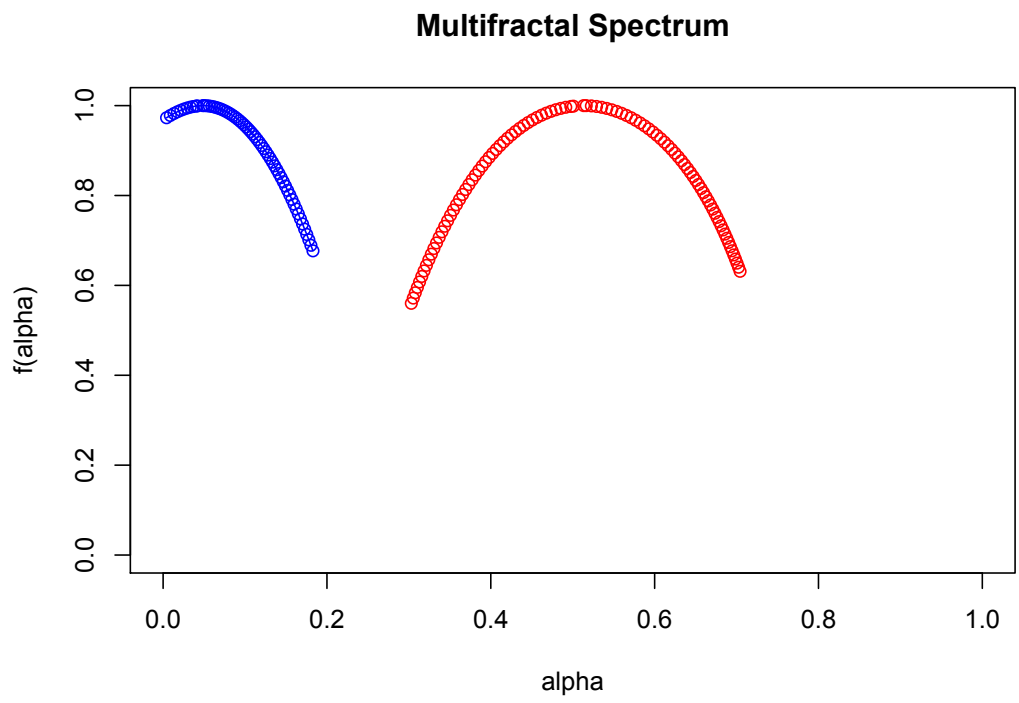


Figure 4.16: The multifractal spectrum from the GE TAQ data set (red) compared with that of the heavy-tailed simulation (blue)

Chapter 5

The Positive-Intelligence Financial Market

5.1 Introduction

In this chapter we expand the double auction order book model in an effort to progress toward a more realistic model of how markets operate. A significant obstacle to this endeavor is establishing a benchmark for that reality. The mechanics of the order book can certainly be enhanced to allow orders of more than one share and to enforce market capitalization by conserving shares. Most exchanges operate in a double auction order book format, with well-defined rules for trading and market clearing. But accurately defining the realistic behavior of market participants is an ongoing debate. Starting with Alfred Marshall around the turn of the twentieth century, economists began modeling the *representative agent* as a method for abstracting the particular behaviors of any one market participant to simplify the modeling of price determination through supply and demand [35]. These early agents were sharply criticized for failing to capture the heterogeneity noted in real markets, and they were subsequently abandoned for the middle part of the century. With the introduction of agent-based modeling and the accompanying computing power available today, the representative agents have seen a resurgence in economic modeling [43]. However, the original concern about heterogeneity still exists. We can now incorporate behavioral traits of market participants, and even learning algorithms that allow them to respond to the market, but we certainly cannot incorporate every such trait. So which ones are appropriate? Which behavior traits impact the market and which ones are obscured at the macrolevel?

In addition to the questions noted above, the debate over the efficient market hypothesis is ongoing [48]. The simplest statement of the hypothesis is that “security prices fully reflect all available information” [24]. But as Fama and others note, there is plenty of empirical evidence to contradict this statement. One such example is the predictability of the magnitude of price movements. A distinct trait of many assets is their price paths exhibit volatility clustering, meaning periods of relative calm alternate with periods of relative turmoil [48]. This means the market is at least partly predictable, and many *technical traders* attempt to exploit this property through the mathematical analysis of price charts. In contrast to technical

traders are the *fundamentalists*, who believe there is a fundamental value associated with the firm, and the asset price will tend toward this fundamental value. These two categories are by no means comprehensive nor mutually exclusive. People change their minds and beliefs. They experience feelings of panic and elation. And their economic situations change, not only through their own consumption levels, but also due to world events that impact the economy in unpredictable ways. Within each group there are disagreements over what method of mathematical analysis to use or what constitutes the fundamental value of the firm. The permutations are innumerable and again we are faced with the question of which combination of these microlevel behaviors and beliefs actually impact the market and which are obscured or cancelled out on the macrolevel.

North and Macal advocate an approach to agent-based modeling that starts with protoagents that can be easily embellished in an incremental fashion [62]. In keeping with this approach, we enhanced the zero-intelligence model to incorporate *positive-intelligence* traders that fall into two groups; fundamental traders we call *Grahamists*, and technical traders we call *Chartists*. We also embellished the mechanics of the order book by conserving the total number of shares in the market and allowing individual orders to specify a desired quantity of shares. The objective of the positive-intelligence model is to progress toward reality in an incremental way while maintaining a simplicity that lends itself to systematic experimentation. As noted above, the economic debate on market behavior is ongoing and unlikely to be captured by simple models. However, insight can be gleaned from systematic exploration of tractable models. Our intention is to analyze the impact of added intelligence on the multifractal properties of the simulated price paths. The zero-intelligence model exhibited both monofractal antipersistent price paths and multifractal antipersistent price paths. To induce multifractal properties, the zero-intelligence agents had to utilize extremely unrealistic price offsets. Our objective is to induce multifractal properties through more reasonable agent behavior. Additionally our analysis of high-frequency trades of GE stock yielded multifractal spectra that exhibit both antipersistence and persistence in different size fluctuations. This begs the question of whether positive-intelligence traders can induce persistence in the market while still interacting with a double auction order book in a plausible way.

The remainder of this chapter is organized as follows. In Section 5.2 we review the pertinent literature to place our model in context of the ongoing discussion on modeling financial markets. In Section 5.3 we describe the enhancements we employed to transform the zero-intelligence model into a positive-intelligence model. In Section 5.4 we present our exploratory analysis of the simulated time series conducted in order to better focus our more detailed experiments. We utilize standard time series analysis techniques, as well as a multifractal analysis. In Section 5.5 we present more detailed results of specific experiments conducted over multiple replications of the simulation. We conclude in Section 5.6 with a discussion of results, along with comparisons with those of the zero-intelligence model and the properties observed in some real asset prices.

5.2 Literature Review

Though the zero-intelligence model with various modifications can provide an excellent research tool [19], our intention is to more accurately represent real market behavior. It is important to note that in advancing to a positive-intelligence model, we bypassed a number of possible enhancements to the zero-intelligence model — specifically, the calibration of limit order and market order interarrival times to empirical trade and quote data. Farmer et al. report considerably more realistic price paths than those we obtained after having performed such a calibration on their model using data from the London Stock Exchange [26]. However, as noted earlier, the impact of heterogeneous agents on the macroeconomic level has become an area of interest, and the zero-intelligence traders are limited in this regard.

A survey of simple heterogeneous agent models by Hommes stressed the interaction between technical traders and fundamental traders [37]. Fundamental traders are generally thought to invest in undervalued assets and sell overvalued assets. They base their assumptions concerning over- versus undervalued assets on economic fundamentals such as dividends, growth, and unemployment rates. The technical traders stand in contrast to the fundamental traders by ignoring these economic indicators, and focusing on the price paths and the perceived patterns they contain. Much focus has been given to these two classifications of traders because of Friedman's hypothesis that speculative traders would ultimately be unsuccessful and therefore driven out of the market. Simple models of differential equations, such as those by Frankel and Froot, were designed to examine the dynamics created by these competing theories [29].

The idea of fundamental trading was popularized by the economist Benjamin Graham. His book, *The Intelligent Investor*, describes an investment approach known as value investing [33]. Graham anecdotally introduces Mr. Market to represent the daily swings of asset prices that he stresses have little to do with actual underlying value of the firms being traded. He encourages investors to ignore these swings and focus their attention on the particular company's performance, and its ability to deliver quality products to customers, as well as dividends to investors. Graham introduces a practical approach for the typical investor to follow, with the intent of enforcing the discipline that avoids the whims of Mr. Market. Specifically each investor should choose a fraction of the individual's wealth β the investor is not willing to risk. This fraction should be invested in low-risk (and therefore lower-yielding) bonds. The remaining fraction $1 - \beta$ should be invested in firms the investor believes possess value. The task of the investor is then to maintain this division of wealth. If the share price increases, the investor sells enough shares to rebalance the chosen bond-to-asset split. If the share price decreases, the investor uses some of the bond money to purchase more shares. The net result is buying low and selling high, while maintaining a steady long-term growth in wealth. This strategy is based on the idea that markets are efficient, but that in the short run irrational investors can cause a mispricing of a given asset that is soon corrected by fundamentals. There are a number of criticisms of this belief, but they are well summarized by a quote of John Maynard Keynes: "Markets can remain irrational a lot longer than you and I can remain solvent" [70]. The obvious implication is that if investors continually shift their bond holdings into a decreasing

market, they may ultimately exhaust all their wealth before the market fundamentals intervene to correct the mispricing.

Since the first publication of *The Intelligent Investor*, the market has failed to reach a steady value. So either the irrational traders are in infinite supply, being driven from the market only to be immediately replaced by more irrational traders; or there is more complexity to the market that overwhelms the impact of fundamentalist traders, and perhaps the principles of fundamental value altogether. This empirical observation coupled with applications of dynamic optimization techniques to derive financial models (e.g., the Black-Scholes options pricing formula) led economists to consider the impact of technical traders on the market in greater depth [29]. Frankel and Froot claim that financial bubbles cause a natural Bayesian response to inferior forecasting techniques, shifting the technical traders from short-term forecasts to longer-term forecasts. They naturally raised the question of which type of forecaster was dominating the market at a given time within the technical trader community. Additionally, studies began to reveal that some degree of predictability exists in the market [14]. As such, utilizing technical analysis seems less like a fool's errand than value investors claim it to be. In 1991, Fama revisited the efficient market hypothesis and agreed that there was some degree of predictability in the market [24]. However, transaction costs associated with entering and exiting the market at high frequency, as well as increased risk often associated with predictability, led him to conclude that predictability alone does not negate the efficient market hypothesis [24]. That is, technical traders may indeed accurately predict market changes, but in the long run they will fair no better than a fundamental trader, as their profits are diminished by transaction costs and increased risks. Setting aside these intriguing debates that are likely to remain unresolved for decades to come, we examine the simpler question of whether select combinations of these behaviors can produce simulated price paths exhibiting the same properties we observe in the real market.

In the literature there are a number of implementations of artificial stock markets containing multiple assets and intelligent agents with behavioral logic involving wealth-motivation and forecasting abilities [47, 17, 63]. LeBaron utilized a market-clearing structure containing different types of forecasting agents to explore a number of stylized facts in price paths, and the impact of learning on market dynamics [50]. In LeBaron's model there were two assets: a risk-free asset available in infinite supply, and a risky asset that pays a stochastic dividend. The dividend D_t consists of a constant growth parameter and a stochastic parameter drawn from a Gaussian distribution. Each agent i is constrained by the agent's available wealth $W_{t,i}$ at time t according to,

$$W_{t,i} = (P_t + D_t)S_{t-1,i} + (1 + r_f)B_{t-1,i}, \quad (5.1)$$

where P_t is the price of the asset at time t , $S_{t,i}$ is the quantity of shares held by agent i at time t , $B_{t,i}$ is the value of the risk-free asset held at time t by agent i , and r_f is the interest rate per time period of the risk-free asset.

The portfolio problem for the agents in LeBaron's model is to maximize their expected wealth at time $t + 1$, constrained by their consumption $C_{t,i}$ at time t and their desired level of overall return R_t^P , which is determined by the fraction of wealth in the risky asset $\omega_{t,i}$. Under certain assumptions this model has an optimal portfolio weight $\omega_{t,i}^*$. LeBaron's focus was to determine the impact of heterogeneous learning on the dynamics of asset prices. His intelligent traders could therefore select between three different forecasting strategies: a filtering technique related to Kalman filtering; a fundamental strategy based on the price-to-dividend ratio; and a simple linear regression strategy. Finally, LeBaron modeled market clearing by setting the sum of individual share demands, $Z_{t,i}$, equal to the aggregate share supply of one — that is,

$$1 = \sum_{i=1}^I Z_{t,i}(P_t). \quad (5.2)$$

Since $\omega_{t,i}$ and $Z_{t,i}$ are functions of the current price, it can be shown that a particular price P_t will clear the market given the aggregate demand at time t . However, given the complexity of the forecasting algorithms, P_t is determined numerically within the simulation. The output of this simulation matched many of the stylized facts associated with real assets, such as large swings in the price-to-dividend ratio. However, LeBaron notes the model is highly stylized, and should be considered a computational thought experiment rather than an accurate representation of market dynamics [50].

What is clear from the above models is that microlevel behaviors can have a profound impact on macrolevel output of dynamical systems. Financial markets are clearly such a system, where the composition of participants and the behavior of those participants are constantly changing. Returning to our objective of analyzing the multifractal properties induced by adding intelligence to the traders interacting with a double auction order book, we borrow a few of the simple assumptions discussed in this section. Our intention is to ground the model on an established foundation that can be easily enhanced in future iterations. To that end, we incorporate two types of traders that fall roughly into the categories of fundamentalist and technical analysts, but within each category we provide them with heterogeneous parameters on which they base their decisions. The next section describes the positive-intelligence model in greater detail.

5.3 The Model

5.3.1 The Order Book

The positive-intelligence financial market model is an expansion of the zero-intelligence model of the previous chapter. The market structure is again represented by a double auction order book, meaning agents can place orders to either buy or sell shares of a single asset. The order book accepts limit orders that do not immediately cross the spread and are therefore placed in a best-price-first queue. In the case

of bid limit orders, the best price is the highest bid; and conversely in the case of ask limit orders, the best price is the lowest ask. Ties are broken by first-come-first-serve logic within the respective queues. The order book also accepts market orders that do not specify a price and are intended to execute at the current best price.

We enhanced the logic of the double auction order book in two ways. First, the order book manages the conservation of shares within the market model. In the zero-intelligence model we were solely focused on how the distribution of price offsets coupled with the interarrival rates of orders impacted the price path. As such, the agents did not keep track of their wealth, and we assumed an infinite supply of shares. In the positive-intelligence model, we require the agents to react to market conditions, which includes the possibilities of excess demand or excess supply. Conserving shares provides a mechanism for such conditions. This means bid orders can only execute if there are orders in the ask-order queue, and ask orders can only execute if there are orders in the bid-order queue.

Second, we adjusted the order process to allow agents to place individual orders for more than one share of the asset. As we discuss in greater detail below, the agents now have limited wealth with which to operate, so their entry and exit from the market requires an additional degree of freedom that is facilitated by being able to buy or sell multiple shares at once. The order book logic was enhanced to search the appropriate queue for crossed orders and satisfy incoming orders up to the available quantity of shares. In the case of market orders, there is no specified price. This means one bid order (respectively, ask order) may be satisfied by multiple ask orders (respectively, bid orders) to meet the quantity of shares being traded. Any time a transaction occurs, the double auction order book updates the market price that is visible to all agents. If the transaction is an incoming market order, the order book calculates a share-weighted average of the transaction to determine the market price. For example, if a market bid order requests three shares and there is one share being offered at \$100.00 and two shares being offered at \$102.00, then the market bid order is fully satisfied and the new market price is $[1(\$100) + 2(\$102)]/3 = \$101.33$. Immediately following a market order, the new bid-ask spread may in fact be negative, meaning existing limit orders are crossed and can be satisfied. The order book handles this situation by taking the midpoint between the two unit share prices. Essentially, the bidding agent is getting his shares at a slightly cheaper price than he was willing to pay, and the asking agent is selling her shares at a slightly higher price than she was willing to offer. The midpoint means their respective gains are as fair as possible.

5.3.2 The Agents

The most significant difference in the positive-intelligence model is the behavior of the agents. In the zero-intelligence model there were patient traders placing only limit orders and impatient traders placing only market orders. Beyond being able to check the order queues for the best price and being able to generate random variables for setting prices and order interarrival times, the agents had no regard for

market conditions. In the positive-intelligence model, the agents must make decisions in the face of scarce resources. Each agent is instantiated with a certain amount of wealth, split between a risk-free asset, called the bond, and an initial stipend of shares. These values are determined randomly when the simulation is started, but the maximum values can be altered by the user. As previously mentioned, the order book conserves shares, so the initial instantiation process determines the market capitalization. Agents can immediately sell the shares they possess or attempt to buy more shares depending on their internal logic and decision thresholds. However, they will only be successful if other agents are simultaneously attempting the opposite operation. Agents are classified into two groups: Grahamists and Chartists. But agents of either classification have the ability to place either market or limit orders. They can query the order book to check the current price of the asset, and use that price to determine their current wealth. Agent i earns interest on that individual's bond and possesses a parameter β_i that establishes the amount of wealth that agent is not willing to risk on the risky asset. All the agents also have a minimum wealth threshold. If their total wealth drops below this threshold, they make no attempt to buy or sell until their wealth increases above the threshold.

Last, for experimentation purposes, the agents have logic that allows them to adapt their behavior in reaction to the changing market. There is a user-controlled checkbox for disabling this logic in all agents. Presently, the checkbox disables adaptation for either all agents or none of them. The algorithm for adaptation is loosely based on prospect theory in that adapted parameters approach their maximum value (as agent wealth increases) slower than they approach their minimum value (as agent wealth decreases). To accomplish this effect we use a modified Gompertz difference equation. Details of the algorithm can be found in Section 5.3.3.

Grahamists

Grahamists, as their name implies, follow the practical rule set forth by Benjamin Graham. Upon instantiation, the Grahamist with agent index i receives a random amount of wealth up to a threshold set by the user, along with the main decision parameter β_i . Each Grahamist's β_i -value is set to a random number in the interval $[0, 1]$, and that individual is immediately allocated enough shares to account for $1 - \beta_i$ of the agent's current wealth at the initial share price. Thus, at time zero, Grahamist agent i holds the fraction β_i of the individual's total wealth in the risk-free bond and the fraction $1 - \beta_i$ of the agent's total wealth in shares of the risky asset. Grahamists then schedule themselves to check the asset price at a time in the near future using an exponential random variable with parameter λ_i . The rate λ_i used in the exponential distribution for interarrival times is set randomly in the interval $(0, 2]$ for each agent i to ensure heterogeneity within the Grahamist community. However, the user can adjust the maximum value of the half-open interval for different runs of the simulation.

Each time a Grahamist checks the market, that individual first queries the double auction order book to determine the share price, and then uses that information along with the risk-free interest rate to update

the individual's wealth. That is, wealth $W_{t,i}$ of Grahamist agent i at time t is determined by

$$W_{t,i} = P_t S_{t,i} + B_{t,i} (1 + r_f)^{t-t_{0,i}}, \quad (5.3)$$

where P_t is the current market price, $S_{t,i}$ is the current quantity of shares held by the agent, and $B_{t,i}$ is amount held in bond since the last time $t_{0,i}$ that agent i checked the market. Note the risk-free interest rate is raised to the power $t - t_{0,i}$ to account for the elapsed calendar time that the bond was held. Within the simulation, calendar time is determined by the agents scheduling themselves on the event calendar, while simulation time is calculated in integer steps corresponding to sequential events on the event calendar.

Once the Grahamists have the current market price, they check to see if they have maintained their bond-to-asset split determined by their individual assigned values of the parameter β_i . If the market price has increased, then the Grahamists attempt to sell the quantity of their shares that would reestablish their desired split. Conversely if the market price has decreased, then they attempt to purchase the quantity of shares that would reestablish the β_i split. The first attempt to reestablish their split is done with a market order. Due to the conservation of shares enforced by the double auction order book, their attempt will be unsuccessful if no other agent has placed a limit order of the opposite operation. If such an attempt fails, then Grahamist agent i offsets the current market price by an offset ε_i taken from the half-normal distribution with mean zero and a variance set by the user. The offset is an increase if agent i is placing a bid and a decrease if agent i is placing an ask. Agent i then recalculates the split based on this new price and places a limit order with this new quantity and price.

It is important to note that there are hundreds of agents all attempting to buy and sell through a single order book. To handle this situation in Java, a certain degree of synchronization is required. Synchronization essentially locks a certain operation when it is seized by an agent. As soon as the agent relinquishes the operation, that operation is free to be seized by the next agent. The Grahamists query the double auction order book for the current price, then make their decision, and finally place a market order. The market order does not specify a price, but it does specify a quantity, which is a function of the price the Grahamists received when they checked the market. By the time their market order is able to seize the double auction order book to place their order, the price may have changed substantially from the original price they used to calculate their split. Given enough agents in the market, this process could place the Grahamists in a constant state of flux trying to reestablish their initial split. We dampened this effect by creating a tolerance level for the β_i -split that can be set by the user. That is, the Grahamists only attempt to reestablish their split when their bond fraction of wealth differs from β_i by more than the tolerance level.

The last aspect of the Grahamists' behavior is their ability to adapt to market conditions. Each Grahamist tracks the number of unsuccessful initial market orders. Upon instantiation of Grahamist agent i , that individual's threshold for unsuccessful orders is set randomly in the interval $(0, 10]$. If the quantity of sequential unsuccessful market orders exceeds the threshold, Grahamist agent i increases

the rate parameter λ_i used to generate the time between market queries. Conversely, if Grahamist agent i has more successful market orders than the individual's threshold value, then agent i decreases the rate parameter λ_i . The increase or decrease in λ_i is done according to the modified Gompertz difference equation in the open interval $(0, 2]$, but the user can change the maximum λ_i value before starting the simulation (see Section 5.3.3 for details). Recall the Grahamists attempt to buy when the market price decreases. Increasing the rate of market activity in a falling market is intended to imitate the fire-sale dynamics that are often observed in real markets.

Chartists

While Grahamists represent our fundamental traders, Chartists represent the technical analysts who depend on technical forecasts of market movements to make their decisions. Like Grahamists, they receive an allocation of wealth at instantiation that is immediately split between the risk-free asset and the risky asset according to the parameter β_i . However, Chartists do not seek to maintain this bond-to-asset ratio. Instead, their parameter β_i serves as a measure of risk aversion in that $1 - \beta_i$ helps them determine the quantity of shares they are willing to risk on their next forecast.

Chartist agent i also possesses a parameter ψ_i that determines the agent's forecast of the next share price. For simplification purposes, all Chartists utilize exponential smoothing as their forecast methodology. That is for Chartist agent i , the forecast $f_{\tau_i,i}$ at forecast step $\tau_i - 1$ corresponding to simulation calendar time $t(\tau_i - 1)$ is given by

$$f_{\tau_i,i} = \psi_i P_{t(\tau_i-1)} + (1 - \psi_i) f_{\tau_i-1,i}, \quad (5.4)$$

where $P_{t(\tau_i-1)}$ is the current price at calendar time $t(\tau_i - 1)$ and f_{τ_i-1} represents the last forecast of the share price made at time $t(\tau_i - 2)$ that will be observed at time $t(\tau_i - 1)$. The Chartists schedule themselves to update their forecast and make decisions about market actions according to a Poisson process with parameter λ_i . So the time between successive forecasts is not necessarily an equal-size interval of calendar time. That is, the amount of calendar time $\Delta t = t(\tau_i) - t(\tau_i - 1)$ elapsed between forecast steps $\tau_i - 1$ and τ_i is exponentially distributed with parameter λ_i .

To maintain a degree of heterogeneity within the Chartist community, the parameter ψ_i is set randomly in the interval $(0, 0.9]$ for Chartist agent i . When Chartist agent i advances to forecast step τ_i at simulation time $t(\tau_i)$, that agent first checks the market price $P_{t(\tau_i)}$ at time $t(\tau_i)$ and then updates the agent's wealth according to Equation (5.3) in which $t = t(\tau_i)$. Chartist agent i then establishes a forecast according to Eq. (5.4). The goal of the Chartist is to make money on market movements rather than long-term growth. So if they forecast an increase in price, the Chartists place a market order to buy shares up to $1 - \beta_i$ of their current wealth, and simultaneously place a limit order to sell that same quantity of shares at the forecasted increased price. Assuming both orders are successfully executed over some interval of calendar time Δt required for the limit order to be crossed, the Chartist will realize a profit of

$(f_{\tau_i,i} - P_{t(\tau_i-1)})S_{t(\tau_i-1),i}$. If the Chartist is unable to execute the market order to purchase shares, they still attempt to place a limit order to sell either the original quantity of shares or their current holding of shares, whichever is less. The structure of our market does not allow short selling, so the Chartists are limited by their buy market order and their current holdings.

If the Chartists forecast a decrease in price, they place a market order to sell shares up to $1 - \beta_i$ of their current wealth or the amount they are currently holding, whichever is less. They simultaneously place a limit order to buy back those shares at the lower price. Regardless of whether they are able to execute the sell market order, the Chartists proceed with the buy limit order. The idea is that purchasing at the lower price will get them back in the market to profit on moves in the future.

All limit orders are limited by the agent's wealth in that they cannot place an order to buy at a value greater than their current holdings. This is not to say that agents cannot go bankrupt. Due to synchronization, they may believe they can afford a market order at the current price, but market orders ahead of theirs may shift that price before they are able to execute. If the shift is large enough, the agent will buy an order that exceeds their current wealth, causing them to exit the market altogether.

The last aspect of Chartists' behavior is their ability to adapt their forecast parameter based on past success. Chartists maintain an average forecast error. If this error exceeds their forecast error threshold, then the Chartists change their parameter ψ_i according to the modified Gompertz difference equation described in the next section. Note that in the case of Chartists, it is not immediately clear whether an increase in ψ_i or a decrease in ψ_i will reduce their forecast error. As such, when employing the Gompertz difference equation, each Chartist increases their parameter ψ_i with probability one-half, and decreases their parameter ψ_i with probability one-half.

5.3.3 The Modified Gompertz Differential Equation

An important aspect of Prospect theory, as introduced by Kahneman and Tversky, is the concept of an s-shaped value function [40]. This function assigns value to an economic outcome, and is asymmetrical in that losses subtract greater value than gains add to the utility of the decision-maker. In an attempt to mimic this behavior in our intelligent traders, we adapted the Gompertz differential equation to serve as a recursive method for updating a parameter [78]. The following procedure allows us to increase a parameter towards its maximum b slower than we decrease the parameter towards its minimum a . The advantage of this adaptation is that only the current parameter value and the direction of change are required to update to the new parameter value.

If we wish to update some parameter λ_t such that $a \leq \lambda_t \leq b$ for $t = 1, 2, \dots$, and if at each time t we are given the direction (sign) of the next increment

$$\Delta\lambda_t = \lambda_{t+1} - \lambda_t, \quad (5.5)$$

where

$$s_t = \text{sgn}(\Delta\lambda_t) = \begin{cases} -1, & \text{if we want } \Delta\lambda_t < 0, \\ 0, & \text{if we want } \Delta\lambda_t = 0, \\ 1, & \text{if we want } \Delta\lambda_t > 0, \end{cases} \quad (5.6)$$

then we can adapt the dynamics captured in the Gompertz differential equation to determine the actual value of $\Delta\lambda_t$ for each time t .

Choose $\varepsilon > 0$ as an arbitrarily small constant that we need to avoid numerical difficulties when λ_t gets too close to the minimum a . For example, in this dissertation we take $\varepsilon = 10^{-10}$. Let

$$d_t = \theta s_t \lambda_t \ln \left(\frac{b-a}{\max\{\lambda_t, a+\varepsilon\}-a} \right), \quad (5.7)$$

and take

$$\lambda_{t+1} = \text{mid}\{a, \lambda_t + d_t, b\}. \quad (5.8)$$

Note that when λ_t is close to the maximum b ($\lambda_t \approx b$) and $s_t = +1$, then from (5.7) we see that

$$d_t \approx \theta b \ln \left(\frac{b-a}{b-a} \right) = 0. \quad (5.9)$$

On the other hand, when λ_t is close to a ($a \leq \lambda_t \leq a+\varepsilon$) and $s_t = -1$, then from (5.7) we see that

$$d_t \approx -\theta a \ln \left(\frac{b-a}{\varepsilon} \right) \rightarrow -\infty \text{ as } \varepsilon \rightarrow 0, \quad (5.10)$$

provided $\theta a > 0$. We assume $a > 0$ so the user-specified growth parameter θ must be positive. The user can set θ to control the rate of approach to the lower limit a when λ_t is close to a and $s_t = -1$.

5.3.4 Model Mechanics

Both for troubleshooting during development and for illustration purposes we added a fair amount of animation to the simulation. One advantage of MASON is the fact that it decouples the animation from the computational aspects of the simulation. This allows the simulation to run at increased speeds if the animation is turned off. Nonetheless, good modeling practices encourage animation to assist in verification of the simulation. MASON's built-in inspectors allow us to analyze the variables within specific agents while the simulation is running. These aspects of the software greatly assisted in model development, and were invaluable during the verification process.

The animation consists of a central market that is surrounded by participating agents. The agents are differentiated by color, red for Chartists and blue for Grahamists. All agents increase their radius from the

central market as their wealth increases, and they decrease their radius as their wealth decreases. Chartists change their color to gray if they are holding zero shares of the asset. Given that their trading strategy involves constant entering and exiting of the market, they are constantly switching from red to gray. Similarly, the Grahamists change their color to black if they are holding zero shares. Since Grahamists always attempt to maintain their bond-to-asset ratio, this typically indicates the agent has gone bankrupt.

Additionally, we provide the user with complete control over the following model parameters: the initial price of the asset; the risk-free rate of return; the variance of the Grahamists' offset normal distribution; the total number of traders in the market; and the percentage of traders that are Grahamists as opposed to Chartists. The user can also manipulate other parameters on an aggregate level. Since we wish to maintain heterogeneity within each trader classification, we set the parameters β_i and ψ_i using a random number between $[0, 1]$ multiplied by the maximum value each parameter can take for each agent i . The user can manipulate the maximum values β_i and ψ_i can take. Similarly, we set the step rate parameter λ_i for the Poisson process the agents use to schedule themselves and the maximum wealth they are given upon instantiation using a random variable between zero and a maximum value the user can change. All of the above parameters, and their initial default values, are shown in Table 5.1.

Table 5.1: Positive-intelligence user controlled parameters and default values

Parameter	Symbol	Default Value
Initial Asset Price	P_0	\$50
Risk-Free Rate of Return	r_f	3% annually
Variance of Grahamists' Offset	σ^2	1.0
Total Number of Traders	N	500
Percent Grahamists	—	50%
Maximum β_i	b_i	0.7
Maximum ψ_i	b'_i	0.9
Maximum Step Rate	λ_i	2.0 trades/day
Maximum Wealth	$W_{0,i}$	\$100,000

Note the minimums for β_i , ψ_i , and λ_i used in the Gompertz equation are all $\varepsilon = 10^{-10}$

Last we allow the user to turn off the logic that allows the agents to update their decision parameters. This allows the user to isolate the effect this logic has on the market. All the agents and the double auction order book incorporate Java Bean technology that provides graphical access to their variables. By clicking on any one agent, we can stream time series charts and data as their situation changes within the simulation. Figure 5.1 shows our conceptualization of the positive-intelligence financial market.



Figure 5.1: Double auction order book with 250 Grahamists (blue) and 250 Chartists (red)

5.4 Exploratory Analysis

As previously mentioned, our objective was to analyze the changes in the multifractal properties caused by adding positive intelligence to the agents, while simultaneously incorporating only plausible behavioral traits. In the zero-intelligence model, the nature of the double auction order book appeared to create only antipersistent behavior, as large market orders create a deeply negative spread that gives rise to very low bids and very high asks being satisfied in rapid succession. Since real markets also exhibit persistent behavior, we tested whether a double auction order book combined with intelligent traders could produce this effect. We also analyzed the impact of different market compositions on the multifractal spectrum. There is still the open question of which microlevel behaviors interact to produce notable macrolevel effects versus those that are obscured on the aggregate level. By systematically increasing the proportion of Grahamists in the model, we analyzed the changes to price time series and the multifractal properties induced by shifting the predominant thinking in the market from Chartist to Grahamist. Finally, we analyzed the effect of agent adaptation on the financial market by running comparable simulations with the adaptive logic turned off. For all of the experiments, we conducted standard exploratory time series analysis to confirm the claims by other researchers that agent-based models can replicate the stylized facts of real financial markets [47, 50, 26]. To these analyses we added multifractal analysis to confirm that generalized Hurst exponents and self-similarity are also properties that can emerge from agent-based models of financial markets.

In our preliminary exploratory analysis, we conducted three runs of the simulation for 252 trading days using the same random number seed. Each run had a different composition of Chartists and Grahamists to give us an indication of the impact they might have on the price path. Note that due to the initial condition that each trader's bond is exactly the fraction β_i of their wealth, Grahamists have no incentive to trade until the market price changes. Therefore some quantity of Chartists must be present to cause any movement in the price. Similarly, the Chartists must have an initial "last forecast" that is not equal to the initial price. Otherwise, their next forecast will predict a zero change in price. Since Chartists attempt to profit from market changes, they do nothing when they predict a zero change in price. Although Chartists and Grahamists operate independently of each other in terms of their decision making, they both operate through the double auction order book, and thus their actions interact considerably to create the market dynamics. Figure 5.2 shows the three initial runs with the proportion of Grahamists being 20%, 50%, and 80%.

Adjusting the proportion of Grahamists to Chartists has three main effects on the price path. First, in 252 trading days, the volume of trades increases as the proportion of Grahamists increases. With 20% Grahamists, there were 26,656 trades, with 50% there were 67,739 trades, and with 80% there were 93,776 trades in the same elapsed calendar time. The reason for this increased volume is the relatively impatient nature of the Grahamists' trading strategy. Grahamists primarily use market orders, and attempt to maintain a constant split between the risk-free bond and the risky asset. However, incoming market

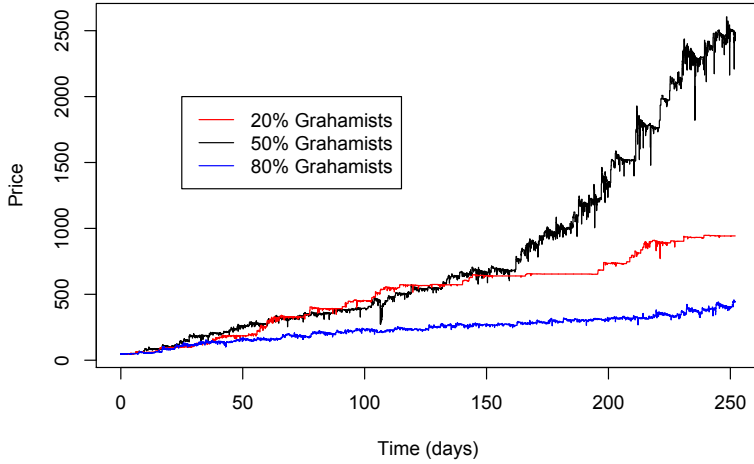


Figure 5.2: Price time series for 252 simulated trading days with 20% (red), 50% (black), and 80% (blue) Grahamists

orders cause ripples in the price by removing limit orders from the bid- and ask-queues. Those ripples in turn disrupt the bond-to-asset split of other Grahamists, causing them to place market orders. The more Grahamists there are, the more pronounced this feedback loop becomes.

The second effect is that fewer Grahamists — and therefore more Chartists — appears to correlate with greater displacement in the overall price level. The initial price in our model was always \$50. With 20% Grahamists the price climbed to \$947 in just 26,656 trades. In the same number of trades, with 50% Grahamists the price only reached \$378 and with 80% Grahamists the price was only \$175. Recall that when Chartists predict an increase they first place a market order to buy the risky asset. This market order removes the lowest ask price thereby making the new best ask price slightly higher. Chartists then place an ask limit order to sell at the forecasted higher price, which further encourages a price increase. The net effect is larger price movements per trade. However, since there are fewer trades per calendar day, the closing price after 252 trading days with 20% Grahamists was still much less than that of 50% Grahamists. The effect of greater price displacement can be noted visually by plotting the price against the double auction order book steps (i.e., trades) rather than calendar time (Figure 5.3).

The third effect is that increased Grahamists appears to dampen volatility in price movements. If we restrict our analysis to the first 26,656 trades in each data set, the variance in price changes drops from around 5.5 with 20% Grahamists to 1.7 with 80% Grahamists. This can be noted visually by examining the price differences in Figure 5.4. The reason for this dampening is that Grahamists rely mostly on market orders, and place limit orders with thin-tailed offsets when they are unable to buy or sell immediately. The more Grahamists there are, the more β_i portfolios there are needing to be balanced. This competition

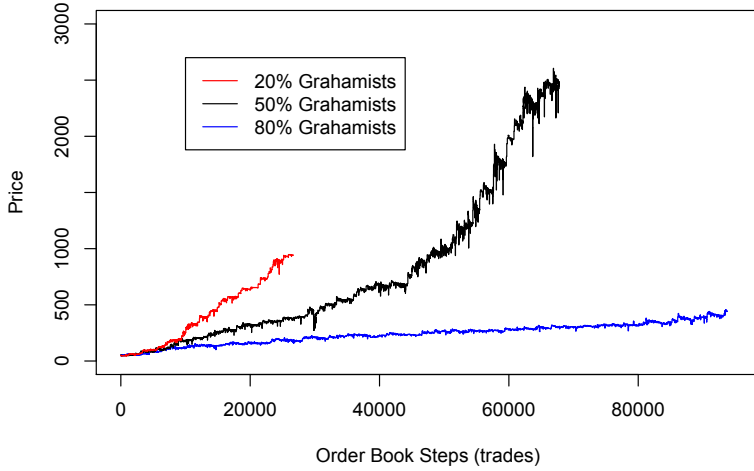


Figure 5.3: Price time series for 252 simulated trading days with 20% (red), 50% (black), and 80% (blue) Grahamists plotted against order book steps

to balance the bond-to-asset split results in increased trading, while the thin-tailed offsets ensure the price movements remain relatively small. Additionally, the Chartists may well be forecasting big changes, but the thin-tailed bids and asks from the Grahamists will outnumber the Chartists' limit orders, and thus cause them to expire before being traded.

All three time series exhibit volatility clustering and long memory in the first difference, observed in both the autocorrelation functions and the partial autocorrelation functions. This implies that GARCH is likely to be a more appropriate model for the time series than ARMA models, and that multifractal properties are potentially present. Given our objective of moving closer to reality, we narrowed our focus to the 80% Grahamists composition. In our analysis of the GE TAQ data, we rarely observed single price changes beyond a couple of dollars, but we also observed close to one million trades in 252 trading days. For these reasons, the time series with the most trades, but smaller average movements, seemed the most appropriate place to focus our initial efforts.

Analyzing the 80% Grahamists simulation output in greater detail, we start by observing the first price difference shown in Figure 5.5. Note the first difference exhibits the distinct triangular shaped bursts of volatility we observed in the zero-intelligence heavy-tailed model, but with considerably more noise interspersed among the clusters. The effect makes the price difference appear more similar to what we see in empirical financial data. Figures 5.6 and 5.7 show the autocorrelation function and partial autocorrelation function of the price difference from the first replication of the 80% Grahamists run. Given the lack of decay in autocorrelation and the volatility clusters observed in the first difference we apply a GARCH(1,1) fit to the differenced price time series. However, as with the zero-intelligence

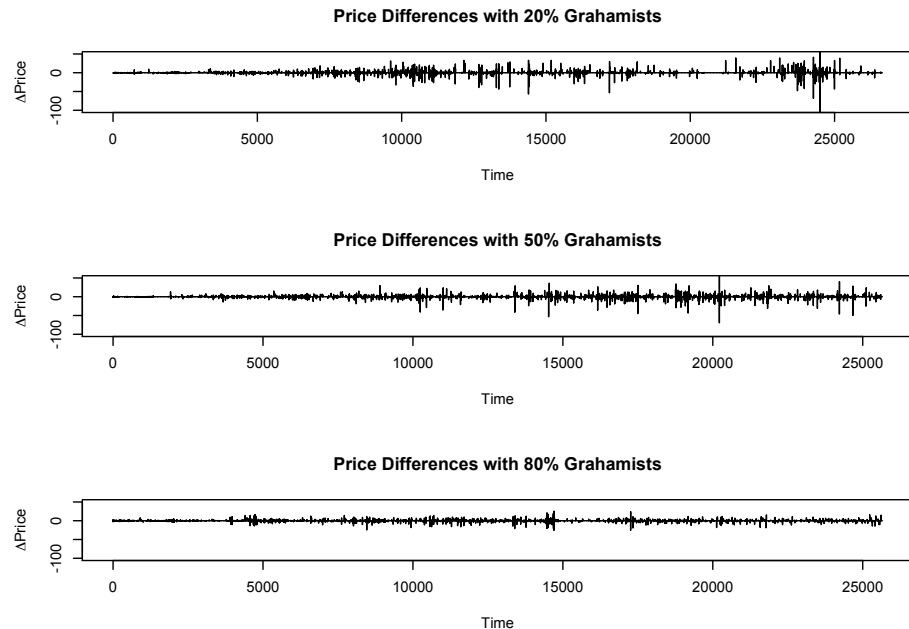


Figure 5.4: Price differences for 26,656 trades by proportion of Grahamists

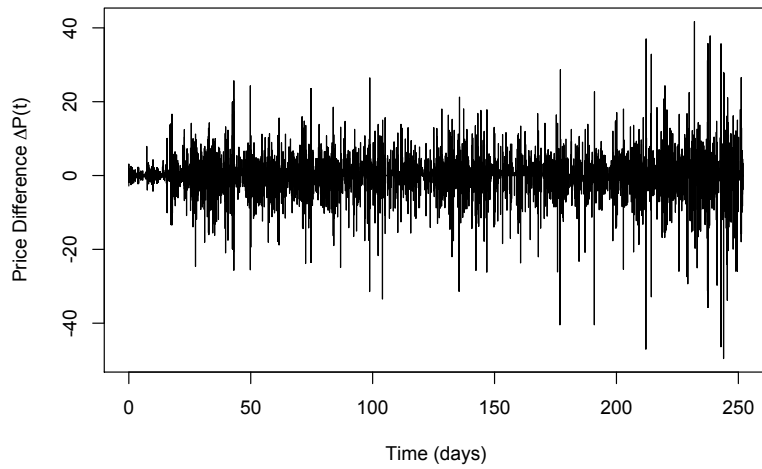


Figure 5.5: Price difference for 80% Grahamists first replication

model, the GARCH fit residuals failed the Box-Ljung-Pierce lack-of-fit test. A histogram of the residuals revealed a leptokurtic structure, and the Q-Q plot (shown in Figure 5.8) reveals a substantial departure from the normal in the tails.

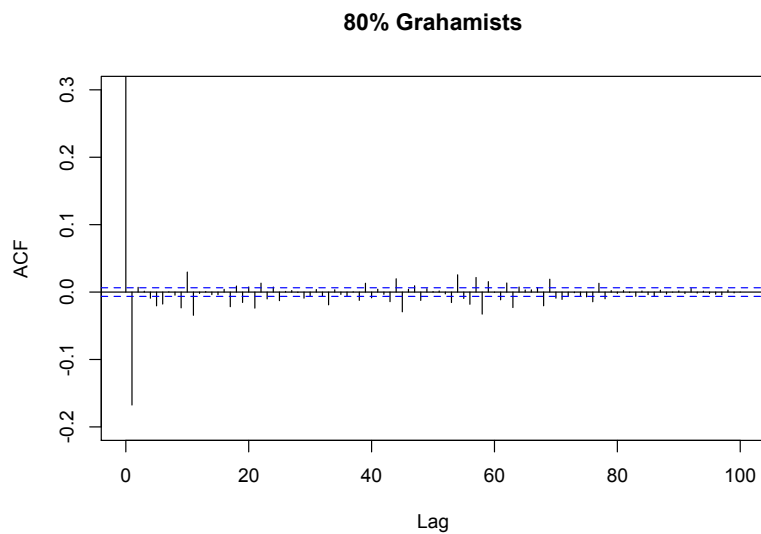


Figure 5.6: Autocorrelation function for 80% Grahamists on the first replication

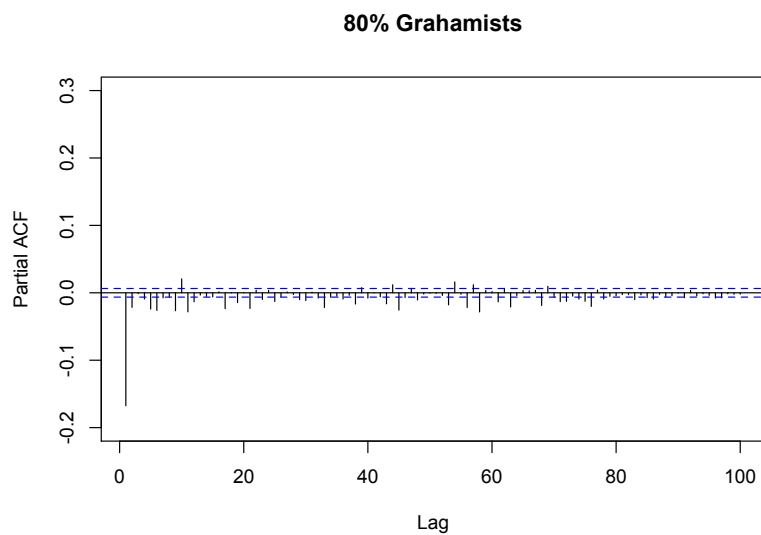


Figure 5.7: Partial autocorrelation function for 80% Grahamists on the first replication

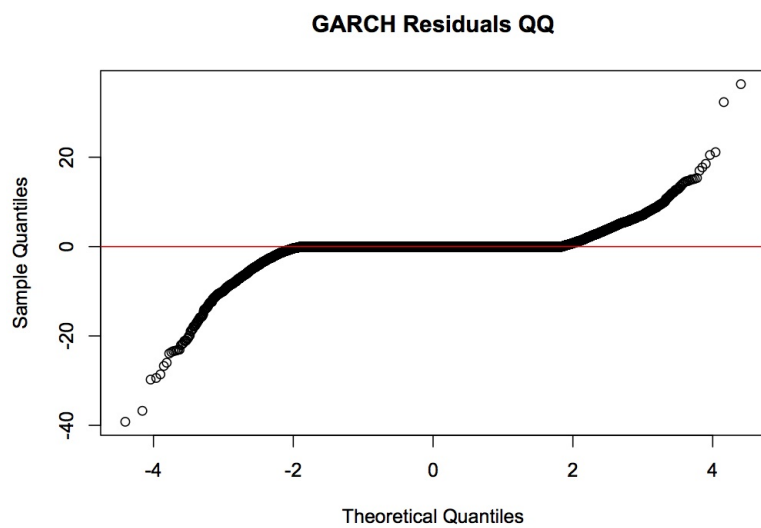


Figure 5.8: Q-Q plot of residuals from the GARCH(1,1) fit for 80% Grahamists on the first replication

Our final step in exploratory analysis was to apply MF-DFA to the simulated data. All three market compositions did produce multifractal properties in the time series. In the case of the 20% Grahamists, the minimum and maximum scales s had to be adjusted considerably to find the range where the multifractal properties were evident. However, this is expected for smaller data sets in general. Figure 5.9 shows the multifractal spectra of all three market compositions. Note that as the proportion of Grahamists increases, the multifractal spectrum narrows and shifts to lower Hölder exponents. What is of greater interest is that all the multifractal spectra now exhibit Hölder exponents greater than one-half. That is, many of the fluctuations exhibit persistent behavior rather than the antipersistent behavior we observed in the zero-intelligence model. In the sections that follow, we present the results of multiple replications of the 80% Grahamists simulation, and compare the multifractal properties of the positive-intelligence model to the zero-intelligence model and the GE TAQ data.

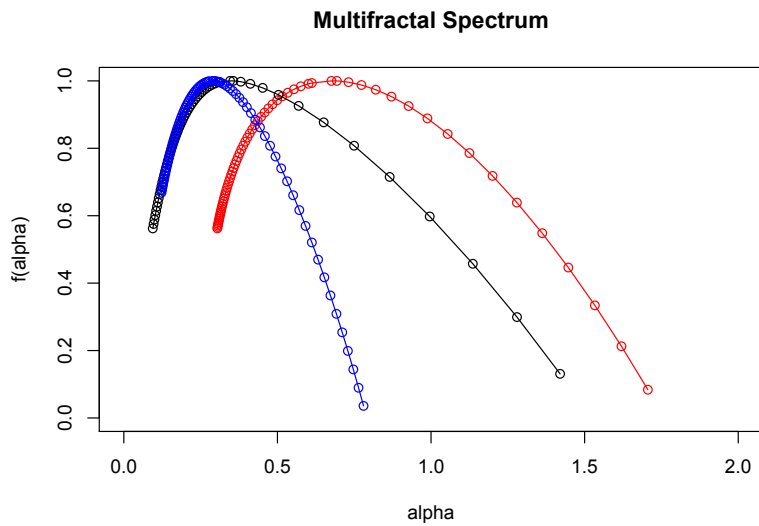


Figure 5.9: Multifractal spectra for different proportions of Grahamists: 20% (red), 50% (black), and 80% (blue)

5.5 Multifractal Results

In the case of monofractals such as Brownian motion or multifractals with closed-form multifractal spectra such as the stochastic binomial measure, the underlying mechanics governing the process are constant and well defined. As a result, the process may take any number of paths, but the multifractal spectrum remains unchanged. Due to Brownian motion being defined by the normal distribution, its increments always scale with the same Hölder exponent, $\alpha = 0.5$, making it a monofractal. Similarly, the stochastic binomial multifractal measure maintains the same spectrum of Hölder exponents determined only by the parameter used to allocate the mass during its construction. However, the mechanics underlying dynamically evolving systems are neither constant nor well defined, as illustrated in the previous sections. As such, we would expect a certain degree of variation in the multifractal spectra produced.

To investigate further the multifractal properties produced by the positive-intelligence financial market, we ran ten replications of the simulation with 80% Grahamists, starting with different random number seeds. Figure 5.10 shows the multifractal spectra obtained from the replications. The most central spectrum is shown in red, while the others are in gray for illustration purposes.

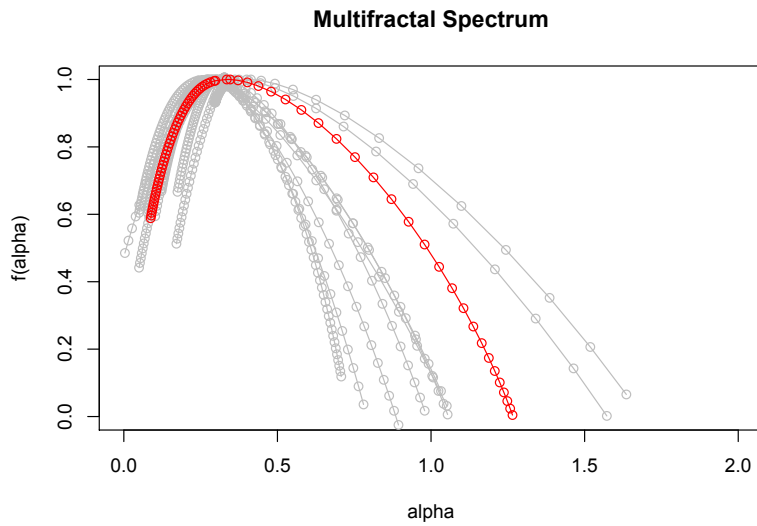


Figure 5.10: Multifractal spectra for ten runs of 80% Grahamists simulation

Although there is significant variation in the range of Hölder exponents α , there is very little variation in the $E[\alpha]$. For ten replications the average α -value corresponding to $f(\alpha) = 1$ was 0.319 with a 95% confidence interval of [0.287, 0.350]. This indicates there is some aspect of the system that remains relatively constant that determines the dominant Hölder exponent in the output of the simulation. As we

noted in Chapter 2, the multifractal spectrum identifies events that contribute to the overall price path at a vanishing frequency. These contributions appear to be enough to change the multifractal spectrum from one run to the next, but not enough to alter the expected value of the Hölder exponent. Table 5.2 shows the numerical results from the multifractal analysis of the ten runs.

Table 5.2: 80% Grahamists simulation multifractal results

Run	$\widehat{\text{Min }} \alpha$	$\widehat{\text{Max }} \alpha$	$\hat{E}[\alpha]$
1	0.123	0.780	0.291
2	0.050	1.032	0.272
3	0.087	1.265	0.341
4	0.050	0.979	0.322
5	0.102	1.051	0.273
6	0.004	1.054	0.283
7	0.175	0.894	0.303
8	0.171	0.708	0.326
9	0.297	1.636	0.407
10	0.079	1.572	0.368

Our next experiment was to analyze the impact of agent-adaptation on the multifractal spectrum. Figure 5.11 shows a comparison of the price path taken from the first run of the simulation with agent-adaptation off (red) and on (black). The time series are similar in length, but the average absolute price change is \$0.22 with adaptation turned on and \$0.50 with adaptation turned off. The net effect is a price that increases much faster when adaptation is off. Recall that Grahamists adapt by decreasing the rate at which they check their bond-to-asset split as their wealth increases. When adaptation is turned off, the Grahamists continue to trade more frequently, which in turn gives rise to larger price movements in an increasing market.

The multifractal spectra produced by the ten runs with agent-adaptation turned off are shown in Figure 5.12. It is interesting to note that although the price path has larger increments on average, the variation in the range of Hölder exponents is reduced slightly when the agents are not adapting. Recall that the right-hand side of the multifractal spectrum corresponds to the negative q -values and therefore the small fluctuations, while the left-hand side represents the large fluctuations. By comparing Figures 5.10 and 5.12 we see that adaptation has a greater effect on the large fluctuations as opposed to the small fluctuations. That is, the left-hand side of the multifractal spectrum shows much less variation when adaptation is turned off. The right-hand side appears to be less affected by adaptation, as the different replications continue to produce widely different Hölder exponents. It is interesting to note, however,

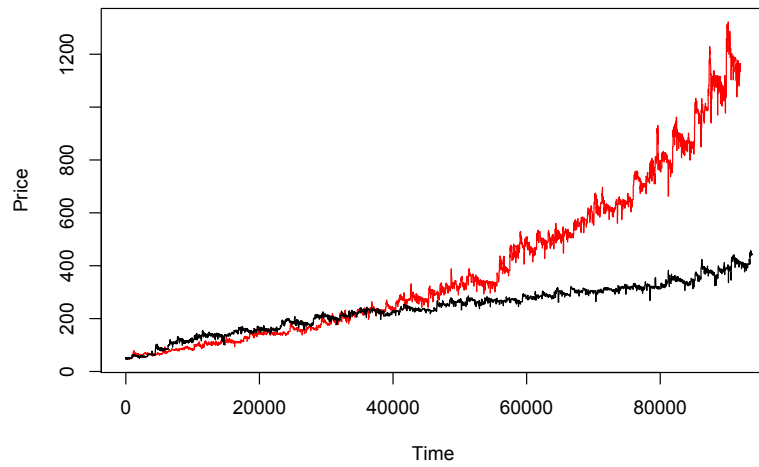


Figure 5.11: Price output from first run of the 80% Grahamists with adaptation on (black) and off (red)

that the $E[\alpha]$ is unchanged. The confidence interval from a paired t-test of the dominant Hölder exponent from the adaptation-on versus adaptation-off runs was $[-0.011, 0.050]$. Table 5.3 shows the numerical results of the multifractal analysis with adaptation off.

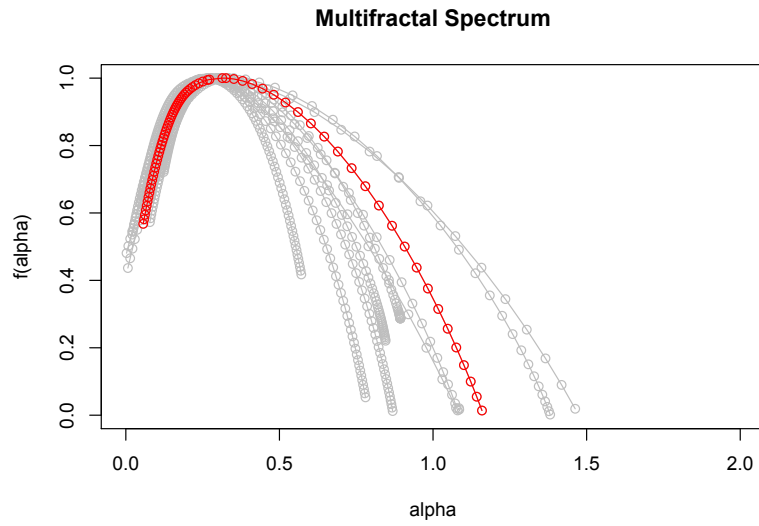


Figure 5.12: Multifractal spectra for ten runs of the 80% Grahamists simulation with adaptation turned off

Table 5.3: 80% Grahamists simulation multifractal results - adaptation off

Run	$\widehat{\text{Min } \alpha}$	$\widehat{\text{Max } \alpha}$	$\hat{E}[\alpha]$
1	0.107	0.780	0.266
2	0.021	0.869	0.275
3	0.057	1.159	0.320
4	0.007	1.075	0.277
5	0.078	0.846	0.301
6	0.081	0.571	0.271
7	0.074	1.383	0.342
8	0.002	0.894	0.331
9	0.048	1.462	0.301
10	0.123	1.085	0.307

Next, we conducted comparable runs of the simulation with 20% Grahamists and 50% Grahamists with adaptation turned on. Table 5.4 shows the mean value for the dominant Hölder exponent for each of the runs along with their respective 95% confidence intervals. We also conducted paired t -tests for the difference in $E[\alpha]$ between each combination of 20%, 50%, and 80% Grahamists. The results (Table 5.5) indicate there is enough evidence to reject the null hypothesis that the difference between the two values is equal to zero for all combinations. This suggests that the behavioral traits of traders in the market is instrumental in determining the dominant Hölder exponent in the price path.

Table 5.4: Expected value of the dominant Hölder exponent for 20%, 50%, and 80% Grahamists

Proportion of Grahamists	Mean $\hat{E}[\alpha]$	95% Confidence Interval
20%	0.532	[0.454, 0.611]
50%	0.388	[0.355, 0.420]
80%	0.319	[0.287, 0.350]

Our final step was to employ the shuffling heuristic to test whether the multifractal properties originate from heavy tails in the distribution of price changes or long memory in the process. Given the increased intelligence of agents and the thin-tailed offsets utilized by the Grahamists, we expect the source of the multifractal properties to be correlation in the price changes rather than heavy tails. Recall that if the price increments are i.i.d. random variables governed by a heavy-tailed distribution, then shuffling the

Table 5.5: Paired t -tests of the difference between dominant Hölder Exponents for 20%, 50%, and 80% Grahamists

Difference Tested	Mean Difference	95% Confidence Interval
20% – 50%	0.144	[0.042, 0.247]
20% – 80%	0.214	[0.112, 0.315]
50% – 80%	0.069	[0.052, 0.087]

increments should have no impact on the multifractal spectrum. Conversely, if the price increments exhibit long-term correlation, the shuffled series will have a distinctly different multifractal spectrum. Figure 5.13 shows the original 80% Grahamists multifractal spectrum in red, and the multifractal spectrum from the shuffled series in blue. The spectra differ substantially, indicating that the multifractal properties are most likely the result of long-term correlation in the price changes. Note also that the shuffled series is closer to being a monofractal, with all of the Hölder exponents clustered around $\alpha = 0.57$.

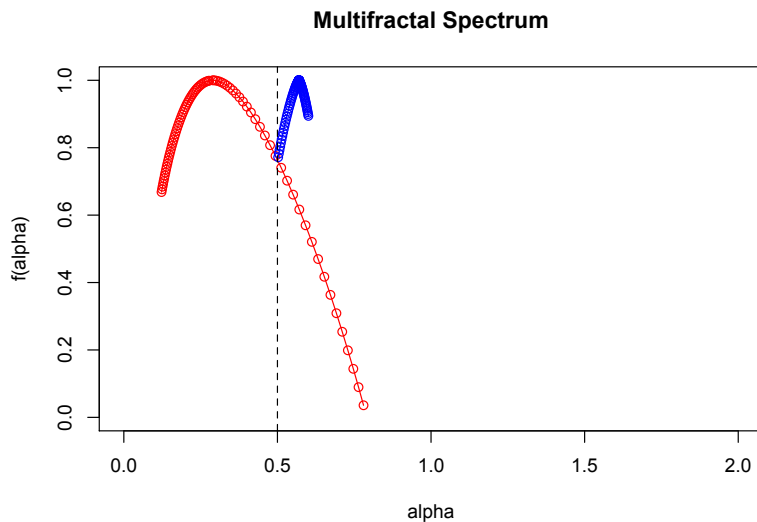


Figure 5.13: Multifractal spectra from the 80% Grahamists first replication (red) and the shuffled series (blue)

5.6 Discussion

From the results of the positive-intelligence financial market, we can conclude that a double auction order book structure coupled with informed agents, making decisions with publicly available information, and utilizing basic philosophies of market dynamics, can produce multifractal time series exhibiting persistence in the price increments. We have also shown that altering certain aspects of the market, such as agent-adaptation, has only minor effects on the multifractal properties, while other aspects, such as the composition of competing philosophies, can have more substantial effects on the multifractal properties. These results suggest that agent-based models have the potential to be tuned to multifractal properties observed in the price paths of real financial assets.

When analyzing the effect of different random number streams on the same configuration of our model, we noted that the dominant or expected Hölder exponent remained statistically unchanged, while the less prominent α -values showed greater variation. In a real asset, there is obviously only one price path, but we can analyze the multifractal properties of different years in isolation. It turns out that when we conducted such an analysis for the four years of GE TAQ data we analyzed in Chapter 3, we discovered that the dominant Hölder exponent remained unchanged, while the less prominent α -values varied more readily. Although the effect was less pronounced in the GE data than in the simulation, it indicates that certain aspects of real financial assets appear to dominate the price increments over many years and many millions of trades, while other aspects with less of an impact on the multifractal properties vary from year to year. Figure 5.14 shows the four multifractal spectra in gray, along with the spectrum taken from all years together in red.

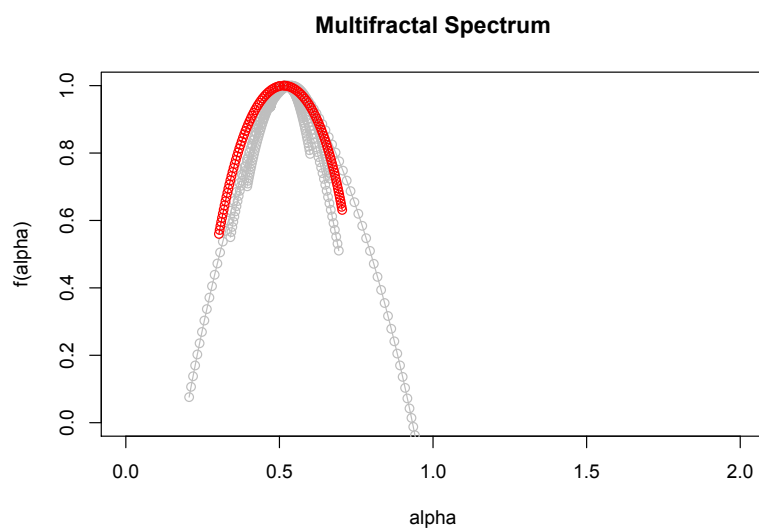


Figure 5.14: Multifractal spectra for GE's stock price in 2000, 2001, 2002 and 2003 (gray) and all years together (red)

Our analysis also indicates that positive agent intelligence is required if agent-based models hope to imitate the properties we observe in empirical financial data. Our thin-tailed experiment with the zero-intelligence model produced a plausible price path, but failed to exhibit the scaling properties we see in the real market. Conversely, the heavy-tailed experiment yielded a completely implausible price path, but did produce multifractal properties. The positive-intelligence model only incorporated thin-tailed distributions for price offsets. Yet, the model produces plausible price paths, some persistence in price increments, and multifractal properties. It is our contention that without multifractal analysis, we might conclude that the zero-intelligence model with thin-tailed offsets is a reasonable representation of a real financial market. However, running MF-DFA on the output of the thin-tailed zero-intelligence experiment reveals an antipersistent, monofractal price path. Multifractal analysis, therefore, illuminates the relative simplicity of the simulation and its inability to replicate the complexity we observe in real data.

Figure 5.15 shows the multifractal spectra from the heavy-tailed experiment, the GE stock data, and the 20% Grahamists positive-intelligence simulation. Like LeBaron's model, our positive-intelligence financial market could be classified as a computational thought experiment [50]. However, it is clear that the addition of agent intelligence brings the output of agent-based financial market models closer to reality. Much research and market analysis is required to further ground the behavior of agents on more realistic footing. But, the mechanics of the order book and the behavioral traits of the agents in our model are intended to be advancements toward a real financial market. And the model is constructed in such a way that additions and embellishments can be easily added for future research. In the next chapter we summarize the advancements made in this dissertation, and discuss avenues for future research in greater depth.

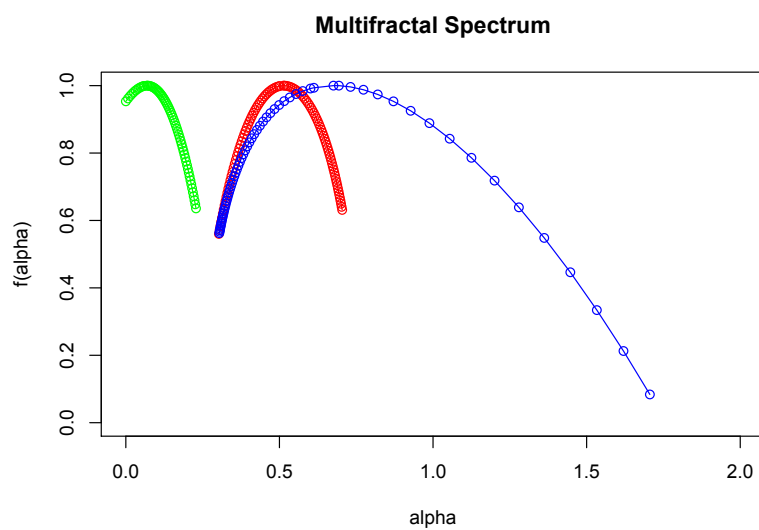


Figure 5.15: Multifractal spectra for GE's stock price (red), the heavy-tailed zero-intelligence simulation (green), and the positive-intelligence 20% Grahamists (blue)

Chapter 6

Conclusions and Future Research

6.1 Summary

We began this dissertation with a discussion of objects that are too rough or irregular to be measured using traditional Euclidean geometry. Mandelbrot introduced the term *fractal* to describe such objects, and derived the mathematics required to analyze their properties [57]. The critical value needed to describe a fractal is its Hausdorff dimension D , which in the case of time series data, is captured by the Hurst exponent H through the relationship $H = 2 - D$. However, many time series, most notably financial data, exhibit such complex scaling properties that a single exponent is insufficient to describe their behavior. These time series are characterized by a spectrum of more local Hölder exponents, $\alpha(t)$. The set of time points within the series that support a given $\alpha(t)$ are dispersed throughout the domain and constitute a fractal set. The Hausdorff dimension of each such set is given by the multifractal spectrum $f(\alpha)$. The range of $\alpha(t)$ and the corresponding Hausdorff dimension of the points supporting each $\alpha(t)$, $f(\alpha)$, stochastically quantify a multifractal time series. A number of algorithms exist for extracting the multifractal spectrum, but we focused on multifractal detrended fluctuation analysis (MF-DFA) due to its accuracy and ease of implementation. We developed a robust, fully portable software application in Java that enables the user to manipulate the necessary parameters needed for the algorithm, and performs statistical goodness of fit tests for the interim steps to ensure the appropriate detrending is employed for a given data set. Using this application, we conducted a thorough analysis of General Electric's stock price from the beginning of 2000 to the end of 2003. We used fine-scale trade and quote data for this analysis, and showed that GE's stock does in fact exhibit multifractal properties. We also illustrated the difficulty in describing the GE data using more traditional time series techniques.

The multifractal spectrum can also be described as a renormalized density of Hölder exponents. It essentially captures scaling properties that contribute to the construction of a multifractal time series only briefly, before giving way to more dominant effects. And it has been shown by us and others (see [13] for example) that empirical financial data exhibit multifractal properties. It follows that any model of a

financial market that hopes to capture true market dynamics, must also produce multifractal properties. With the growing use of agent-based modeling in economics, we set out to analyze the output of an agent-based model of financial markets using MF-DFA. We first constructed a simple model known as the zero-intelligence model. The agents in a zero-intelligence model blindly place orders to buy and sell through a double auction order book. We determined that the order book structure coupled with zero-intelligence agents created antipersistent price paths that did exhibit fractal properties. By manipulating the price offset used by the agents when placing their buy and sell orders, we were able induce both monofractal and multifractal time series. Both series exhibited many of the stylized facts observed in real financial data, such as heavy-tailed returns and volatility clustering.

Given the ongoing debate in economics over how market participants behave, and whether individual behavior actually has a significant impact on the price of an asset on the aggregate level, we expanded our zero-intelligence model in a first step towards a more realistic structure. We incorporated two different strategies for trading into our agents and gave them increased intelligence (i.e., behavioral logic). This positive-intelligence model produced more plausible price paths than our prototype zero-intelligence model, and exhibited multifractal properties and persistent price increments similar to what we observed in the empirical data. These results indicate that multifractal analysis is a critical tool for analyzing certain complex systems, and that agent-based models have enormous potential for gaining insight into financial market dynamics.

6.2 Conclusions

In order to validate a simulation model, Law advocates utilizing quantitative techniques whenever possible, as well as statistical procedures to compare simulation output with output from the real system [46]. He goes on to say that for time series output, confidence interval approaches based on nonparametric analysis are preferable to hypothesis tests, and that Fourier transformations of the autocovariance function are one such approach. When analyzing complex systems, like financial markets, the outputs of the real system can potentially exhibit such wild properties that many quantitative analyses are ill-defined. In Chapter 3, we attempted to apply ARMA and GARCH models to the fine-scale GE price time series with little success. As noted, we could have continued to manipulate the parameters of these models to obtain better fits, but the parametric nature of that endeavor would make the resulting fit all the more delicate and harder to replicate in a simulated environment. Multifractal analysis, on the other hand, makes no assumptions about the underlying distributions of the observations in a time series. It simply breaks the data into smaller and smaller time scales, performs an appropriate regression based on the data in question, and checks for power law relationships in the variance of that regression at different time scales. If no such relationship exists, the output of MF-DFA will exhibit a spectrum that violates the properties $f(\alpha)$ is known to possess, indicating that the time series is not multifractal. Thus, our main conclusion is that multifractal analysis is well suited for validating agent-based models of financial markets and other

complex systems.

There is continuing debate over which parametric models best describe heavy-tailed returns and volatility clustering that are exceedingly common in financial time series. Mandelbrot suggested that we relinquish our reliance on the Gaussian approach started by Bachelier over a century ago, and focus on the scale invariant properties that are ubiquitous in finance [54]. His pioneering work in fractal geometry paved the way for this analysis, and with advances in computing power, we can extract multifractal properties from data in a matter of seconds. It is our contention that multifractal analysis should become a standard technique for analyzing complex systems, along side the other parametric approaches that often have difficulty capturing the multi-scaling nature of certain time series.

By utilizing MF-DFA to analyze the output of our agent-based financial market models, we were able to quickly recognize that our zero-intelligence model with thin-tailed offsets did not exhibit enough complexity to represent a real financial time series. Although qualitatively it appeared to be a more plausible price path than our heavy-tailed experiment and did exhibit volatility clusters, its increments scaled with only a single exponent. Conversely, by forcing our zero-intelligence agents to place very implausible orders, we produced multifractal properties in the simulation output at the expense of creating an implausible price path. Enhancing the agent-based financial market with more realistic structure gave us both a plausible price path and multifractal properties. We concluded that agent-based financial markets are ideal for modeling financial structure, but that the simplest models are likely to be insufficient. Given the advances in computer power and in agent-based modeling software and techniques, we contend that the finance and simulation communities should continue to move these models toward a more realistic structure. LeBaron noted that the double auction order book is the most realistic mechanism for market clearing [48]. A number of studies have been conducted on agent behavior and the psychology governing real market participants [74, 29, 40, 37]. Our positive-intelligence model is one of the first models we have seen that tries to incorporate both the order book structure and some of these competing theories of market psychology. Though our intention here was to illustrate the application of MF-DFA, we believe the positive-intelligence model should be enhanced and embellished for future study. The multifractal analysis clearly showed an improvement toward more realistic time series in the positive-intelligence model. The positive-intelligence output was qualitatively more plausible, but subtly contained the persistent price increments and multifractal properties we observed in empirical data. In the next section we discuss some of the possible avenues for this and other future research.

6.3 Future Research

The positive-intelligence model in its current form offers several opportunities for future research. We discovered in exploratory analysis that more than 100 agents were required to prevent the model from reaching an equilibrium price in only a few thousand trades. Once the equilibrium was reached, no further trades occurred. The impact of changing the quantity of agents, step rates of agents, β - and

ψ -values for each group of agents, and the initial price of the asset, could all be analyzed with little or no modification to the current model. One especially interesting extension of the positive-intelligence model would be to implement an adaptive exponential smoothing technique that effectively improves the forecast accuracy for each Chartist over time; see, for example, Trigg and Leach, "Exponential Smoothing with an Adaptive Response Rate," [77] and Ekern, "Adaptive Exponential Smoothing Revisited" [20]. However, these essential next steps still fall into the category of computational thought experiments. The most intriguing opportunity is the calibration of a positive-intelligence order book model to an actual asset or collection of assets. The typical steps to building a simulation model involve collecting data and validating assumptions. Although we based our modeling assumptions on published literature, surveys of actual market participants, the calibration of order rates to real markets, and the incorporation of more than one risky asset are all endeavors that should be undertaken to enhance the positive-intelligence model and its agents. Another addition to such models would be the shock of external events. Currently the model is a closed system with no outside influence. However, pundits and economists alike, claim that certain world events bolster or rattle the confidence of investors. One relatively simple inclusion could be a representation of a Federal Reserve agent that adjusts interest rates periodically. By allowing the investing agents to borrow capital to invest in the risky market, the concepts of leverage and the impact of interest rate control by a federal entity could be analyzed.

Similarly, the analysis of the multifractal properties of both empirical data and agent-based simulation output offers a number of possibilities for future research. One area that has already begun to incorporate multifractal analysis is large deviation theory and, by extension, risk modeling and assessment. One of the central quantities in risk analysis is the probability that after some elapsed time x from the last event exceeding a threshold Q , the next event above Q will occur within a very short interval of time. Bogachev et al. showed that for multifractal data sets with nonlinear correlation in the returns, this probability is dependent on the threshold Q through the function $\delta(Q)$. The function $\delta(Q)$ presents as a power law in multifractal data sets and can therefore be obtained empirically [9]. Utilizing MF-DFA to first extract these properties from empirical data, and then formulate a risk estimation model from the results is a natural next step. Additionally, the multifractal spectrum, may give indications about fundamental changes in the dynamics of a system. As shown in Chapter 5, we analyzed different years of the GE data in isolation. One interesting comparison was the multifractal spectrum from the year 2000 to that of 2001. Noting that the terrorist attacks on the World Trade Center happened in 2001, it is fascinating to see the change in the multifractal spectrum between these two years (see Figure 6.1). The positive-intelligence model also revealed that altering the proportion of different market behaviors could shift the peak of the multifractal spectrum, while different random number streams only seem to affect the breadth of the spectrum and the concentration of Hölder exponents on either side of the peak. Connecting these changes in the multifractal spectrum with changes in the underlying system deserves considerably more attention. It is common to present a plausible story, such as the World Trade Center attacks, for large changes in the economic climate. However, the expected Hölder exponent in the GE data remained unchanged

from 2000 to 2003, while the less prominent exponents varied more readily. Perhaps multifractal analysis can lend weight to these explanations or dispel their validity if the impact of such changes can be better quantified.

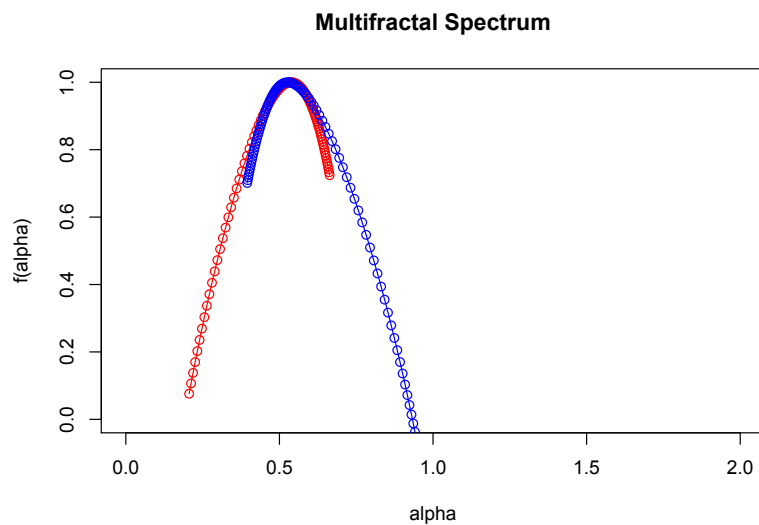


Figure 6.1: Multifractal spectra for GE's stock price in 2000 (red) and 2001 (blue)

REFERENCES

- [1] General Electric: www.ge.com.
- [2] JAMA matrix package: <http://math.nist.gov/javanumerics/jama/>.
- [3] JFree Chart: <http://www.jfree.org/jfreechart/>.
- [4] Wharton Research Data Services: <http://wrds-web.wharton.upenn.edu/wrds/>, 2013.
- [5] P. S. Addison. *Fractals and Chaos: An Illustrated Course*. The Institute of Physics, London, 1997.
- [6] E. Bacry, A. Kozhemyak, and J. Muzy. Continuous cascade models for asset returns. *Journal of Economic Dynamics and Control*, (32):156–199, 2008.
- [7] J. Beran. *Statistics for Long Memory Processes*. Chapman and Hall CRC Press, 1998.
- [8] P. Bloomfield. *Fourier Analysis of Time Series*. New York: Wiley, 1976.
- [9] M. I. Bogachev, J. F. Eichner, and A. Bunde. Effect of nonlinear correlations on the statistics of return intervals in multifractal data sets. *Physical Review Letters*, 99(4):24061–1:24061–4, December 2007.
- [10] G. Box and G. Jenkins. *Time Series Analysis: Forecasting and Control*. Prentice Hall, 3rd edition, 1994.
- [11] T. Brenner. *Handbook of Computational Economics: Agent Based Computational Economics*, volume II, chapter Agent Learning Representation: Advice on Modelling Economic Learning. Amsterdam: Elsevier, 2006.
- [12] C. Burrus, R. Gopinath, and H. Guo. *Introduction to Wavelets and Wavelet Transforms: A Primer*. New Jersey: Prentice Hall, 1998.
- [13] L. Calvet and A. Fisher. Multifractality in asset returns: Theory and evidence. *The Review of Economics Statistics*, 84(3):381–406, 2002.
- [14] J. Y. Campbell and R. Schiller. The dividend-price ratio and expectations of future dividends and discount factors. *Review of Financial Studies*, 1(3):195–227, 1988.
- [15] M. E. Cates and J. M. Deutsch. Spatial correlations in multifractals. *The American Physical Society - Physical Review A*, 35(11):4907–4910, 1987.
- [16] W. K. Chan. Interaction metric of emergent behaviors in agent-based simulation. *Proceedings of 2011 Winter Simulation Conference*, 2011.
- [17] S. Chen and C. Yeh. On the emergent properties of artificial stock markets: the efficient market hypothesis and the rational expectations hypothesis. *Journal of Economic Behavior and Organization*, 49:217–239, 2002.

- [18] J. Courtalt, Y. Kabanov, B. Bru, P. Crepel, I. Lebon, and A. Marchand. Louis Bachelier on the centenary of *Theorie de la Speculation*. *Mathematical Finance*, 10(3):341–353, 2000.
- [19] J. Duffy. *Handbook of Computational Economics: Agent Based Computational Economics*, chapter Agent-based Models and Human Subject Experiments. Amsterdam: Elsevier, 2006.
- [20] S. Ekeren. Adaptive exponential smoothing revisited. *The Journal of Operational Research*, 32(9):775–782, 1981.
- [21] R. F. Engle. Autoregressive conditional heteroscedasticity with estimates of the variance of United Kingdom inflation. *Econometrica*, 50(4):987–1007, July 1982.
- [22] J. M. Epstein and R. L. Axtell. *Growing Artificial Societies: Social Science from the Bottom Up*. MIT Press, Cambridge, MA, 1996.
- [23] A. Etheridge. *A Course in Financial Calculus*. Cambridge University Press, 2002.
- [24] E. Fama. Efficient capital markets: II. *The Journal of Finance*, 46(5):1575–1617, 1991.
- [25] M. Farge, K. Schneider, O. Pannekoucke, and R. Nguyen Van Yen. *Handbook of Environmental Fluid Dynamics*, volume 2, chapter Multiscale Representations: Fractals, Self-similar Random Processes and Wavelets, pages 311–332. CRC Press, 2013, in press.
- [26] J. D. Farmer, P. Patelli, and I. Zovko. The predictive power of zero intelligence in financial markets. *Proceedings of the National Academy of Sciences*, 102(6):2254–2259, 2005.
- [27] R. A. Fisher and F. Yates. *Statistical tables for biological, agricultural and medical research*. London: Oliver and Boyd, 1948.
- [28] M. Frame, B. B. Mandelbrot, and N. Neger. Fractal geometry: <http://classes.yale.edu/fractals>.
- [29] J. A. Frankel and K. A. Froot. Chartists, fundamentalists and the demand for dollars. *The American Economic Review*, 80(2):181–185, 1990.
- [30] U. Frisch and G. Parisi. *Fully Developed Turbulence and Intermittency in Turbulence and Predictability in Geophysical Fluid Dynamics and Climate Dynamics*. Amsterdam: North-Holland, 1985.
- [31] B. V. Gnedenko. *The Theory of Probability*. New York: Chelsea Publishing Co., 4th edition, 1968.
- [32] D. K. Gode and S. Sunder. Allocative efficiency of markets with zero-intelligence traders: Market as a partial substitute for individual rationality. *Journal of Political Economy*, 101(1):119–137, 1993.
- [33] Benjamin Graham. *The Intelligent Investor*. Harper and Brothers, 2003 ed edition, 1949.
- [34] M.A. Graneroa, J.E. Segoviab, and J. G. Perez. Some comments on hurst exponent and the long memory processes on capital markets. *Physica A*, 387:5543 – 5551, 2008.
- [35] James E. Hartley. The origins of the representative agent. *Journal of Economic Perspectives*, 10(2):169–177, 1996.

- [36] A. Harvey, E. Ruiz, and N. Shephard. Multivariate stochastic volatility models. *Review of Economic Studies*, (61):247–264, 1994.
- [37] C. H. Hommes. *Handbook of Computational Economics: Agent Based Computational Economics*, chapter Heterogeneous Agent Models in Economics and Finance, pages 1111–1186. Amsterdam: Elsevier, 2006.
- [38] P. Ivanov, L. Amaral, A. Goldberger, S. Havlin, M. Rosenblum, Z. Struzik, and H. Stanley. Multi-fractality in human heartbeat dynamics. *Nature*, (399):461–465, June 1999.
- [39] J. S. Jordan. Bayesian learning in normal form games. *Games and Economic Behavior*, 3(1):60–81, 1991.
- [40] D. Kahneman and A. Tversky. Prospect theory: An analysis of decision under risk. *Econometrica*, 47(2):263–292, March 1979.
- [41] J. Kantelhardt, E. Koschielny-Bunde, H. Rego, S. Havlin, and A. Bunde. Detecting long-range correlations with detrended fluctuation analysis. *Physica A*, (295):441–454, 2001.
- [42] J. Kantelhardt, S. A. Zschiegner, E. Koschielny-Bunde, S. Havlin, A. Bunde, and H. Stanley. Multifractal detrended fluctuation analysis of nonstationary time series. *Physica A*, (316):87–114, 2002.
- [43] Alan P. Kirman. What does the representative individual represent? *Journal of Economic Perspectives*, 6(2):117–136, 1992.
- [44] M. Kuhl, S. Sumant, and J. Wilson. An automated multiresolution procedure for modeling complex arrival processes. *INFORMS Journal on Computing*, 18(1):3–18, Winter 2006.
- [45] B. Lashermes, P. Abry, and P. Chainais. New insights into the estimation of scaling exponents. *International Journal of Wavelets, Multiresolution and Information Processing*, 2(4):497–523, 2004.
- [46] A. M. Law. *Simulation Modeling and Analysis*. McGraw-Hill, 2007.
- [47] B. LeBaron. Empirical regularities from interacting long- and short-memory investors in an agent-based stock market. *IEEE Transactions on Evolutionary Computation*, 5(5):442–455, October 2001.
- [48] B. LeBaron. *Handbook of Computational Economics: Agent Based Computational Economics*, chapter Agent-Based Computational Finance. Amsterdam: Elsevier, 2006.
- [49] B. LeBaron. *Post Walrasian Macroeconomics: Beyond the DSGE Model*, chapter Agent-based Financial Markets: Matching Stylized Facts with Style. Cambridge University Press, 2006.
- [50] B. LeBaron. Heterogeneous gain learning and the dynamics of asset prices. *Journal of Economic Behavior and Organization*, 83(3):424–445, 2011.
- [51] M. Lettau. Explaining the facts with adaptive agents: The case of mutual fund flows. *Journal of Economic Dynamics and Control*, (21):1117–1147, 1997.

- [52] S. Luke. Mason: A multiagent simulation environment. *Simulation*, 81(7):517–527, July 2005.
- [53] S. Mallat and W. Hwang. Singularity detection and processing with wavelets. *IEEE Transactions on Information Theory*, 38(2):617–643, March 1992.
- [54] B. B. Mandelbrot. The variation of certain speculative prices. *Journal of Business*, 36(4), October 1963.
- [55] B. B. Mandelbrot. How long is the coast of Britain? statistical self-similarity and fractional dimension. *Science*, 156(3775):636–638, May 1967.
- [56] B. B. Mandelbrot. Possible refinement of the lognormal hypothesis concerning the distribution of energy dissipation in intermittent turbulence. *Physics*, 12:331–351, 1972.
- [57] B. B. Mandelbrot. *The Fractal Geometry of Nature*. W. H. Freeman and Company: New York, 1977.
- [58] B. B. Mandelbrot. Multifractal measures, especially for the geophysicist. *PAGEOPH*, 131(1/2):5–42, March 1989.
- [59] B. B. Mandelbrot, A. Fisher, and L. Calvet. The multifractal model of asset returns. *Cowles Foundation Discussion Paper*, Yale University(1164), 1997.
- [60] B. B. Mandelbrot and R. Hudson. *The Misbehavior of Markets: A Fractal View of Risk, Ruin, and Reward*. Basic Books, 2004.
- [61] B. B. Mandelbrot and J. W. van Ness. Fractional brownian motions, fractional noises and applications. *SIAM Review*, 10(4):422–437, 1968.
- [62] M. J. North and C. M. Macal. *Managing Business Complexity*. Oxford University Press, 2007.
- [63] R. G. Palmer, W. B. Arthur, J. H. Holland, and B. LeBaron. An artificial stock market. *Artificial Life and Robotics*, 1998.
- [64] C. Peng, S. Buldyrev, S. Havlin, M. Simons, H. Stanley, and A. Goldberger. Mosaic organization of DNA nucleotides. *Physical Review E*, 49(2):1685–1689, February 1994.
- [65] S. F. Railsback, S. L. Lytinen, and S. K. Jackson. Agent-based simulation platforms: Review and development recommendations. *Simulation*, 82(9):609–623, 2006.
- [66] R. H. Reidi. Multifractal processes. Technical Report ADA531331, Defense Technical Information Center, 1999.
- [67] S. A. Rice. *Advances in Chemical Physics, Fractals, Diffusion and Relaxation in Disordered Complex Systems*. John Wiley and Sons, 2006.
- [68] S. P. Robbins. *Organizational Behavior*, volume 9th. New Jersey: Prentice Hall, 2001.
- [69] T. C. Schelling. Dynamic models of segregation. *Journal of Mathematical Sociology*, 1:143–186, 1971.

- [70] A. G. Schilling. Scorboard. *Forbes*, 151(4):236, 1993.
- [71] R. Shumway and D. Stoffer. *Time Series Analysis and Its Applications*. Springer Science and Business Media, LLC, 2nd edition, 2006.
- [72] N. N. Taleb. *The Black Swan*. New York: Random House, 2007.
- [73] M. Taqqu and V. Teverovsky. Estimators for long-range dependence: An empirical study. *Fractals*, 3(4), 1995.
- [74] L. Tesfatsion. *Handbook of Computational Economics: Agent Based Computational Economics*, volume II, chapter Agent-based Computational Economics: A Constructive Approach to Economic Theory. Amsterdam: Elsevier, 2nd edition, 2006.
- [75] Y. Tessier, S. Lovejoy, P. Hubert, D. Schertzer, and S. Pecknold. Multifractal analysis and modeling of rainfall and river flows and scaling, causal transfer functions. *Journal of Geophysical Research*, 101(D21):26,427–26,440, 1996.
- [76] V. Teverovsky, M. Taqqu, and W. Willinger. A critical look at Lo's modified R/S statistic. *Journal of Statistical Planning and Inference*, (80):211–227, 1999.
- [77] D.W. Trigg and A.G. Leach. Exponenital smoothing with an adaptive response rate. *Operational Research*, 18(1):53–59, 1967.
- [78] C. P. Winsor. The gompertz curve as a growth curve. *Proceedings of the National Academy of Sciences*, 18(1), 1932.
- [79] Z. Yi, W. Zhang, and X. Du. Nonlinear correlation tracking technique in data mining of financial markets. *Journal of Software*, 11(12):1581–1587, 2000.

APPENDIX

Appendix A

A.1 The Multifractal Binomial Measure

The multifractal binomial measure is an example of a simple multiplicative cascade. Expansions on this general procedure lead to more complex multifractals. The concept of a multiplicative cascade forms the basis for *trading time* in the multifractal model of asset returns (MMAR) [13].

Let m_0 and m_1 be two positive numbers such that $m_0 + m_1 = 1$. Let $\mu_0(t)$ represent a uniform probability measure (p.d.f.) on the interval $[0, 1]$. The multiplicative cascade is constructed through an infinite iteration process. In the first step, we define a new measure $\mu_1(t)$ such that $\mu_1(t) = m_0$ for $0 \leq t \leq \frac{1}{2}$ and $\mu_1(t) = m_1$ for $\frac{1}{2} < t \leq 1$. In the second step we repeat this process for each subinterval. That is, for the interval $[0, \frac{1}{2}]$ we assign the portion m_0 of its mass to the interval $[0, \frac{1}{4}]$ and the portion m_1 of its mass to the interval $[\frac{1}{4}, \frac{1}{2}]$. This same process is also applied to the interval $[\frac{1}{2}, 1]$ so that the measure $\mu_2(t)$ is defined as

$$\mu_2(t) = \begin{cases} m_0m_0, & \text{if } 0 \leq t \leq \frac{1}{4}, \\ m_0m_1, & \text{if } \frac{1}{4} < t \leq \frac{1}{2}, \\ m_1m_0, & \text{if } \frac{1}{2} < t \leq \frac{3}{4}, \\ m_1m_1, & \text{if } \frac{3}{4} < t \leq 1. \end{cases} \quad (\text{A.1})$$

If we repeat this process *ad infinitum* we generate an infinite sequence of measures $\{\mu_k(t) : k = 1, 2, \dots\}$.

We can represent the ever smaller intervals using binary representation such $\frac{1}{2} = 0.1000$ and $\frac{1}{4} = 0.0100$, etc. Define η_k to be the binary digit in the k^{th} position of the binary representation of a number in $[0, 1]$. Then we can represent the dyadic number t as

$$t = 0.\eta_1\eta_2\dots\eta_k = \sum_{i=1}^k \eta_i 2^{-i} \quad (\text{A.2})$$

So for the interval $[t, t + 2^{-k}]$ in the k^{th} step of the cascade, we uniformly distribute the portion m_0 of the mass on the subinterval $[t, t + 2^{-k-1}]$ and distribute the portion m_1 of the mass on the interval $[t + 2^{-k-1}, t + 2^{-k}]$. If we now define φ_0 as the relative frequency of 0's in the binary representation of t and φ_1 as the relative frequency of 1's in the binary representation of t , then we can quantify the measure of $\mu_k(x)$ as

$$\mu_k(x) = m_0^{k\varphi_0} m_1^{k\varphi_1}, \text{ for } t \leq x \leq t + 2^{-k}. \quad (\text{A.3})$$

Like many multifractals, the limiting multifractal binomial measure as $k \rightarrow \infty$ is a continuous probability measure, but it has no density and no point mass [59].

A.2 Simulating the Multifractal Binomial Measure

The following is an iterative procedure for simulating the binomial multifractal process and its associated measure on $[0, 1]$ presented in pseudocode.

We seek to perform a sufficiently large number of iterations, n , of the following procedure to obtain a multifractal time series of length $N = 2^n$,

$$\{x_{i,n} = m_0^{\varphi_1} m_1^{N-\varphi_1} : i = 1, \dots, N\} \quad (\text{A.4})$$

where $0 < m_0 < 1$, $m_1 = 1 - m_0$, and $\varphi_1 = \{\text{the number of 1's in the binary representation of } i\}$. The algorithm is as follows:

```

 $x_{i,n} \leftarrow \text{NULL}$ , (initialize the time series)
 $\mu_n \leftarrow \text{NULL}$ , (initialize the measure)
 $n_{\max} \leftarrow 12$ , (maximum # of iterations)
 $n \leftarrow 1$ , (current iteration #)
 $N \leftarrow 2^n$ , (# of cells)
 $\delta \leftarrow \frac{1}{N}$ , (cell length)
 $M_{0,n} \leftarrow 0$ , (fractal measure (c.d.f.) up to current cell)
Define the function  $m_{(i) \bmod 2} \leftarrow \begin{cases} m_0, & \text{if } i \bmod 2 = 0 \\ m_1, & \text{if } i \bmod 2 = 1 \end{cases}$ 

Initialization {
    For  $i = 0$  to  $N - 1$  {
        define the  $i^{\text{th}}$  cell as  $C_{i,n} = (a_{i,n}, b_{i,n}]$ , where
    }
}

```

```

 $a_{i,n} \leftarrow i\delta$  (cell lower limit)
 $b_{i,n} \leftarrow a_{i,n} + \delta$  (cell upper limit)
 $p_{i,n} \leftarrow m_{(i) \bmod 2}$  (cell probability)
 $x_{i,n} \leftarrow p_{i,n}$  (latest observation of the time series on the current iteration)
If ( $i \neq 0$ ) {
     $M_{i,n} \leftarrow M_{i-1,n} + p_{i,n}$  (fractal measure of  $(0, b_{i,n}]$ )
} (End If)
} (End For loop)
call mainRun()
} (End Initialization)

mainRun() {
     $n \leftarrow n + 1$ 
    If ( $n < n_{\max}$ ) {
        For  $j = 1$  to  $(n_{\max} - 1)$  {
             $N \leftarrow 2N$ 
             $\delta \leftarrow \delta/2$ 
             $\mu_n = \text{nextIteration}()$ 
        } (End For loop)
    } (End If)
    return  $\mu_n$ 
    Stop
} (End mainRun)

nextIteration() {
    For  $i = 0$  to  $N - 1$  {
        define the  $i^{\text{th}}$  cell as  $C_{i,n} = (a_{i,n}, b_{i,n}]$ , where
         $a_{i,n} \leftarrow (i)\delta$  (cell lower limit)
         $b_{i,n} \leftarrow a_{i,n} + \delta$  (cell upper limit)
         $p_{i,n} \leftarrow p_{\lceil i/2 \rceil, n-1} m_{(i) \bmod 2}$  (cell probability)
         $x_{i,n} \leftarrow p_{i,n}$ , (latest observation of time series on the current iteration)
        If ( $i \neq 0$ ) {
             $M_{i,n} \leftarrow M_{i-1,n} + p_{i,n}$  (fractal measure of  $(0, b_{i,n}]$ )
        } (End If)
    } (End For loop)
    return  $M_{i,n}$ 
}

```

} (End nextIteration)

The above procedure converges to the multifractal binomial measure as n approaches infinity. However, taking $12 \leq n_{\max} \leq 16$ is sufficient for a good approximation to the multifractal measure.